ALPHA FOUNDATION FOR THE IMPROVEMENT OF MINE SAFETY AND HEALTH

Final Technical Report

Project Title: Development of A Stability Mapping Platform for Stone Mines That Will Combine Numerical Modeling and Empirical Criteria

Grant Number: AFCTG22r2-160

Organization: University of Kentucky

Principal Investigator: Dr. Zach Agioutantis

Contact Information:

Phone – (859) 257-2953 Fax – (859) 323-1962 Email – zach.agioutantis@uky.edu

Period of Performance: June 2023 – August 2025

Acknowledgement/Disclaimer: This study was sponsored by the Alpha Foundation for the Improvement of Mine Safety and Health, Inc. (ALPHA FOUNDATION). The views, opinions and recommendations expressed herein are solely those of the authors and do not imply any endorsement by the ALPHA FOUNDATION, its Directors and staff.

Contents

1	Exec	cutive Summary	. 5
2	Prob	lem Statement and Objective	. 6
3	Rese	earch Approach	. 7
	3.1	Overview	. 7
	3.2	Design Guidelines	. 7
	3.3	The Project – Scenario Concept	. 8
	3.4	Testing	. 9
	3.4.	Internal Testing	. 9
	3.4.2	2 External Testing	. 9
4	Rese	earch Findings and Accomplishments	10
	4.1 Variati	Assessing Pillar Stability in Underground Stone Mines: Impact of Geological Structures and Stre	
	4.2 Operat	Calibration of LaModel In-Seam Material Properties for Underground Stone Mine Benchi	
	4.3	Comparison of Rectangular and Spalled Stone Pillars	15
	4.4	Adjustment of the Elastic Modulus for Benched Pillars	20
	4.5	Using LaModel for Analyzing Stress Distribution in Benched Areas for Possible Massive Stone Pil	
	Collap	se	20
	4.5.	Case Study 1	20
	4.5.2	2 Case Study 2	32
	4.6	Development of the StabMap Windows Application	35
5	Publ	ication Records and Dissemination Efforts	37
	5.1	Published Papers	37
	5.2	Planned Papers	37
	5.3	Past Presentations	37
	5.4	Upcoming Presentations	37
6	Con	clusions and Impact Assessment	39
7	Reco	ommendations for Future Work	41
8	Refe	rences	42
9	App	endix A: Stone Mine Literature Review	45
10) A	ppendix B: Stabmap Installation	53

11	Appendix C: Stability Mapping Application Help File	57
Table o	of Figures	
	1: Stand-alone Windows application with database back-end	ç
	2: Photographs and LIDAR scans of the same pillar	
	3: Point cloud data visualization in Cloud Compare software	
	4: DSE Software interface and joint distribution.	
	5: Stages of multiple-pass benching operation in underground stone mines (modified a	
•	uizen et al., 2011)	
	6: Elements used in LaModel as a function of pillar width.	
_	7: Element distribution layouts in a pillar using LaModel	
	8 Modeled area	
_	9: LaModel grid for (a) development and (b) benched stages	
	10: LaModel element safety factors for (a) development and (b) benched stages	
_	11: Comparison of LaModel in-seam material properties with FLAC3D models and Equation 1: (a)	
	to-height ratio of 0.5, (b) final width-to-height ratio of 0.75	
	12: Selected pillar map design and LIDAR scan comparison	
_	13: LaModel pillar's grid comparison. Left) Designed. Right) LIDAR scanned	
	14: Map of the case study mine (Esterhuizen et al., 2019)	
	15: Digitized Mine map in AutoCAD and generated LamPre grid	
	16: Topography grid for overburden stress	
_	17: LamPre Grid for development and benched pillars with elements	
_	18: Calculated peak strength and strain values for development pillars for each element (Stab)	
_	To Catedrate pour energer and examination in development pittare for each element (etab.	
	19: Calculated peak strength and strain values for benched pillars for each element (StabMap)	
_	20: S-Pillar results for case study mine 1	
	21: Total vertical stress distribution in LamPLT	
_	22: Element strain safety factors visualized in LamPLT	
	23: Pillar stress safety factors visualized in LamPLT	
_	24: Safety factors obtained with different lamination thicknesses	
_	25: Pillar selected for collapse scenario	
_	26: Pillar's SF values before and after simulated collapse	
_	27: Safety factors obtained with different spalling levels	
_	28: Map of the study area for case study 2	
_	29: Calculated peak strength and strain values for development pillars in Mine 2 (StabMap)	
_	30: Simulated overburden stress and pillar stress safety factors for case study 2	
	31: S-Pillar results for case study mine 2	
	32: Change detection from two LIDAR scans 9-months apart	
	33: Low resolution LIDAR data	
_	34: High resolution point cloud data of a pillar (after Bishop, 2022)	
•	35: High resolution point cloud data of a pillar wall (after Bendezu, 2021)	

Figure 36: Pillar stress and geological ratings (after Esterhuizen et al. 2011)	47
Figure 37: Pillar stress and geological ratings (after Johnson et al., 2014).	48
Figure 38: Benching stages and pillar strength (after Esterhuizen et al., 2011)	49
Figure 39: Total vertical stress with reduced stiffness in benched pillars (after, Escobar, 2021)	49
Figure 40: S-Pillar Database GSI Representation.	50
Figure 41: CMRR application with stability mapping software.	51
Figure 42: Application of the local large discontinuity factor.	51
Figure 43: Mine layout is divided in sub-sections.	52
Figure 44: StabMap Setup Wizard	53
Figure 45: License Agreement	54
Figure 46: Component Selection	54
Figure 47: Install Location Determination	55
Figure 48: Selecting Install Options	55
Figure 49: Completion and Commencement	56
Table of Tables	
Table 1: Material properties calculated for development and benched stages	14
Table 2: Length Benefit Ratio values calculated for corresponding width-to-height ratios	16
Table 3: Discontinuity Dip Factor Table (Esterhuizen et al., 2011)	17
Table 4: Frequency Factor Table (Esterhuizen et al., 2011)	17
Table 5: Pillar strength values for the mapped pillar and the LIDAR-scanned pillar without adjustmen	ıt 18
Table 6: Pillar strength values for adjusted widths for the mapped pillar and the LIDAR scanned pill	lar with
adjustment	18
Table 7: Calculated peak strength and strain values for development pillars for each element	24
Table 8: Calculated peak strength and strain values for benched pillars for each element	24
Table 9: S-Pillar and LaModel safety factor comparison	29
Table 10: S-Pillar and LaModel safety factor comparison including LDF	29
Table 11: Calculated peak strength and strain values for development pillars in case study 2	33

1 Executive Summary

This report details the successful development and validation of a new stability mapping platform, StabMap, designed to mitigate severe safety risks associated with pillar stability and ground control in underground stone mining. The primary objectives were two-fold: first, to validate the use of the boundary element software LaModel—historically used for coal—as an enhanced design tool for stone mines, improving upon the limitations of the existing S-Pillar program; and second, to develop StabMap as a user-friendly, database-driven front end to LaModel that streamlines scenario preparation and analysis.

The research confirmed that LaModel can be used to model both development and benched areas in underground stone mines, a conclusion supported by comparisons with FLAC3D simulations. Furthermore, the study emphasized the critical influence of geological discontinuities. The analysis also confirmed the value of LIDAR scanning in capturing realistic, irregular pillar geometries, which often resulted in narrower dimensions than those on mine maps, leading to strength reduction estimates that were notably different between the numerical and empirical models.

The report also discusses the successful launch of StabMap, a brand new, database-driven software platform that functions as an efficient pre- and post-processor for LaModel and is independent of AutoCAD. It incorporates the necessary elasto-plastic analysis developed by Escobar (2021) to generate material models for both development and benched stone pillars.

This platform integrates the functionality of previous tools (LamPre and the Stability Mapper AutoCAD plugin) into a single environment. StabMap expands upon previous limitations by extending the grid dimension limit beyond 2000 x 2000 elements and allowing the analysis of more than four steps and four seams simultaneously.

The stability mapping platform is provided as a free tool and has been officially approved by the MSHA Technical Support Branch for installation on their computers, projecting that it will eventually be adopted by most consultants and mine operators evaluating pillar stability. While currently StabMap supports only one development and one benched level for stone seams, this functionality is planned to be expanded in the near future to accommodate two and three bench level operations.

Avenues for future work are discussed. These include the improvement of methodologies regarding multiseam stone operations and the refinement of the lamination thickness estimation.

2 Problem Statement and Objective

Underground stone mining represents around 21% of the total underground mining operations in the United States (NIOSH, 2021). In 2019, more than 2000 people worked in underground stone mining (NIOSH, 2021). Approximately 40% of fatalities have been linked with falls of ground from roofs and pillars in underground stone mines since 2006, and the time lost related to ground control issues represents about 15% of the total lost working days in underground stone mining (MSHA, 2016). Five massive pillar collapses (Crab Orchard Mine – August 2021, Torrance mine - November 2020 and July 2021, Subtropolis Mine – October 2020 and Whitney Mine – May 2015) occurred between 2015 and 2021 in older workings of active limestone mines. On January 7, 2022, a massive roof fall claimed the life of a dozer operator in an underground mine operating in the Loyalhanna formation and reports of extensive regionalized roof falls in other mines demonstrated the potentially severe risk to the safety of miners in underground stone mines.

In the U.S., the S-Pillar program was developed by the National Institute for Occupational Safety and Health (NIOSH) to assist in designing stable pillars in underground stone mines (Esterhuizen et al., 2011). S-pillar considers the influence of a large joint set intersecting a pillar on the stability of the pillar. This approach does not consider the relative location of geological structures with respect to pillars or that multiple joint sets may intersect a pillar. Moreover, the S-Pillar program conservatively calculates the pillar load as the maximum depth over the pillar layout, and the tributary-area stress calculation is only truly valid if the mine uses regularly-sized pillars (Esterhuizen et al., 2011). Currently, the S-Pillar program calculates the stability factor of underground stone mines by assuming that the full weight of the overburden is evenly distributed among the pillars and is only valid if large areas are mined using regularly-sized pillars (Esterhuizen et al., 2011). Therefore, the S-Pillar program can be further improved by extending the stability analysis of pillar systems to variable topographies and geometries.

LaModel is a software program used by mining operators to analyze stresses, displacements, and safety factors in underground mines, particularly for thin, tabular ore bodies like coal seams. It can model single and multiple seams, irregular pillars, and variable topography, calculating outputs such as seam convergence, pillar safety factors, and surface subsidence. It was originally developed in 1993 for the analysis of coal mine related stresses.

The main objectives of this project were to (a) utilize LaModel to provide enhanced capability beyond that provided by the empirical S-Pillar program and (b) develop a front end to LaModel that would incorporate the methodology developed so that stone mine scenarios could be easily prepared and fed into LaModel.

3 Research Approach

3.1 Overview

The ultimate goal of this project was to develop a stability mapping platform (software package) that is independent of the AutoCAD package, which would allow mine operators to assess stone mine pillar stability to identify potential hazard zones in the mine.

The project included two main objectives.

- The first objective (objective 1) was related to a research component that would target (i) the extension of the stone mine pillar concentric zone capacities derived by Escobar and Tulu (2021) to semi benched pillars, (ii) the development of laminated overburden models for stone mine stress analysis that could be addressed either through LamPre (v3) or under the stability mapping platform.
- The second objective (objective 2) was related to the development of a stand-alone, user-friendly software tool based on the Microsoft Windows platform that comprises the stability mapping platform (StabMap). The platform would allow for different input parameter groups that would be used to develop the stability maps of each project.

The literature review for the research component is presented in Appendix A.

A number of case studies were modeled under Objective 1, and the results are presented in Section 4 and Appendix A. The material models that were developed using Escobar's equation (Escobar 2021), were applied to both development pillars and benched pillars. In the initial phases of the project, the values pertaining to the elasto-plastic material models were developed through Excel and manually entered into LamPre. It should be noted that LamPre was developed for coal pillar analysis and, therefore, it can not generate material properties for stone.

While developing the stability mapping application for stone mines, it was considered prudent to extend the scope of the program to also include material model generation and other features applicable to coal mine projects. Thus, StabMap was expanded to include both, while maintaining compatibility with LamPre.

The Windows application was developed as a database-driven back end and a Windows front end (Figure 1). In addition, a project and scenario-based structure was built into the platform. Thus, multiple iterations of a given project can be analyzed as scenarios and can be easily compared.

3.2 Design Guidelines

The design guidelines adopted for this project include the following:

- The application should be fully parametric.
- o The application should be developed for a collaborative or stand-alone office environment.
- The application should be a database-driven application (operating on a client server concept) that should be able to store primary data as well as results.

- o The user should be able to set/change parameters when needed.
- Logs should be kept to document user actions at every step.
- Imported data should be easily accessible and reusable.
- o The application and database back-end should be optimized to store and retrieve large datafiles.
- o Data generated based on imported data should be easily accessible and reusable.
- The installer should be able to update both the application as well as the back-end database without affecting any user data already in the database.
- o There should be tools to backup and restore a database (see the users manual in Appendix C).
- There should be options and settings that the user can set at the local level (see the users manual in Appendix C).
- The application should follow the project/scenario framework where scenarios and all their data can be managed as a single entity (i.e., copied, deleted, saved, etc.).

3.3 The Project – Scenario Concept

The project–scenario concept has been successfully implemented in a number of other database applications developed by the PI (e.g., Wetbud, TreeSpec)

The project-scenario concept is briefly described below:

- A project, as defined in this application, includes general information about the project, such as description, comments, location, units used, etc. A typical entity identified as a project could represent a mine site.
- The user can create multiple scenarios under a given project. For example, different locations (panels, sections, etc.) within a project can be identified as scenarios. Scenario-level information should include data used for input as well as outputs related to the particular scenario. In this particular case, a scenario may include a CAD drawing file (*.DWG or *.DXF), the actual input data used, as well as data generated by LaModel. For a different set of analysis parameters, it would be very easy for the user to duplicate the current scenario and change the relevant parameter in the newly created scenario.

Data management was optimized for the particular application. Appropriate data indices were developed to ensure fast and reliable system response. Grouping queries was developed to enable the quick retrieval of data. LaModel output data, which served as input data, is also stored along with the parameters used to process such data.

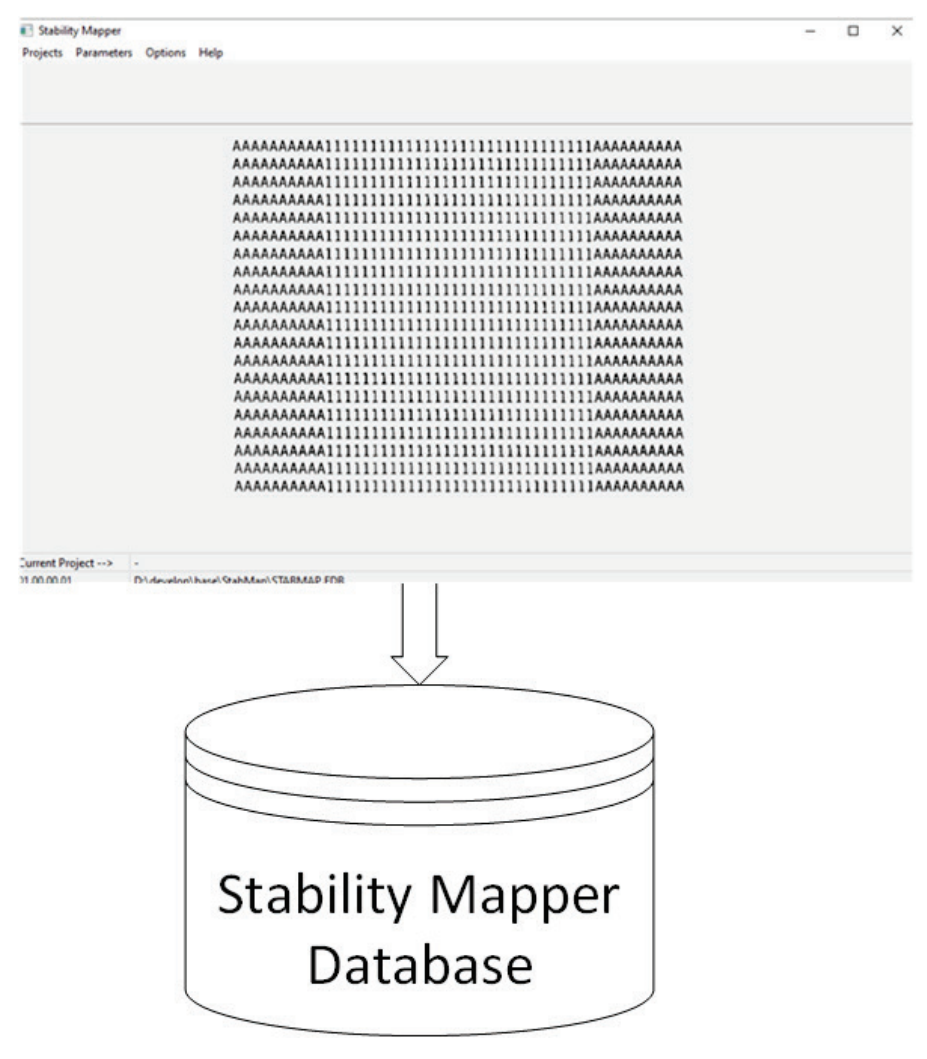


Figure 1: Stand-alone Windows application with database back-end

3.4 Testing

3.4.1 Internal Testing

The new stability mapping application was continually tested during development by sharing different builds with the research team, both at the University of Kentucky and West Virginia University. Over 140 internal versions were generated during the course of this package development.

3.4.2 External Testing

The new stability mapping application was also shared with two consultants who routinely run LaModel either for coal or for stone applications. In addition, it was shared with the MSHA Technical Support personnel. Feedback received was incorporated into the application. At the time of writing this report, the IT group of the MSHA technical support team had officially approved this package for installation on MSHA computers.

4 Research Findings and Accomplishments

4.1 Assessing Pillar Stability in Underground Stone Mines: Impact of Geological Structures and Stress Variations in the Appalachian Region

The research aimed to enhance stability assessments by examining the relationship between regional stress variations and geological discontinuities, a relationship often inadequately addressed by existing tools like the S-pillar software, particularly when multiple intersecting joint sets are involved. The methodology involved acquiring pillar surface data from four case study mines using Light Detection and Ranging (LIDAR) sensors, which generated point clouds, as shown in Figure 2.



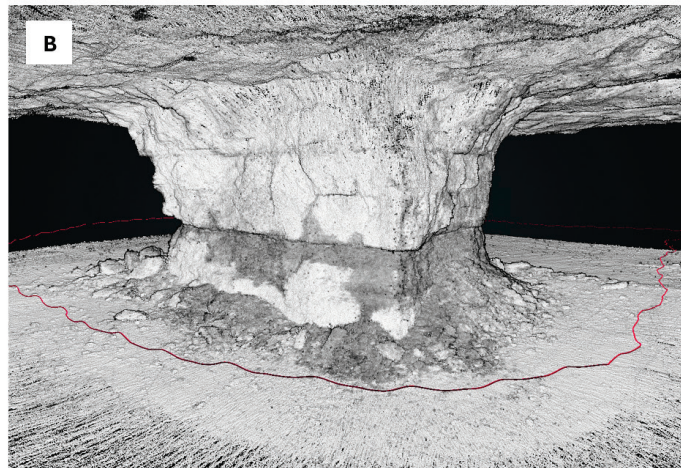


Figure 2: Photographs and LIDAR scans of the same pillar.

This data was processed using Cloud Compare for visualization (Figure 3) and subsequently analyzed by the Discontinuity Set Extractor (DSE) software to calculate normal vectors and identify distinct sets of discontinuities within the rock mass.

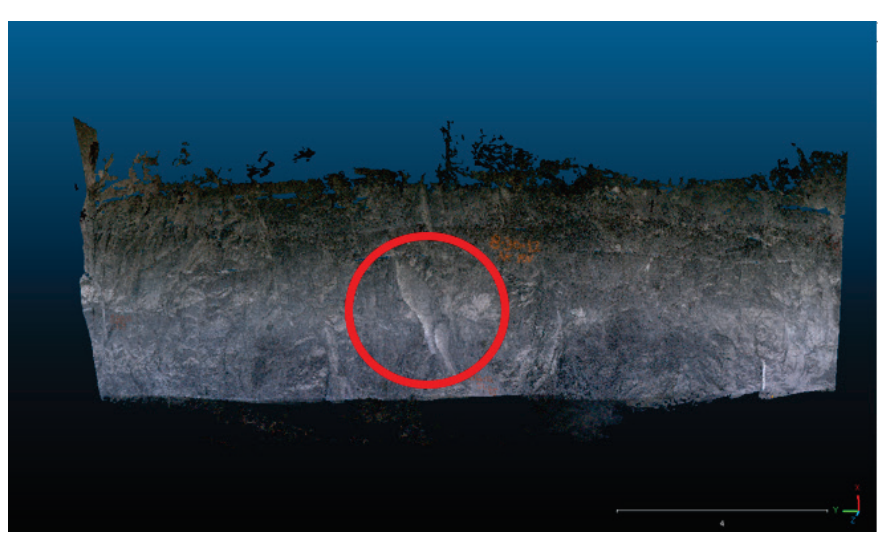


Figure 3: Point cloud data visualization in Cloud Compare software

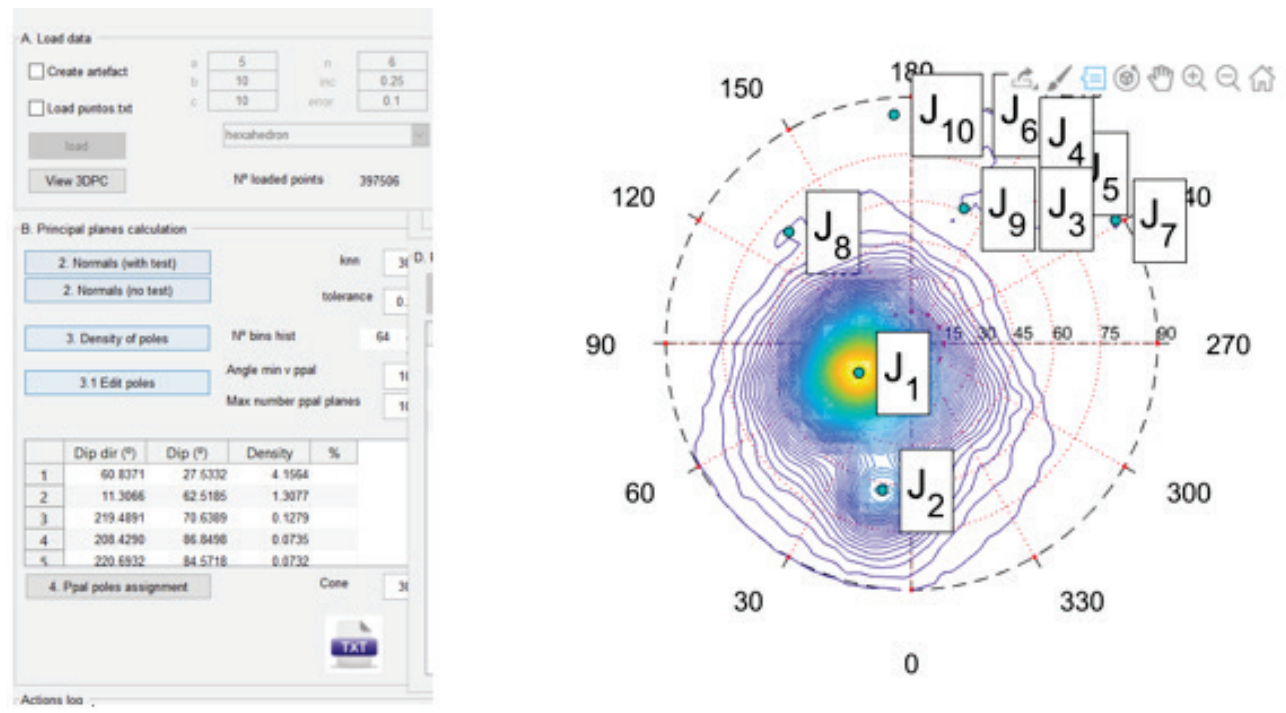


Figure 4: DSE Software interface and joint distribution.

Stress distribution data was integrated from the World Stress Map (WSM) to understand the tectonic behaviors of the Appalachian area. The geological setting is defined by the Alleghenian orogeny, which generated folds, faults, and discontinuities, and the regional maximum horizontal stresses generally align along the NE-SW direction. By comparing the global orientations of the extracted joint sets against nearby WSM measurements, the research concluded that the strikes of the observed joint sets were typically found to be at an angle less than 45° with respect to the major horizontal stresses, and their dip angles generally ranged between 60° and vertical. The overall findings support the need to expand pillar stability analysis to incorporate varying topographies, geometries, and detailed geological information, thereby enhancing mine safety considerations.

4.2 Calibration of LaModel In-Seam Material Properties for Underground Stone Mine Benching Operation by Employing Brittle Failure Criteria in FLAC3D

This work focuses on calibrating the LaModel software for multi-stage underground stone mines that employ benching. The methodology employed FLAC3D numerical simulations utilizing an implemented S-shaped brittle failure criterion routine to estimate pillar strength and failure mechanisms across different benching stages and width-to-height ratios. Figure 5 presents the stages of benching from the initial development to the final stage.

This criterion models rock mass cohesive and frictional strength components as a function of confinement (minimum principal stress). Key findings from the FLAC3D analysis showed that both slender and square pillar models resulted in a near-linear strength reduction, losing up to 35% of their initial development strength, whereas squat pillars experienced an exponential strength reduction, losing about 55% of development strength at the final stage. Furthermore, the study introduced a prototype metric, the confined

surface index, to quantify strength reduction during benching, demonstrating that reduced confinement—particularly evident in slender pillars after the first benching operation—leads to lower ultimate strength.

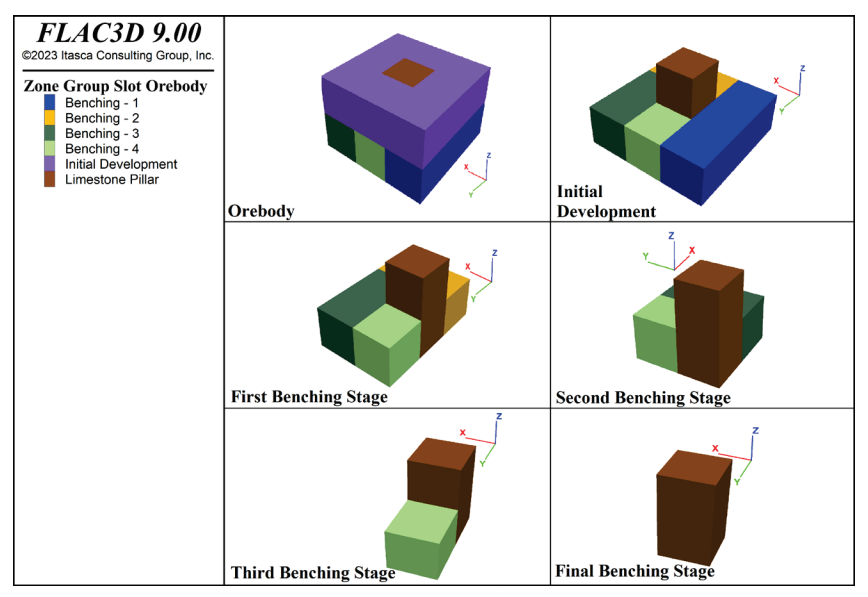


Figure 5: Stages of multiple-pass benching operation in underground stone mines (modified after Esterhuizen et al., 2011)

Finally, the estimated pillar strengths and stress gradients from FLAC3D were used to calibrate LaModel inseam material properties by applying the empirical stone mine pillar strength equations (eqn 1, 2, 3) as a function of pillar element position where σ_0 represents the intact rock strength, which is similar to k in eqn 1 (e.g., $0.65 \cdot UCS$ for the international system of units and $0.92 \cdot UCS$ for the imperial measurement system), x is the average location within the pillar, W is the width of the pillar, and h is the height of the pillar. Pillar elements as a function of element width are shown in Figure 6 for square and rectangular pillars. As the pillar width increases, the number of elements used to assess pillar stress increases too. In Figure 6, E_W stands for element width.

Pillar Strength Equation Modified for Stone Mines = $k \cdot LDF \cdot \frac{w^{0.3}}{h^{0.59}}$	(1)
$\sigma_{rib}(x) = 1.84 \cdot \sigma_0 \cdot \frac{x^{0.3}}{h^{0.59}}$	(2)
$\sigma_{corner} = \frac{1.23 \cdot \sigma_0}{h^{0.59} \cdot W} \cdot \left[\left(x + \frac{W}{2} \right)^{2.3} - 2.3 \cdot \left(x + \frac{W}{2} \right) \cdot \left(x - \frac{W}{2} \right)^{1.3} + 1.3 \cdot \left(x - \frac{W}{2} \right)^{2.3} \right]$	(3)

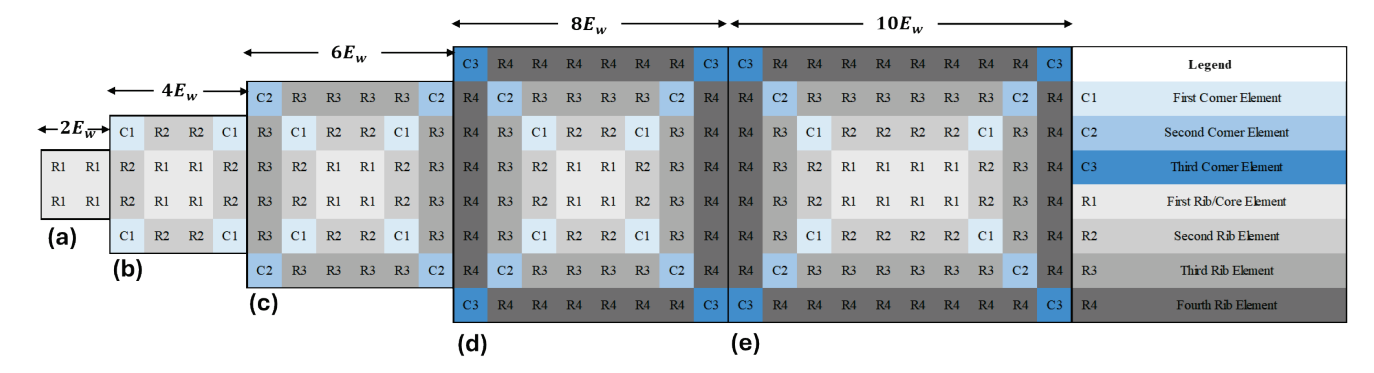


Figure 6: Elements used in LaModel as a function of pillar width.

In order to capture similar trends with FLAC3D simulations, a layout is implemented to distribute grid elements as the benching operations are performed as shown in Figure 7.

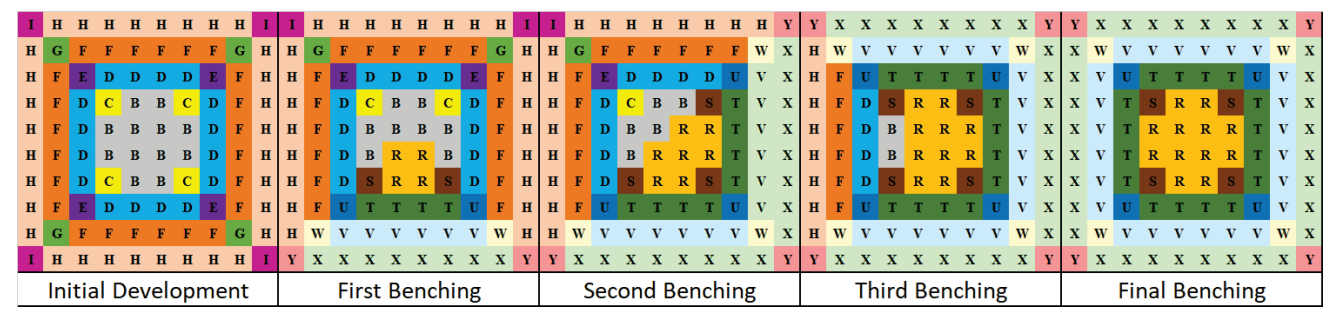


Figure 7: Element distribution layouts in a pillar using LaModel

The following briefly describes a LaModel application that was created for a case study mine for one of the benched areas. The mine extracts the Loyalhanna limestone with an average mining height of 28 ft. The modeled area has an additional benching height of 25 ft (Figure 8 – red dashed area).

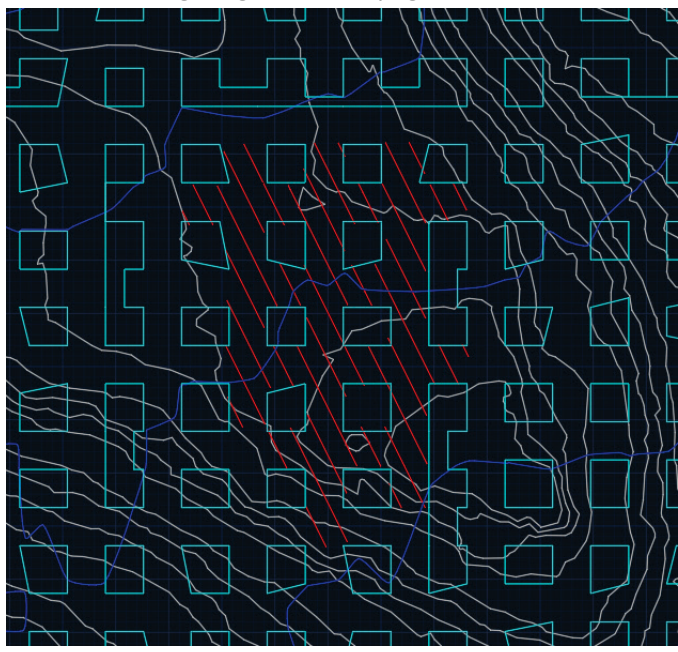


Figure 8 Modeled area

The model was generated with 2.5 ft elements, and the in-seam material properties were calculated using the equations derived by Escobar (2021) and the geotechnical properties suggested by Rashed et al. (2023) (see Table 1). The generated grid and the safety factor results are shown in Figure 9 and Figure 10.

Table 1: Material properties calculated for development and benched stages

Element	Yield Strength (psi)	Yield Strain		Element	Yield Strength (psi)	Yield Strain	
В	9011	0.00342	Development	L	6184	0.00235	Benched
С	8901	0.00338	Development	М	6108	0.00232	Benched
D	8356	0.00317	Development	N	5735	0.00218	Benched
Е	8225	0.00312	Development	0	5645	0.00214	Benched
F	7554	0.00287	Development	Р	5184	0.00197	Benched
G	7387	0.00281	Development	Q	5069	0.00193	Benched
Н	6481	0.00246	Development	R	4448	0.00169	Benched
I	6232	0.00237	Development	S	4277	0.00162	Benched
J	4661	0.00177	Development	T	3199	0.00122	Benched
K	3836	0.00146	Development	U	2633	0.00100	Benched

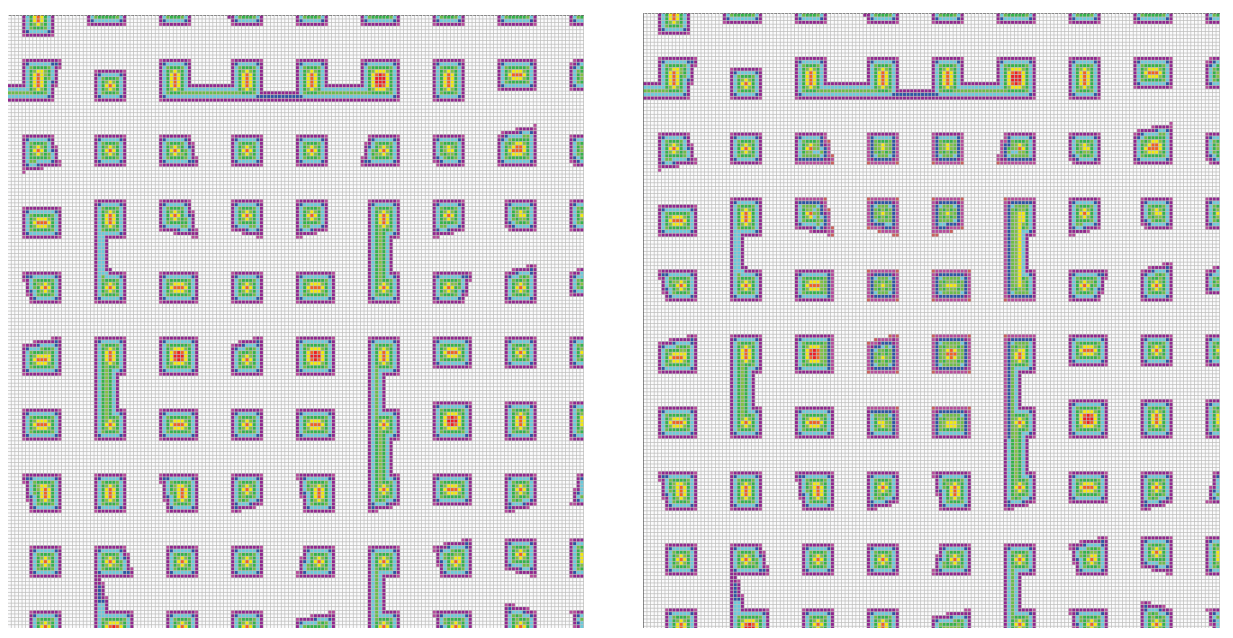


Figure 9: LaModel grid for (a) development and (b) benched stages

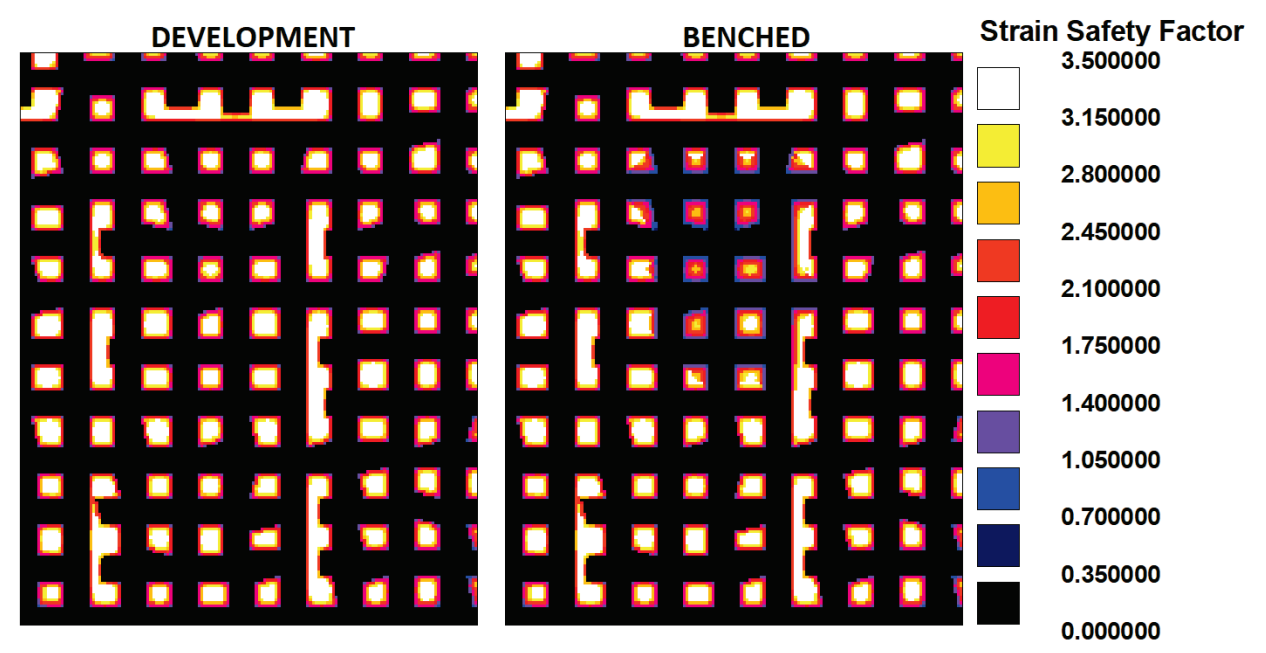


Figure 10: LaModel element safety factors for (a) development and (b) benched stages

In conclusion, the comparison between the calibrated LaModel and the FLAC3D simulations showed a reasonable agreement, validating this approach and providing a framework to incorporate strength changes during bench mining into robust design layouts for enhanced mine safety (Figure 11).

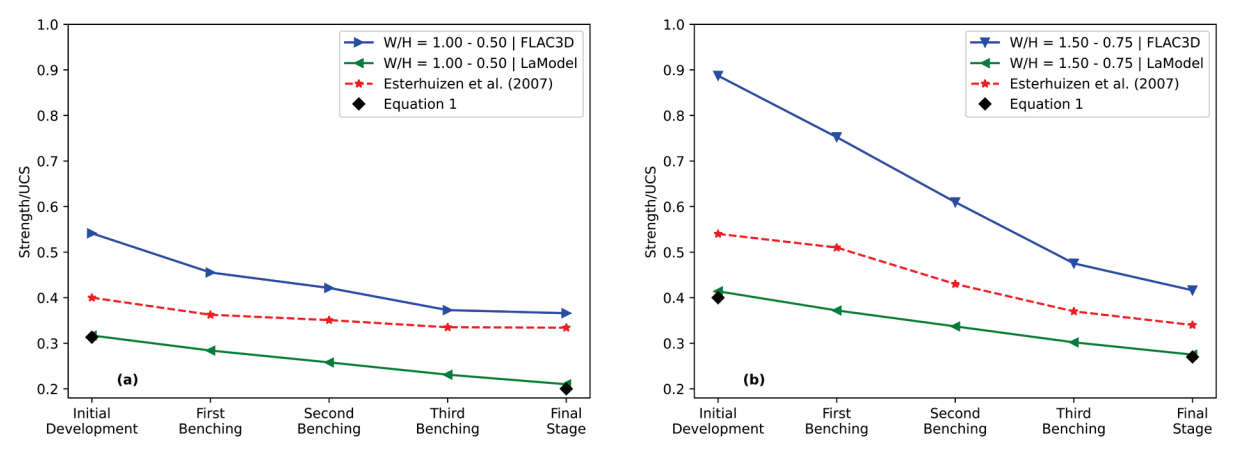


Figure 11: Comparison of LaModel in-seam material properties with FLAC3D models and Equation 1: (a) final width-to-height ratio of 0.5, (b) final width-to-height ratio of 0.75

4.3 Comparison of Rectangular and Spalled Stone Pillars

A mathematical model of rock pillar failure in brittle rock reveals that thinner pillars gain less from increased length than thicker pillars, due to their unconfined nature. The model demonstrates that the LBR is 0 when the width-to-height ratio is 0.5, but increases to 1.0 as the ratio approaches 1.4, as shown in Table 2. The method calculates the length benefit in terms of an equivalent pillar width increase used in the equation for pillar strength. The calculation of the equivalent width follows Wagner's formula (1992), presented in eqn 4,

which incorporates parameters such as the pillar's actual width, plan area, circumference, and the LBR value.

$$w_e = w + \left(\frac{4A}{C} - w\right) * LBR \tag{4}$$

Where A is the area of the pillar, C is the circumference of the pillar, w is the width of the pillar, and LBR is the length benefit ratio calculated according to Table 2. For square pillars, the equivalent width is simply the actual width. A chart of LBRs for different ratios of width to height is available, illustrating that as the ratio increases, the LBR approaches 1.0. This implies that rectangular pillars benefit proportionally more from length when they are wider, as shown in Table 2.

Table 2: Length Benefit Ratio values calculated for corresponding width-to-height ratios

Width-to-height ratio	Length benefit ratio (LBR)
0.5	0.00
0.6	0.06
0.7	0.22
0.8	0.50
0.9	0.76
1.0	0.89
1.1	0.96
1.2	0.98
1.3	0.99
1.4	1.00

A case study was developed to compare stresses between a rectangular pillar (as designed) and the pillar that is actually in place as determined by LiDAR scans (Figure 12).



Figure 12: Selected pillar map design and LIDAR scan comparison

Thus, two different sets of pillar width and length measurements were analyzed: one obtained from a mine map layout and the other from a LIDAR scan. The pillar dimensions from the mine layout were recorded as 9.14 m (30 ft) and adjusted width as 9.28 m (30.44 ft) and 15.24 m (50 ft) in length. For the LIDAR scan measurements, the width was measured as 6.61 m (21.69 ft), where the adjusted width is calculated as 6.75 m (22.14 ft). To determine the pillar strength, the large discontinuity factor (LDF) was required. The LDF is calculated using eqn 5,

$$LDF = (1 - DDF) * FF \tag{5}$$

where DDF (discontinuity dip factor) is derived from the width-to-height ratio, and FF (frequency factor) is based on Table 3 and Table 4. The DDF was specifically calculated using LIDAR scan data analyzed with DSE software, which identified the LDF for the mine as 0.77. And the LIDAR-scanned pillar had dimensions of 6.61 m (21.69 ft) in width and 13.45 m (44.15 ft) in length. To analyze the worst-case scenario with greater accuracy in real-life applications, LDF is considered with a value of 0.77. LDF is a direct multiplier for pillar strength, and it can be applied directly to pillar safety factors obtained from LaModel. Ates (2022) demonstrated how LDF can be implemented into LaModel by locating the pillars that are intersected by large discontinuities on a mine layout and reducing the load-bearing capacity of the pillar by LDF.

Table 3: Discontinuity Dip Factor Table (Esterhuizen et al., 2011)

Discontinuity	Pillar width-to-height ratio					atio			
dip (deg)	≤0.5	0.6	0.7	0.8	0.9	1	1.1	1.2	>1.2
30	0.15	0.15	0.15	0.15	0.16	0.16	0.16	0.16	0.16
40	0.23	0.26	0.27	0.27	0.25	0.24	0.23	0.23	0.22
50	0.61	0.65	0.61	0.53	0.44	0.37	0.33	0.3	0.28
60	0.94	0.86	0.72	0.56	0.43	0.34	0.29	0.26	0.24
70	0.83	0.68	0.52	0.39	0.3	0.24	0.21	0.2	0.18
80	0.53	0.41	0.31	0.25	0.2	0.18	0.17	0.16	0.16
90	0.31	0.25	0.21	0.18	0.17	0.16	0.16	0.15	0.15

Table 4: Frequency Factor Table (Esterhuizen et al., 2011)

Average frequency of large	Frequency
discontinuities per pillar	Factor
0.0	0.00
0.1	0.10
0.2	0.18
0.3	0.26
0.5	0.39
1.0	0.63
2.0	0.86
3.0	0.95
>3.0	1.00

Table 5: Pillar strength values for the mapped pillar and the LIDAR-scanned pillar without adjustment.

	Development
	$\sigma_p = 0.65 * \sigma_0 * LDF * \frac{w^{0.3}}{h^{0.59}}$
Pillar Strength Value with Mine Map	56.21 MPa
Pillar Strength Value with LIDAR Scan	51.03 MPa

Table 6: Pillar strength values for adjusted widths for the mapped pillar and the LIDAR scanned pillar with adjustment.

	Development
	$\sigma_p = 0.65 * \sigma_0 * LDF * \frac{w_e^{0.3}}{h^{0.59}}$
Pillar Strength Value with Mine Map	56.47 MPa
Pillar Strength Value with LIDAR Scan	51.36 MPa

The pillar strength values shown in Table 5 and Table 6 present a comparison derived from mine maps and LIDAR scans using the empirical strength formula. Table 5 shows the values without any width adjustment, while Table 6 includes adjusted effective widths (w_e) for the mapped pillars and LIDAR Scan pillars. In Table 5, the LIDAR scan results in lower pillar strength values than the mine map, with a difference of 5.18 MPa in development pillars.

This suggests that the actual pillar geometries captured by LIDAR are more irregular or narrower than those represented on the mine maps, leading to reduced strength estimates. As shown in Table 6 adjusting the pillar widths using the LiDAR scans slightly decreases the strength values by 5.11 MPa for development pillars. However, even after this adjustment, the LIDAR values remain lower, suggesting that LIDAR provides a more realistic view of pillar dimensions. The pillar strength values in Table 6 were 56.47 MPa for the mapped development pillar and 51.36 MPa for the LIDAR-scanned development pillar. The corresponding width reduction was approximately 1.53 %, resulting in a 9.9% decrease in strength, indicating how even modest changes in geometry and discontinuities can significantly affect pillar strength. Overall, the analysis demonstrates that LIDAR scanning is a valuable tool for capturing true pillar geometries and estimating pillar strength more accurately, while also emphasizing the importance of accounting for width adjustments and zone-specific conditions, especially in benched areas.

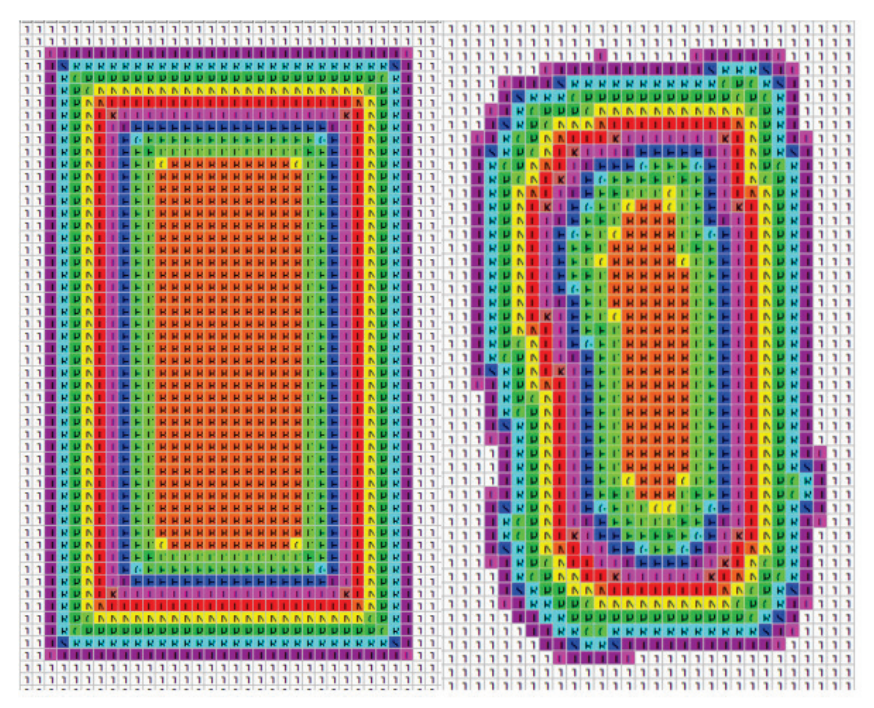


Figure 13: LaModel pillar's grid comparison. Left) Designed. Right) LIDAR scanned

With a 27.7% overall width reduction from the mine-designed pillar width to the LIDAR-scanned pillar width, a model is generated using LaModel (Figure 13). The element size was set to 1 ft. A pillar was generated according to the mine layout, and another pillar was generated according to LIDAR scans, with five (5) less elements in terms of width and nine (9) less elements in terms of length.

In summary, for pillars with a width-to-height (W/H) ratio of 0.5, the strength decreases significantly when a 60° discontinuity dip angle is present in the direction of the pillar's inclination. This occurs regardless of whether the pillar is vertical or inclined (Jessu, 2018). In our case, the W/H ratio is almost 1.3, and some discontinuities have almost 70 dip angles. According to the LaModel results, the calculated pillar strength is 59.68 MPa for the designed pillar and 58.03 MPa for the LIDAR-scanned pillar. This reflects a reduction of approximately 2.75% in pillar strength due to the observed dimensional changes. Although the percentage decrease may seem modest, Table 10 highlights the sensitivity of pillar strength to geometric variations, especially in the presence of high-angle discontinuities. In critical areas of the mine where ground conditions are less favorable, even small reductions in strength could impact long-term stability and safety.

According to the S-Pillar analysis, the estimated pillar strength is 56.47 MPa for the designed pillar and 51.36 MPa for the LIDAR-scanned pillar, indicating a 9.05% reduction in strength due to dimensional changes observed in the scan. In contrast, LaModel results show a pillar strength of 59.68 MPa for the designed pillar and 58.03 MPa for the LIDAR-scanned pillar, reflecting a smaller reduction of approximately 2.75%.

This discrepancy highlights how different modeling approaches respond to changes in geometry. S-Pillar, being an empirical tool, may be more sensitive to width and height changes, particularly under assumptions of uniform loading and simplified geometry. LaModel, on the other hand, incorporates stress distribution

and load transfer across the seam, providing a more nuanced response to dimensional changes, especially when confinement and boundary effects are present.

Overall, both tools indicate a loss in pillar strength due to narrowing, but the magnitude of the reduction differs. This suggests that relying solely on empirical methods may overestimate the impact of dimensional changes in certain geomechanical settings. Using a combination of empirical and numerical approaches provides a more comprehensive understanding of pillar stability.

The research indicates that rectangular pillars increase pillar strength, as researched by numerous studies (Wagner, 1992; Mark and Chase, 1997; Galvin et al., 1999; Dolinar and Esterhuizen, 2007). These pillars are also less affected by geological structures when their longer axis is properly aligned, making them a more stable option (Dolinar and Esterhuizen, 2007). However, there remains a research gap regarding the performance of inclined rectangular pillars, highlighting an area for further investigation.

4.4 Adjustment of the Elastic Modulus for Benched Pillars

When one does the benching in a stone mine, or anywhere different seam heights are used in LaModel, the elastic modulus needs to be adjusted to correlate with the different seam heights, to be mechanistically accurate.

For example, let's assume that a limestone regular seam has a height of 7 m. When seam materials for a benched model that was 18 m high are created, these elements have a much smaller w/h ratio, so they are weaker, as determined in the material section. However, they are also 18 m high rather than the 7 m that LaModel is using for the seam height. So, when the 7 m seam converges 1 m, the strain is 1/7 for the 7 m elements but only 1/18 for the taller elements. Unless the modulus is adjusted for the 18 m high elements, LaModel will use a strain of 1/7 on them to calculate the stress and get an unrealistically high stress. To get the correct stress, the modulus on the benched elements needs to be lowered by a factor of the relative seam heights, i.e., 7/18, so that the strain on the thicker elements is not 1/7, but now 1/18. This reduction should be standard practice for a benched seam.

This has been implemented in the new package and is also shown below.

4.5 Using LaModel for Analyzing Stress Distribution in Benched Areas for Possible Massive Stone Pillar Collapse

The objective was to investigate the application and calibration of LaModel, a boundary element software typically used for coal mining, to accurately assess the stability of these benched limestone pillars. A number of case studies were analyzed as discussed below.

4.5.1 Case Study 1

The first case study concerns a limestone mine in Pennsylvania that experienced a pillar collapse in 2015. The details of the mine site and the rock properties have been obtained from the study published by Esterhuizen et al. (2019). The study highlights the catastrophic collapse of 37 slender pillars within the limestone mine, which tragically resulted in fatalities. The study focuses on the role of through-going

discontinuities in compromising pillar stability. A detailed mine map provided by Esterhuizen et al. (2019) (Figure 14) was digitized and converted into an AutoCAD file for further analysis (Figure 15).

The geological context is the Loyalhanna limestone, characterized by structural features such as a thrust fault (N25°E, 15° SE dipping angle) and significant joint sets, including one with a N60°W strike, in an area where 35 pillars had already collapsed.

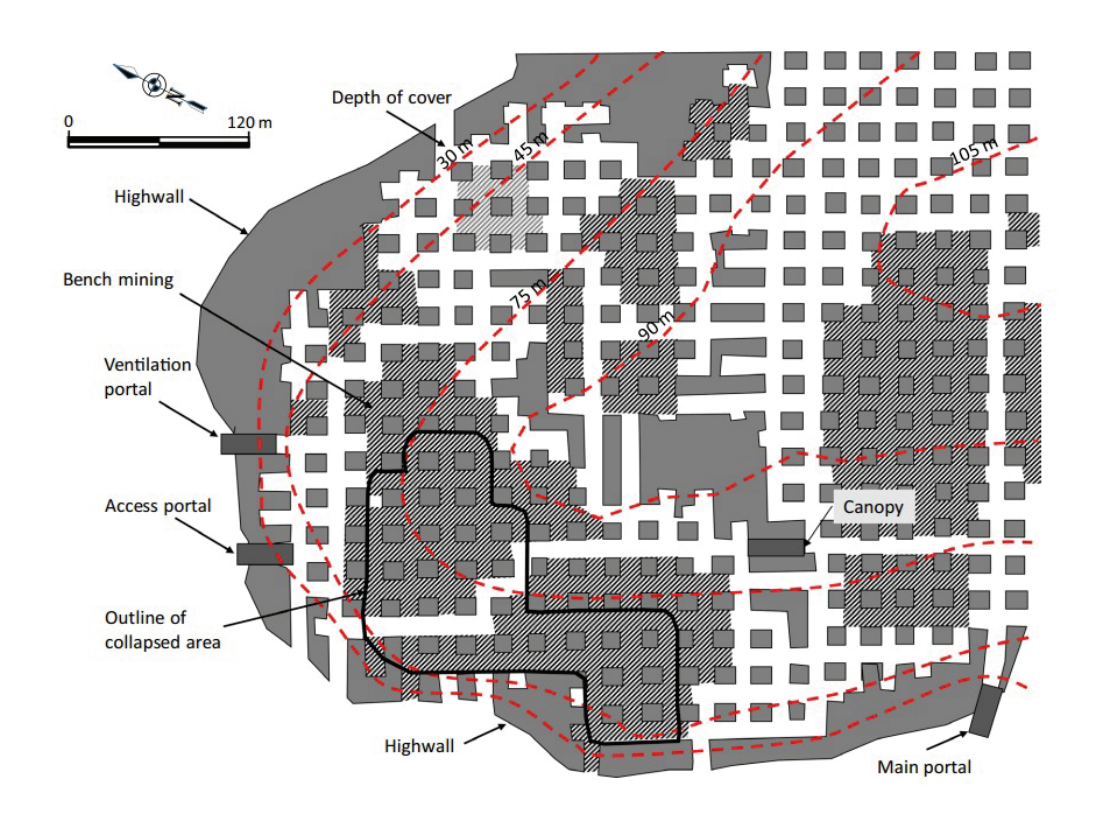


Figure 14: Map of the case study mine (Esterhuizen et al., 2019)

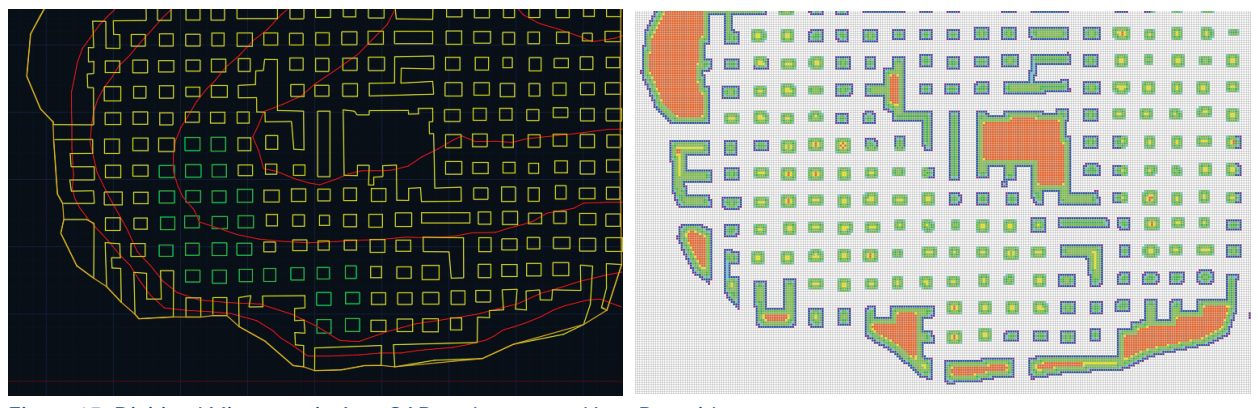


Figure 15: Digitized Mine map in AutoCAD and generated LamPre grid

In AutoCAD, both the Seam Grid and Topography Grid were generated to facilitate accurate modeling and analysis. These grids serve as the foundation for entering geometric and topographical details into LaModel via the LamPre preprocessor. The key parameters implemented in LamPre include the following:

- Number of in-seam materials: 18 (9 codes for development, 9 codes for benched pillars)
- Number of steps: 2 (development and benched)
- Units: LamPre was configured to use MPa and meters.

The seam grid was created with an element width of 2 meters to enhance accuracy. Symmetric boundary conditions were applied to all seam edges. The mine dimensions were set to 600 m x 600 m, resulting in a total of 300 elements along both the x and y directions. The origin points for the x and y axes were set at (0, 0). Key geometric and mechanical parameters include:

- Overburden height: Topography grid is used to determine overburden stresses (Figure 16)
- Seam thickness: 7 m for development and 18 m for benched pillars
- Poisson's ratio: 0.2
- Overburden elastic modulus: 20.7 GPa (this is the default value used in LaMPre)
- In Seam elastic modulus: 46 GPa
- **Element width:** 2 m
- Rock UCS: 181.9 MPa
- Lamination thickness: the default value of 15.25 meters is used (50 ft)
- Vertical stress gradient: 0.025448 MPa/m (default value of 1.125 psi/ft)

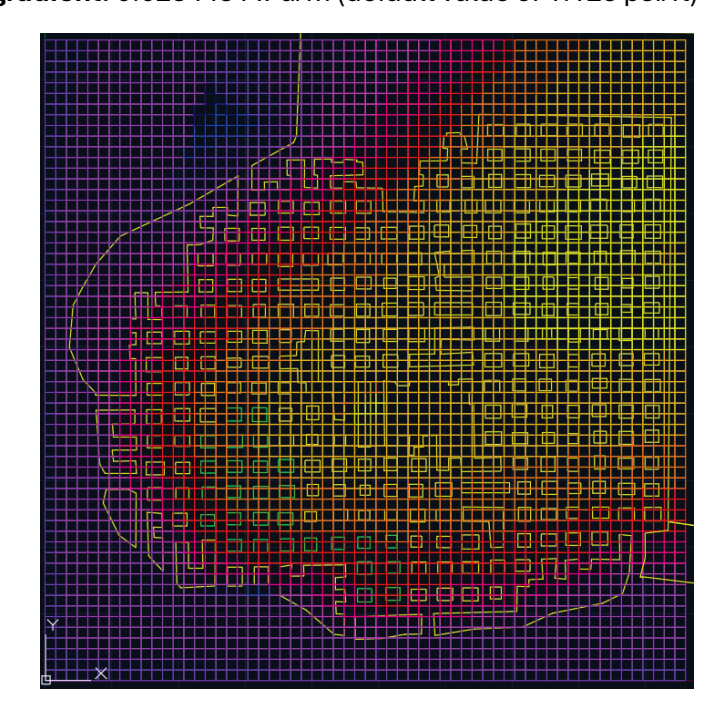


Figure 16: Topography grid for overburden stress

Each seam was divided into nine elements per set, leading to a total of 18 elements for all material configurations. The seam grid data, along with the topography file, were input into LamPre to simulate realistic stress and deformation conditions. To ensure precise analysis of stress distribution and pillar behavior, each individual pillar was subdivided into five elements. This segmentation provides a detailed understanding of how stresses are distributed within and around the pillars, enabling a more accurate assessment of stability and failure mechanisms. The 2-meter element width was critical in achieving this level of detail, particularly for modeling slender and benched pillars. The integration of these parameters into LamPre allows for comprehensive modeling, adhering closely to the conditions described in the case study. The outputs from LaModel will provide critical insights into stress redistribution and potential failure zones within the mine.

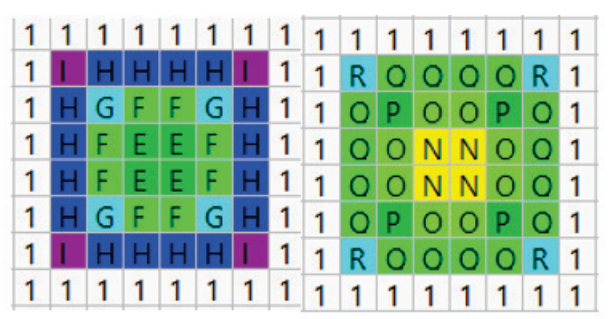


Figure 17: LamPre Grid for development and benched pillars with elements

An Excel spreadsheet was developed to calculate specific parameters for individual elements within the pillars using Eq.1 and Eq.2 (Escobar, 2021). This spreadsheet served as a tool to validate the input data and ensure consistency in the modeling process. The material properties were converted into MPa to align with the units used in LamPre and were subsequently entered into the software.

$$\sigma_{corner} = \left(\frac{1.23 \,\sigma_0}{h^{0.59} \,W^2}\right) \left[\left(\bar{x} + \frac{W}{2}\right)^{2.3} - 2.3 \left(\bar{x} + \frac{W}{2}\right) \left(\bar{x} - \frac{W}{2}\right)^{1.3} + 1.3 \left(\bar{x} - \frac{W}{2}\right)^{2.3} \right] \tag{1}$$

$$\sigma_v(x) = 1.84 \ \sigma_0 \ \frac{x^{0.3}}{h^{0.59}} \tag{2}$$

The case study was evaluated using the S-Pillar tool, which calculates the average stress on the pillars and the pillar strength. This analysis was validated by performing elemental stress calculations in the Excel spreadsheet. While the results from S-Pillar and the calculations in the Excel spreadsheet were largely consistent, minor differences were observed. These differences are likely due to rounding or differences in how stresses are averaged or distributed within the software versus manual calculations. By utilizing the Excel spreadsheet for parameter verification and using LamPre for advanced modeling, the workflow ensured both accuracy and reliability in simulating the stress conditions within the mine pillars. Table 7 provides the calculated peak strength and peak values for the development material properties while Table 8 provides the calculated peak strength and peak values for the benched material properties. The data in both tables were calculated via the Excel spreadsheet. Figure 18 and Figure 19 present the same information as calculated in StabMap.

Table 7: Calculated peak strength and strain values for development pillars for each element

Element Code		Peak Strength (psi)	Peak Strength (MPa)	Peak Strain (%)
В	Rib	17987.4	124.0	0.270%
С	Corner	17705.8	122.1	0.265%
D	Rib	16260.3	112.1	0.244%
E	Corner	15900.6	109.6	0.238%
F	Rib	13950.0	96.2	0.209%
G	Corner	13414.5	92.5	0.201%
Н	Rib	10033.2	69.2	0.150%
I	Corner	8257.2	56.9	0.124%

Table 8: Calculated peak strength and strain values for benched pillars for each element

Element Code		Peak Strength (psi)	Peak Strength (MPa)	Peak Strain (%)
K	Rib	10303	71.04	0.154%
L	Corner	10141.7	69.92	0.152%
М	Rib	9314.2	64.2	0.140%
N	Corner	9108.2	62.8	0.137%
0	Rib	7990.8	39.6	0.086%
Р	Corner	7684.1	53.0	0.115%
Q	Rib	5747.2	39.6	0.086%
R	Corner	4729.9	32.6	0.071%

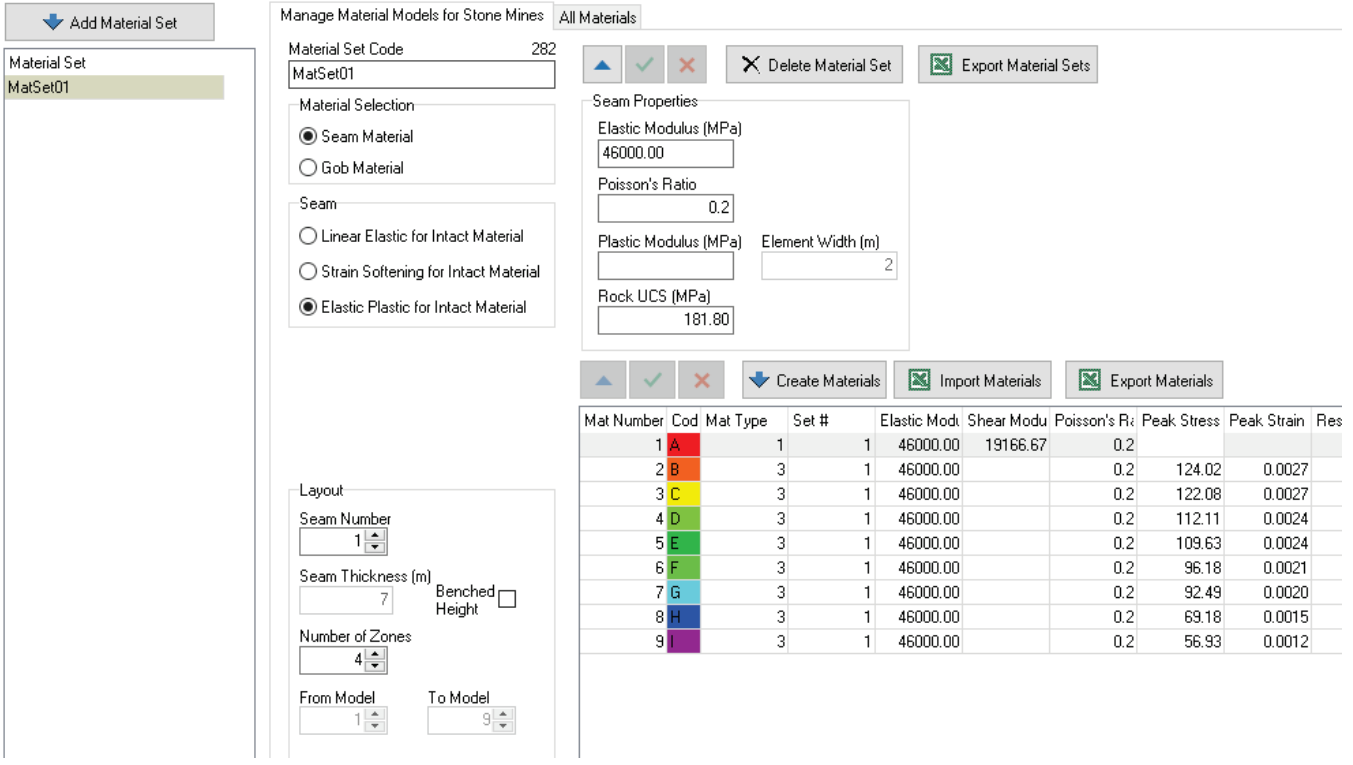


Figure 18: Calculated peak strength and strain values for development pillars for each element (StabMap)

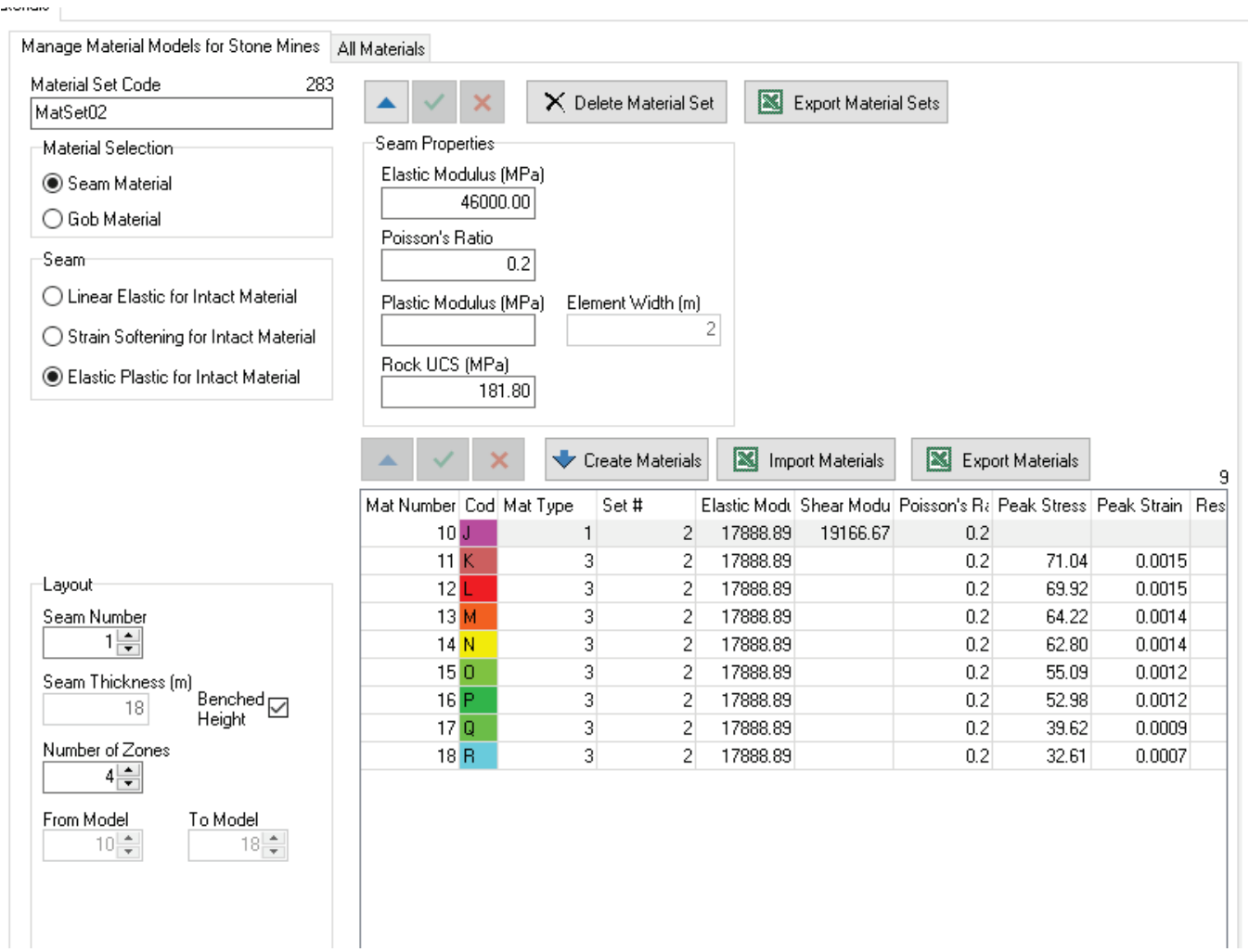


Figure 19: Calculated peak strength and strain values for benched pillars for each element (StabMap)



Figure 20: S-Pillar results for case study mine 1

The AutoCAD grid created earlier was imported into LamPre to serve as the base grid for further modeling. After importing, the benched areas were manually modified within LamPre to accurately reflect the dimensions and structural changes specific to these regions. This step was crucial for ensuring that the model aligned closely with the actual mine layout and conditions. Partially benched pillars were assumed to have a linear strength reduction following the FLAC3D results presented in the previous report. Once the modifications were completed, the overall stress distribution was recalculated by running simulations in LaModel. The results were then visualized using LamPlt.

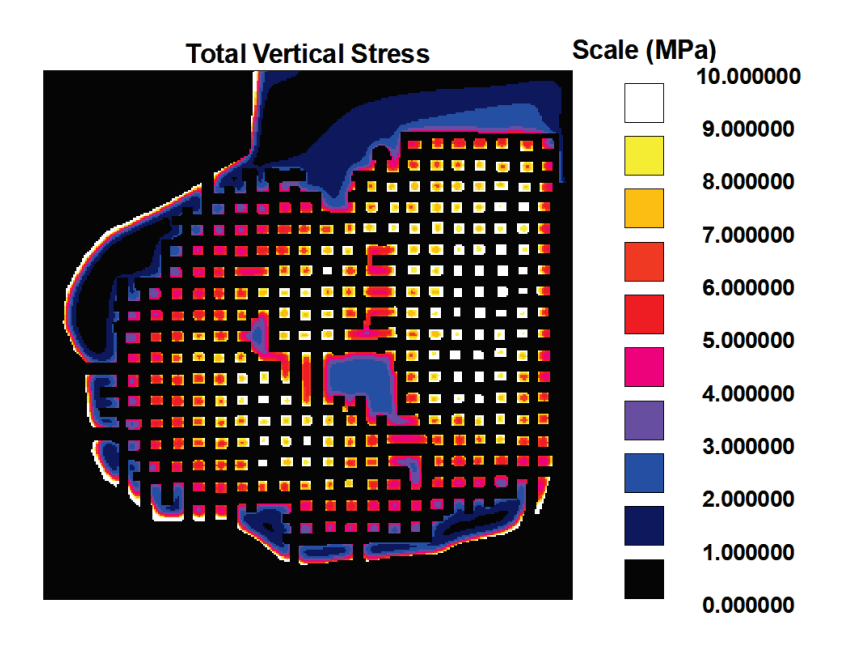


Figure 21: Total vertical stress distribution in LamPLT

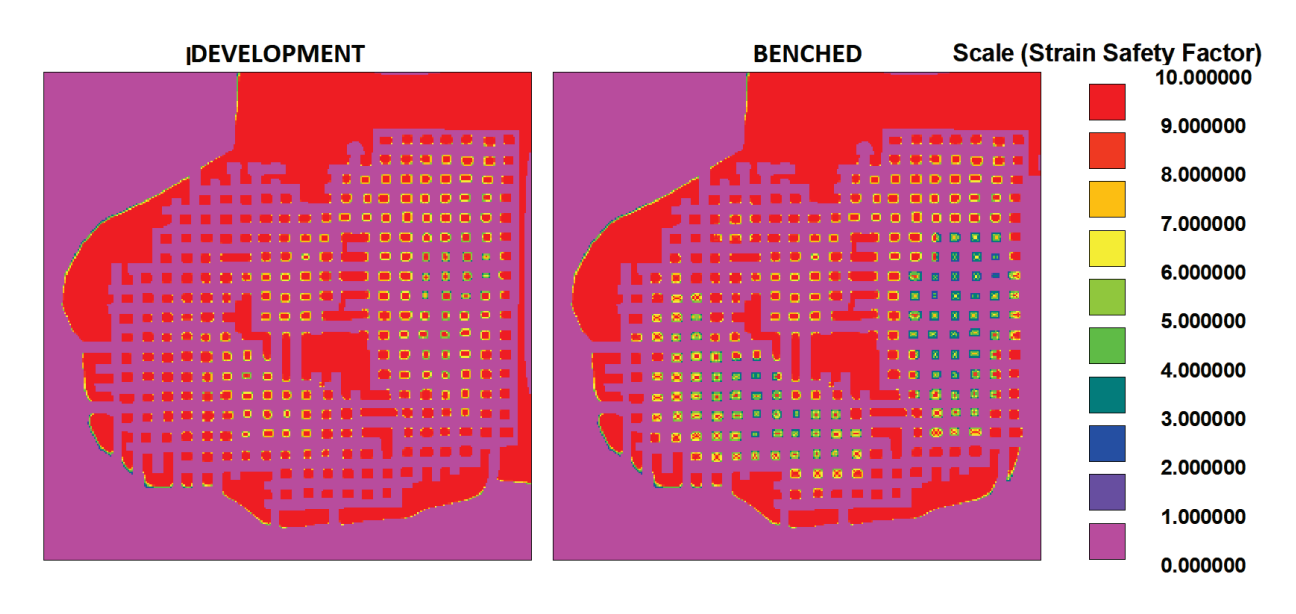


Figure 22: Element strain safety factors visualized in LamPLT

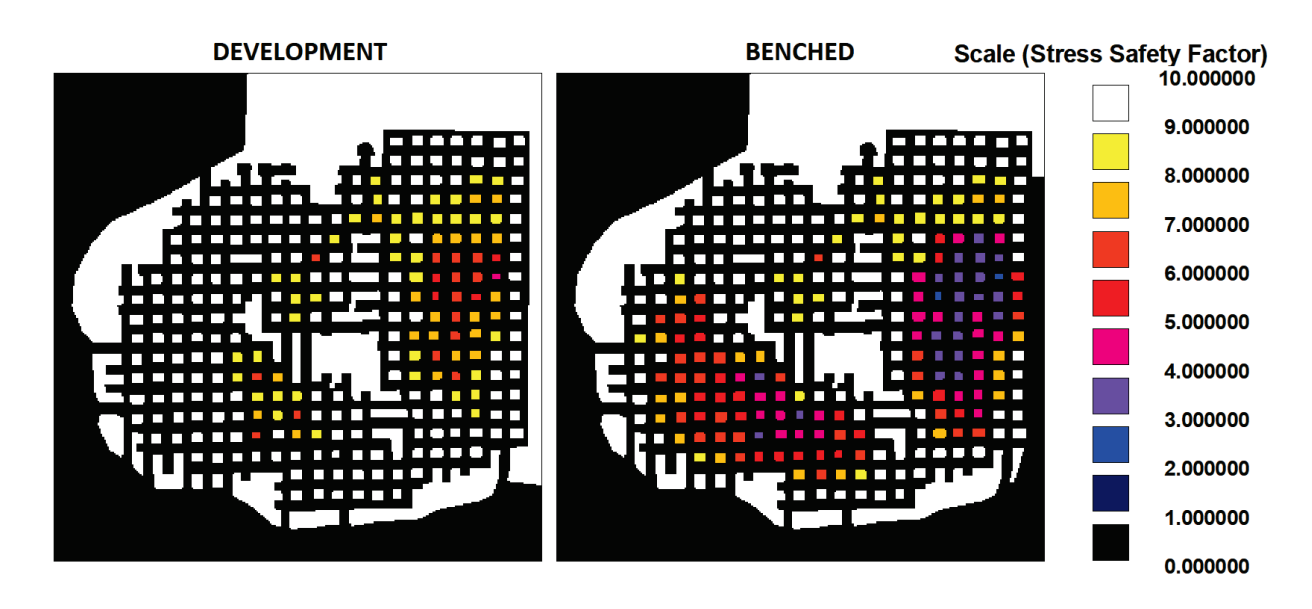


Figure 23: Pillar stress safety factors visualized in LamPLT

Compared to the S-Pillar results, in LaModel, a 10m by 10m pillar in the collapsed area had a safety factor of 7.89 during the development stage, which dropped down to 4.27 during the benching stage (Table 9). The results were in agreement for the development stage, but LaModel showed lower safety factors for the benched pillars, mainly due to load transfer from the surrounding benched pillars.

Table 9: S-Pillar and LaModel safety factor comparison

	S-Pillar Safety Factor LaModel Safety Factor	
Development	7.77	7.89
Benched	4.75	4.27

As reported by Esterhuizen et al. (2019), there were large discontinuities observed in the mine. The reported spacing of the discontinuities was between 2 and 5 m, with dip angles ranging between 50° and 80°. These discontinuities can be accounted for using the large discontinuity factor (LDF) approach (Esterhuizen et al., 2011). When incorporating an LDF based on a worst-case scenario (2 m spacing, 60° dip), the result was a significant reduction of the safety factor of benched pillars to 1.07 (LaModel) or 1.17 (S-Pillar), pushing them below the critical stability threshold of 1.5 (Table 10). For that scenario, the LDF was 0.79 for development pillars and the LDF was 0.25 for the benched pillars. Furthermore, simulations of a single pillar collapse in the benched zone revealed an average safety factor reduction of approximately 9% in adjacent pillars, indicating a potential for cascading failures.

Table 10: S-Pillar and LaModel safety factor comparison including LDF

	S-Pillar Safety Factor LaModel Safety Factor	
Development	6.15	6.23
Benched	1.17	1.07

In LaModel, the stiffness of the overburden is governed by the rock mass modulus and the rock mass lamination thickness. The rock mass will behave stiffer as these parameters increase. The rock mass modulus is usually assumed to be a standard value and kept constant, while the lamination thickness is calibrated to match the abutment extent observations or historical data. However, in stone mines, since there are no retreat operations, this type of calibration cannot be performed. This does not necessarily mean the lamination thickness can be ignored, and through a parametric study, we investigated its effect on stress distribution in the case study mine.

Accurate stress distribution is critical in practical mining applications and in LaModel, it is governed by the overburden stiffness. In this research, the case study mine model was simulated with different lamination thicknesses, and pillar safety factors were examined. Slight differences in safety factors can be seen for different lamination thickness values (Figure 24). It was observed that lower lamination thickness resulted in lower safety factors since a less stiff overburden allowed more convergence and more load to be applied on the pillars.

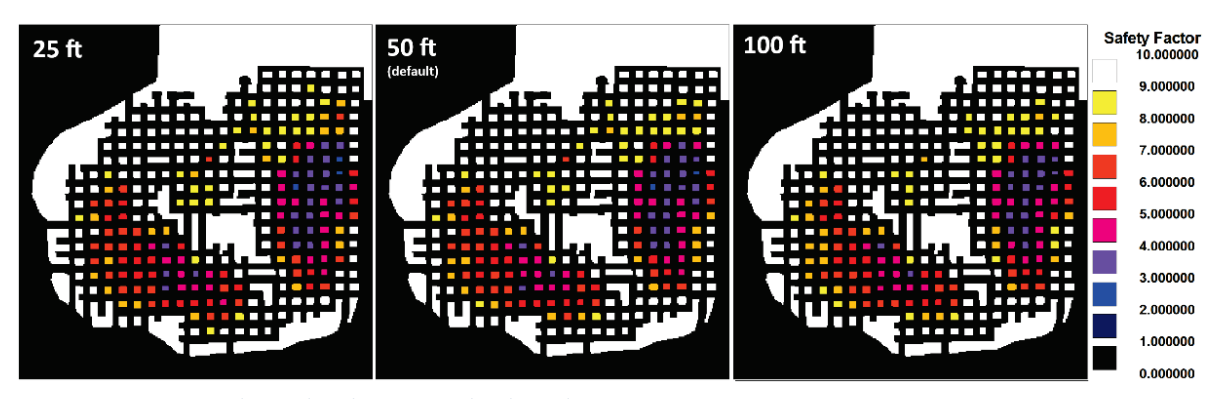


Figure 24: Safety factors obtained with different lamination thicknesses

Two scenarios were then developed in order to replicate certain behavior. The first scenario modeled the simulated collapse of a single pillar located in the benched zone, aimed at assessing whether such a localized failure could trigger instability in adjacent pillars or if the surrounding structure could effectively absorb the redistributed load (Figure 25). In the LaModel simulation, this scenario was modeled by allowing all elements within the selected pillar to fail, thereby simulating a total load transfer rather than a partial failure. This approach enabled an evaluation of stress redistribution in the immediate vicinity of a single collapsed pillar.

The results shown in Figure 26 reveal that the failure of the single, benched pillar resulted in an average safety factor reduction of approximately 9% in the neighboring pillars. These findings suggest that even a single pillar failure—when located in structurally compromised zones such as benched areas—can contribute to cascading failures, especially in regions with large structural discontinuities.

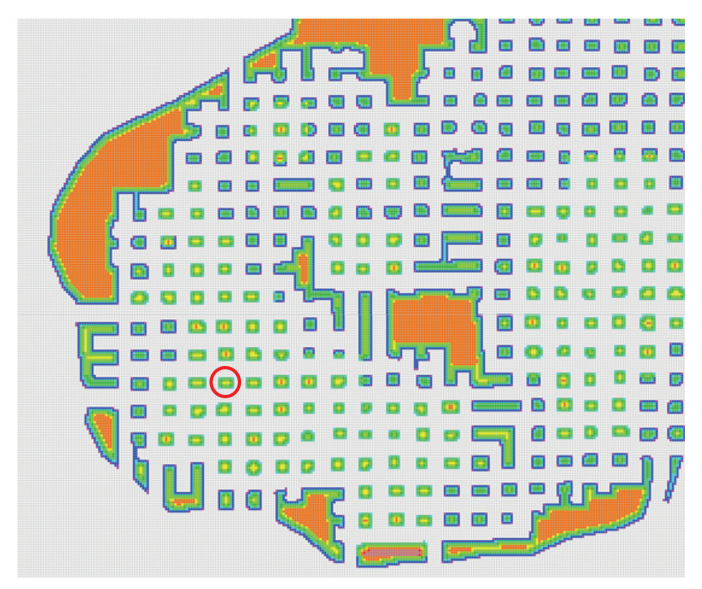


Figure 25: Pillar selected for collapse scenario

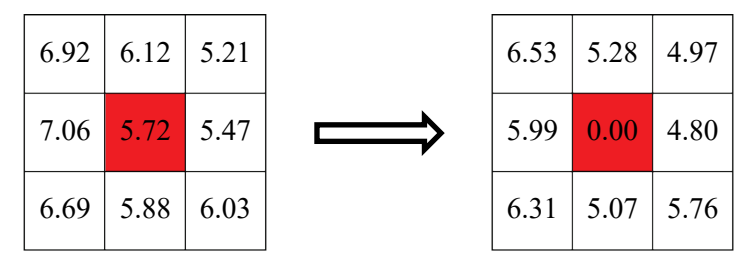


Figure 26: Pillar's SF values before and after simulated collapse

For the second scenario, it was assumed that the benched pillars had reduced widths due to spalling. Referring back to the S-Pillar strength equation, it can be seen that the pillar strength will be reduced by the width reduction to the power of 0.3. The parametric study includes a 10% and 20% reduction in pillar widths, resulting in a 3.1% and 6.48% reduction in pillar strengths, respectively. For a practical implementation of this reduction, the UCS values were adjusted (reduced by 3.1% and 6.48%) and new peak stress and strain values were calculated for the elements.

Assuming LDF = 0.25, the pillars with less than 7.2 safety factor (1.8 if considering LDF) are shown in Figure 27 as expected, some additional pillars fell below the critical safety factor levels, but no stress magnification was observed. The reduction in safety factors was not significantly different from the calculated strength reductions (3.1% and 6.48%).

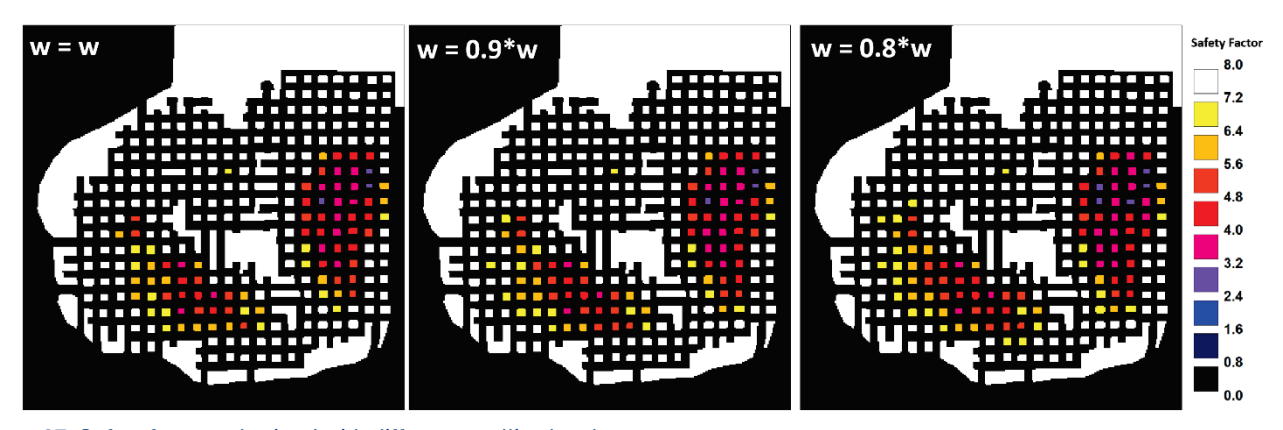


Figure 27: Safety factors obtained with different spalling levels

4.5.2 Case Study 2

The second case study mine is a limestone mine in East Palestine, Ohio, that the project team visited in February and November of 2024. The mine map (Figure 28) and the rock properties have been shared with the project team by the mine. The mine operates in the Vanport limestone seam with a thickness ranging from 16 to 22 feet. Only development mining is used, and the pillars around the study area have a height of around 11 ft. The average overburden depth in the study area is around 200 ft.



Figure 28: Map of the study area for case study 2

The square pillars were 30 ft by 30 ft, and the rectangular pillars were 30 ft by 50 ft, rib-to-rib. The rooms were developed 40 ft wide around the study area. The UCS of the limestone was reported as 17405 psi (120 MPa) and the elastic modulus was 725,189 psi (5 GPa), according to the lab results shared with the team. For the LaModel grid, 2.5 ft elements were used and 13 different materials were generated for one elastic, six corner, and six rib elements. Using these parameters and Eq.1 and Eq.2, the pillar element properties were calculated and are presented in Table 11.

Table 11: Calculated peak strength and strain values for development pillars in case study 2

Element Code		Peak Strength (psi)	Peak Strain (%)
В	Rib	15715.8	2.1671%
С	Corner	15558.5	2.1454%
D	Rib	14797.6	2.0405%
E	Corner	14617.4	2.0157%
F	Rib	13723.0	1.8923%
G	Corner	13508.2	1.8627%
Н	Rib	12405.4	1.7106%
1	Corner	12131.0	1.6728%
J	Rib	10642.8	1.4676%
К	Corner	10234.2	1.4113%
L	Rib	7654.5	1.0555%
М	Corner	6299.6	0.8687%

Figure 29 presents the same information as calculated in StabMap.

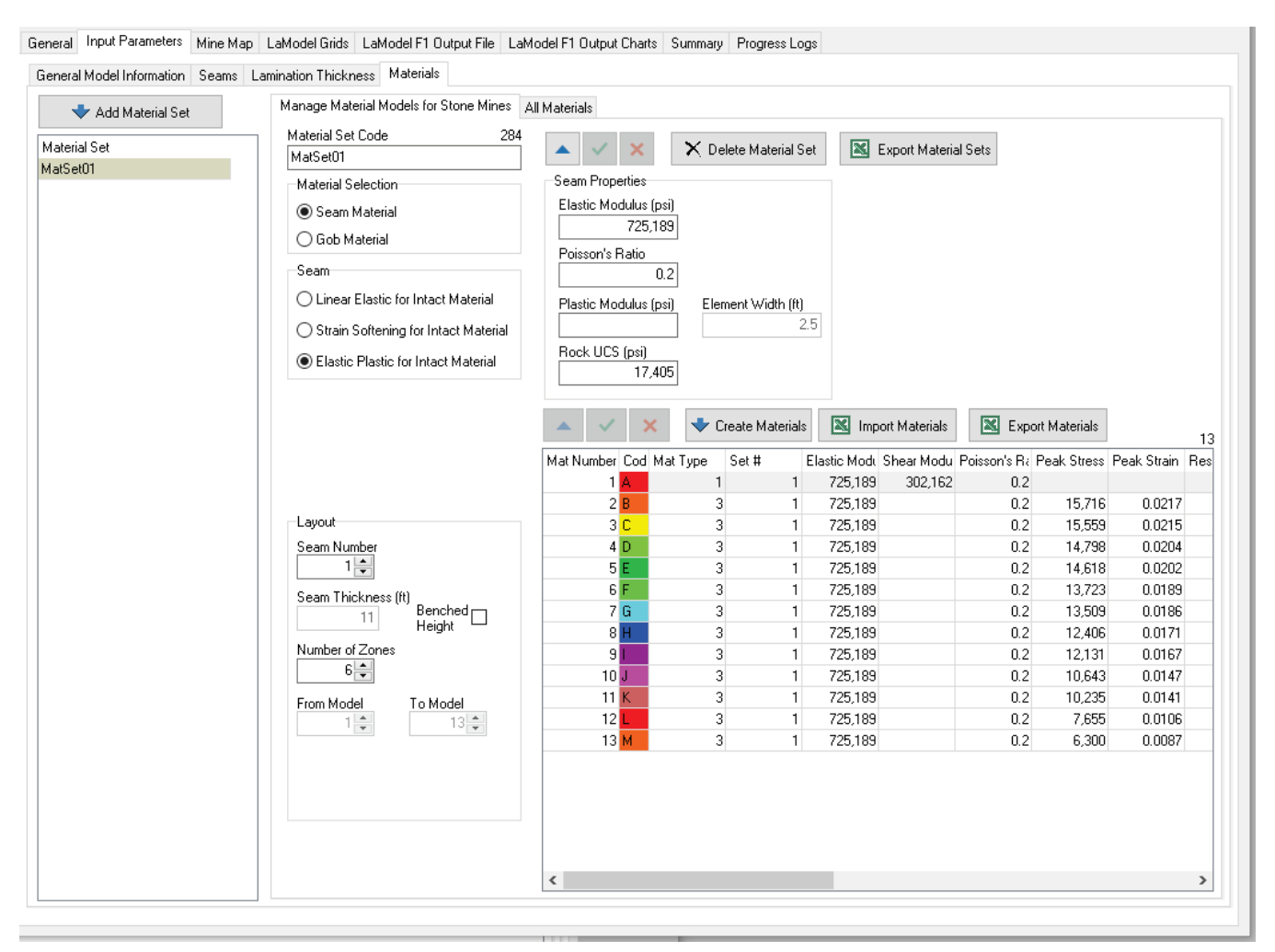


Figure 29: Calculated peak strength and strain values for development pillars in Mine 2 (StabMap)

The results obtained from the LaModel simulation are presented in Figure 30. The lowest safety factor was observed for the small square pillars. The safety factor values for those pillars ranged between 8.9 and 9.2. The same pillar geometries were analyzed using S-Pillar, and the safety factor was calculated as 8.92 (Figure 31).

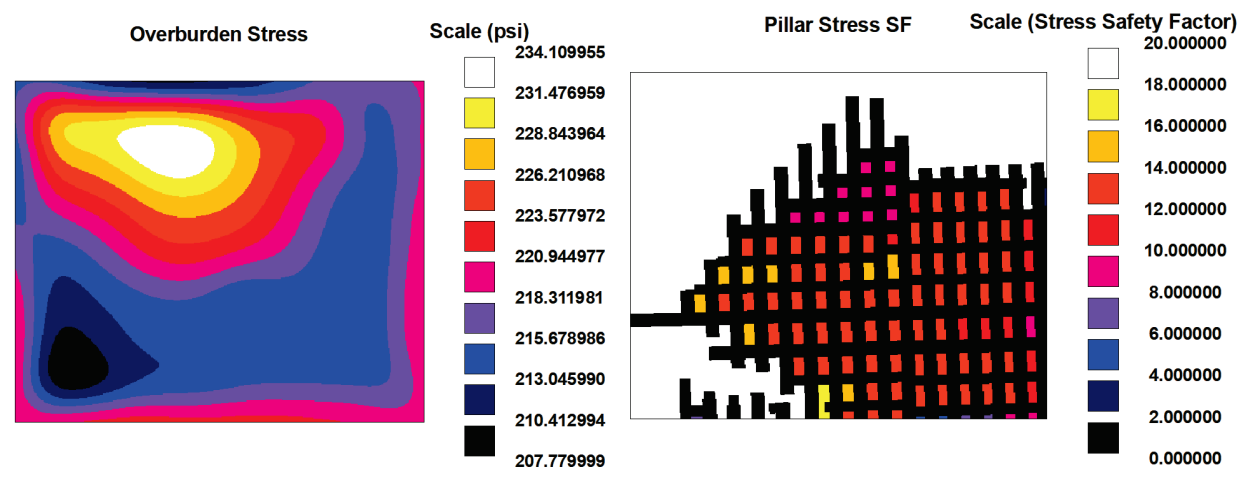


Figure 30: Simulated overburden stress and pillar stress safety factors for case study 2

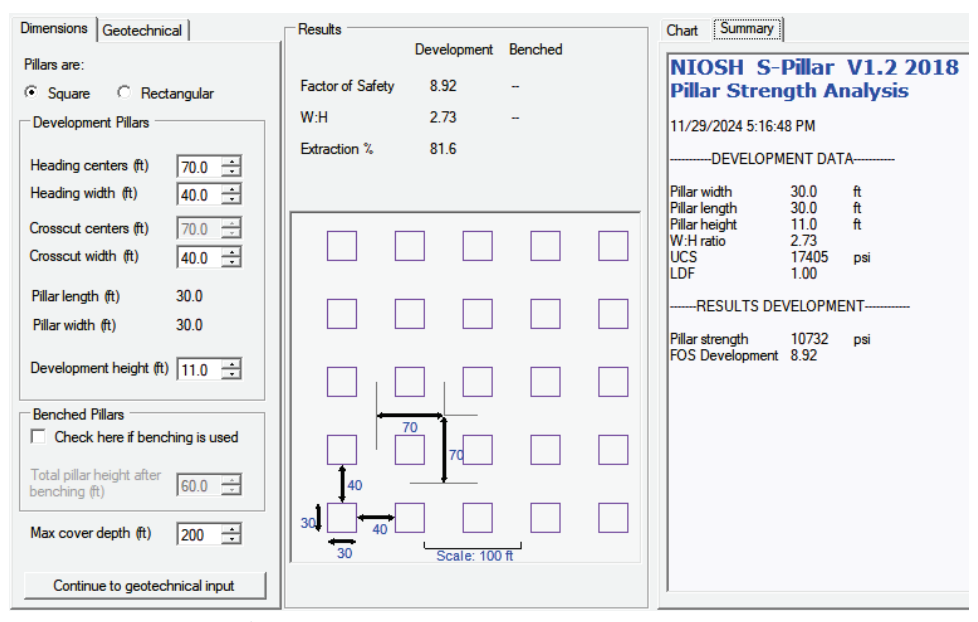


Figure 31: S-Pillar results for case study mine 2

The pillars in Mine 2 were also scanned using handheld LIDAR scanners during both visits, and the point cloud data was analyzed for change detection between the two visits. It was observed that there has been spalling on the pillar ribs, and it was also seen in the point cloud comparison (Figure 32). Even though the pillar safety factors were high enough for stable conditions, the main contributing factor for the spalling was observed as the shale bands running horizontally in the middle of the pillars. The mine has started pushing clay toward the ribs of the pillars, covering the shale band, to contain the spalling and degradation of the shale bands.

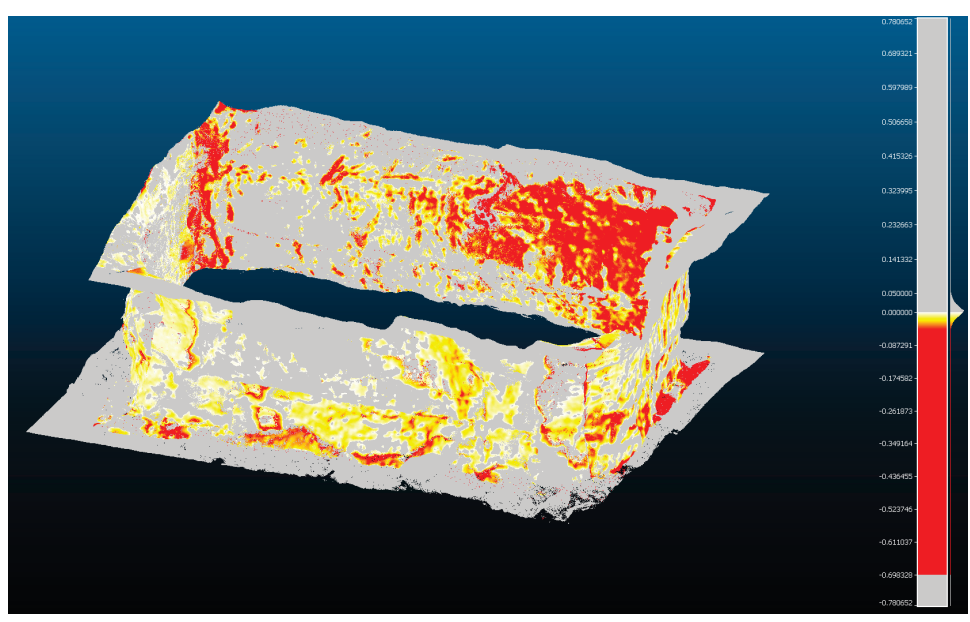


Figure 32: Change detection from two LIDAR scans 9-months apart

4.6 Development of the StabMap Windows Application

The purpose of StabMap is to provide an efficient pre- and post-processor for LaModel that is independent of the AutoCAD package, which allows mine operators to assess both coal and stone mine pillar stability to identify potential hazard zones in the mine. It is designed to be a significant improvement over the current LamPre and LamPlt platforms. In addition to the workflow improvements to existing features, StabMap contains several novel components.

- StabMap is database-driven, meaning all files are saved inside the program. This greatly eases file management and streamlines workflow.
- It combines the functionality of LamPre and the Stability Mapper AutoCAD plugin into a single platform.
- It extends the 2000 x 2000 grid dimension limit in LamPre.
- It allows more than four steps and four seams to be analyzed simultaneously LaModel supports that, but LamPre did not.
- Grids can be easily moved between steps and/or saved for future use.
- Operators may now employ the laminated overburden model in LaModel for stone mine analysis.
- StabMap incorporates the elasto-plastic analysis conducted by Escobar (2021) to generate material properties for both developed and benched stone pillars.
- StabMap includes a self-updating mechanism. When an update becomes available, it will ask the user whether they would like to download and install. All user files are backed up during installation.
- StabMap is installed using an installer package that prompts the user for information regarding the installation process. More information is provided in Appendix B.

Appendix C includes the help manual for the program. Each feature is described in detail.

In addition, four videos were generated and are included as part of the distribution package, which can be downloaded from https://www.minegroundcontrol.com/lamodel/

5 Publication Records and Dissemination Efforts

5.1 Published Papers

- Elibol, A., D. Tuncay, and Z. Agioutantis, Assessing Pillar Stability in Underground Stone Mines: Impact of Geological Structures and Stress Variations in the Appalachian Region, (2024), Proceedings 58th US Rock Mechanics / Geomechanics Symposium (ARMA), 23-26 June 2024, Golden, CO, paper 24- 0578
- Suner, M.C., A. Elibol, R. Jimenez, D. Tuncay, and Z. Agioutantis, (2024), Calibration of LaModel In-Seam Material Properties for Underground Stone Mine Benching Operation by Employing Brittle Failure Criteria in FLAC3D, Proceedings, 43rd International Conference on Ground Control in Mining, July 22-25, Canonsburg, PA.
- Elibol, A., D. Tuncay, Z. Agioutantis, (2025) Using LaModel for Analyzing Stress Distribution in Benched Areas for Possible Massive Stone Pillar Collapse, Proceedings, Ground Control in Mining Industry Seminar, July 25, Beaver, WV.
- Elibol, A., "Enhancing Pillar Stability Assessment in Underground Limestone Mines Using LaModel: Integrating Empirical Strength Equations for Improved Ground Control", (2025), MS Thesis, West Virginia University.

5.2 Planned Papers

 Tuncay D., Z. Agioutantis and B. Diddle, (2026), Application of LaModel for Pillar Stress Analysis in a Moderate-Cover Underground Limestone Mine, 45th Conference on Ground Control

5.3 Past Presentations

- Elibol, A., D. Tuncay, and Z. Agioutantis, (2024), Assessing Pillar Stability in Underground Stone Mines: Impact of Geological Structures and Stress Variations in the Appalachian Region, Proceedings, 58th US Rock Mechanics / Geomechanics Symposium (ARMA), June 23-26, Golden, CO, paper 24-0578.
- Suner, M., A. Elibol, R. Jiminez, D. Tuncay, and Z. Agioutantis, (2024), Calibration of LaModel In-Seam Material Properties for Underground Stone Mine Benching Operation by Employing Brittle Failure Criteria in FLAC3D, Proceedings, 43rd International Conference on Ground Control in Mining, July 22-25, Canonsburg, PA.
- Elibol, A., M. Suner, D. Tuncay, and Z. Agioutantis, (2025), Back-analysis of a Limestone Mine Pillar
 Collapse Using LaModel A Case Study, SME Annual Conference, February 25, Denver, CO.
- Elibol, A., D. Tuncay, and Z. Agioutantis, (2025), Using LaModel for Analyzing Stress Distribution in Benched Areas for Possible Massive Stone Pillar Collapse, Proceedings, Ground Control in Mining Industry Seminar, July 25, Beaver, WV.

5.4 Upcoming Presentations

 Agioutantis, Z., (2025), Stability Mapping Platform for Stone Pillar Analysis, Kentucky Underground Stone Safety Seminar, December 10, Louisville, KY (oral presentation).

Conditions,	SME Annual Co	nference, Febr	uary 24, Denve	er, CO (abstrac	t and oral pre	sentatior

 $\circ \quad \mathsf{Diddle}, \mathsf{B}. \, \mathsf{and} \, \mathsf{Z}. \, \mathsf{Agioutantis}, (2026), \mathsf{Using} \, \mathsf{the} \, \mathsf{Updated} \, \mathsf{Stability} \, \mathsf{Mapper} \, \mathsf{Program} \, \mathsf{to} \, \mathsf{Improve} \, \mathsf{Ground}$

6 Conclusions and Impact Assessment

The main objectives of this project were (a) to determine the validity of utilizing the LaModel program, which works on a plan view of an actual pillar system, as a stone mine design tool instead of the simple approach offered by the S-Pillar program and (b) to develop a front end to LaModel that would incorporate the above methodology so that the stone mine scenarios could be easily prepared and fed into the LaModel program. It should be noted that, in recent years, utilizing LaModel for evaluating pillar ability in underground stone mines has also been addressed by different researchers, as LaModel is much simpler than complicated 3D modeling packages such as FLAC3D.

With respect to the first objective mentioned above, this work built on the thesis by Escobar (2021), which outlines a way to calculate progressively weaker elastoplastic parameters for different zone layers in a pillar. This work also demonstrated that, with LIDAR scanning technology, pillar dimensions can be precisely mapped and used for LaModel seam gridding. This technology is especially useful for areas not easily accessible, where autonomous vehicles (drones, rovers, etc.) equipped with various sensors can be utilized.

Further to that, models in FLAC3D were developed and compared to LaModel output as well as S-Pillar reports. The comparative analysis concluded that LaModel can actually be used to model development as well as benched areas in an underground stone mine.

This research also highlighted that lower lamination thickness values in LaModel led to reduced safety factors due to less stiff overburden and increased convergence. The overall study confirmed the feasibility of using LaModel for stability evaluation in limestone mines when properly calibrated with empirical stone pillar strength equations, providing a framework for analyzing stress changes during bench mining and enhancing safety. While S-Pillar remains a very useful tool for estimating pillar strength under tributary area conditions, LaModel can be successfully utilized to model irregular pillar geometries and variable overburden depth. Therefore, LaModel can be used instead of or in combination with S-Pillar to access the stability of underground stone mines.

With respect to the second objective mentioned above, a brand new database-driven software platform was developed, which can be used to create the necessary material models for development and benched pillars.

The new platform complements the LamPRE functions for coal pillars by allowing stone seams to be defined with multiple extraction heights. Currently, the program only supports one development and one benched level. This will be expanded in the near future to two and three bench level operations.

In addition to that, the new platform allows for CAD files to be imported and processed so that a mine plan can be broken down into square elements for input into the model program. This feature actually provides an alternative to the existing stability mapper plug-in for AutoCAD, which is version-dependent and needs to be updated every couple of years.

To provide a complete working environment, the coal pillar zoning was also implemented into this new stability platform. The user can select either coal or stone mine analysis when creating a new scenario and the program will provide the relevant interface for material generation.

With respect to its impact on the coal and stone mining industry, it is envisioned that most consultants and mine operators who routinely evaluate stone and/or coal pillar stability will eventually embrace the new platform. The MSHA Technical Support Branch has already approved the program for installation on their computers. The program is provided as a free tool and can be downloaded from this URL: https://www.minegroundcontrol.com/lamodel/

Although the platform has been fully tested through internal and external testing, it is projected that additional releases will be made available to the public when issues are submitted to the developer team. The auto update mechanism built into the installer will allow a seamless update of existing installations without any loss of data.

7 Recommendations for Future Work

The conclusions of this work lead to several recommendations for future work. One avenue is the enhancement of the methodology with regard to multi-seam mining operations in LaModel Software. Having knowledge of pillar performance through different levels of mining and within various geological layers would be extremely useful and help enhance empirical and numerical design methodologies.

Another important area for future investigation is the refinement of the lamination thickness input within LaModel when applied to stone mining conditions. While LaModel was originally developed for coal mining and uses lamination thickness as a key input to simulate overburden stiffness, the default assumptions and equations were tailored to coal seam behavior. In this research, a fixed lamination thickness value was used to reflect average geological layering; however, no standardized method currently exists to calibrate lamination thickness specifically for limestone formations. Therefore, future studies can focus on developing limestone-specific empirical relationships or calibration protocols for lamination thickness input. A new implication would be to adapt or derive an equation for lamination thickness estimation tailored for underground limestone mining, improving model accuracy and risk prediction.

8 References

- Ates, M. (2022), "Integrated Large Discontinuity Factor, Lamodel and Stability Mapping Approach for Stone Mine Pillar Stability", MS thesis, West Virginia University, https://researchrepository.wvu.edu/etd/11397
- Bendezu de la Cruz, Mario Alejandro, (2021) Evaluation of LIDAR systems for rock mass discontinuity identification in underground stone mines from 3D point cloud data. MS thesis, West Virginia University, https://researchrepository.wvu.edu/etd/10243
- Bishop, R. (2022), "Applications and Development of Intelligent UAVs for the Resource Industries, Virginia Tech, 2022. https://vtechworks.lib.vt.edu/10919/109724
- Dolinar, D. R. and Esterhuizen, G. S. (2007). Evaluation of the effects of length on strength of slender pillars in limestone mines using numerical modeling. Proceedings, 26th International Conference on Ground Control in Mining. West Virginia University, Morgantown, WV, pp. 304–313.
- Escobar, S., and B. Tulu. (2021) "Calculating Stone Mine Pillar Concentric Ring Zone Capacities for Boundary Element Modeling." Proceedings, 55th U.S. Rock Mechanics/Geomechanics Symposium, June, paper ARMA-2021-2001.
- Escobar, S., "Implementing the Empirical Stone Mine Pillar Strength Equation into the Boundary Element Method Software LaModel" (2021). MS thesis, West Virginia University, https://researchrepository.wvu.edu/etd/10273
- Esterhuizen, G. S., Dolinar, D. R., Ellenberger, J. L., & Prosser, L. J. (2011). Pillar and roof span design guidelines for underground stone mines. Pittsburgh, PA: U. S. Department of Health and Human Services, Public Health Service, Centers for Disease Control and Prevention, National Institute for Occupational Safety and Health, DHHS (NIOSH).
- Esterhuizen, G.S., Tyrna, P.L. & Murphy, M.M. (2019) A Case Study of the Collapse of Slender Pillars Affected by Through-Going Discontinuities at a Limestone Mine in Pennsylvania. Rock Mech Rock Eng 52, 4941–4952.
- Galvin, J. M., Hebblewhite, B. K. and Salamon M. D. G. (1999). University of New South Wales coal pillar strength determinations for Australian and South African mining 129 conditions. Proceedings, 2nd International Workshop on Coal Pillar Mechanics and Design. Pittsburgh, PA: U.S. Publication No. 99-114, IC 9448, pp. 63-71.
- Heasley, K. A. (1998). Numerical Modeling of Coal Mines with a Laminated Displacement-Discontinuity Code. Ph.D. Dissertation. Colorado School of Mines.
- Heasley, K.A. Chekan, G.J. (1998). Practical Stress Modeling for Mine Planning. Proceedings, 17th International Conference on Ground Control in Mining.
- Heasley, K., Sears, M., Tulu, I., Calderon-Artega, C., & Jimison II, L. (2010). Calibrating the LaModel program for deep cover pillar retreat coal mining. Proceedings, 3rd International Workshop on Coal Pillar Mechanics and Design, Morgantown, WV, pp. 47-57.
- Iannacchione, A., Prosser, L., Esterhuizen, G., & Bajpayee, T. (2007). Technique to assess hazards in underground stone mines: the roof-fall-risk index (RFRI). Mining Engineering, 49-57.
- Johnson, J., Whyatt, J., & Loken, M. (2014). A generalized method for calculating pillar cell capacities for boundary element modeling of coal mines. 2014 SME Annual Meeting, (p. 15). Englewood, CO.

- Mark, C. (1992). Analysis of Longwall Pillar Stability (ALPS): An update. Proceedings of the Workshop on Coal Pillar Mechanics and Design (pp. 238-249). U.S. Bureau of Mines.
- Mark C, Gadde MM. (2008), Global trends in coal mine horizontal stress measurements. Proceedings, 27th Int. Conf. Gr. Control Min., Morgantown, WV: West Virginia University; 2008, p. 319–331.
- Mark, C., Iannacchione, A. T. (1992). Coal pillar mechanics: theoretical models and field measurements compared. Proceedings, Workshop on Coal Pillar Mechanics and Design. Pittsburgh, PA: US Department of the Interior, Bureau of Mines, IC (Vol. 9315, pp. 78-93).
- Mark, C., Agioutantis, Z. (2019) Analysis of Coal Pillar Stability (ACPS): A new generation of pillar design software, International Journal of Mining Science and Technology, 2019, Vol. 29, Issue 1, January, pp. 87-91, https://dx.doi.org/10.1016/j.ijmst.2018.11.007
- Mark, C., Stephan, R., Agioutantis Z. (2020), Analysis of Mine Roof Support (AMRS) for US Coal Mines, Mining, Metallurgy & Exploration, 37, (2020),1899–1910, https://dx.doi.org/10.1007/s42461-020-00301-x
- Mark, C., Chase, F. E. (1997). Analysis of retreat mining pillar stability (ARMPS). In C. Mark & R. J. Tuchman (Eds.), Proceedings: New Technology for Ground Control in Retreat Mining NIOSH Information Circular 9446, pp. 17–34.
- MSHA (2016). Mine Data Retrieval System (Accident Injuries Data Set). Retrieved from Mine Safety and Health Administration (MSHA): https://www.msha.gov/mine-data-retrieval-system (accessed June 25, 2022)
- MSHA (2020). Roof Control Plan and Ground Support Review Procedures: https://arlweb.msha.gov/READROOM/HANDBOOK/PH20-V-2.pdf (accessed June 25, 2022)
- Nandula, A., Heasley, K.A., Tulu, I.B. (2018), "An Area Calculations of the ARBS Support Intensity." Proceedings, 37th International Conference on Ground Control in Mining, Morgantown, WV, July.
- National Institute for Occupational Safety and Health. (2021). Number and percentage of nonfatal lost-time injuries by accident class at underground mining locations, stone operators, 2011 2019.
 Retrieved from https://wwwn.cdc.gov/NIOSH-Mining/MMWC/Injuries/Count?StartYear=2011&EndYear=2019&SelectedMineType=1&SelectedCommodity=4 (accessed June 25, 2022)
- National Institute for Occupational Safety and Health. (2021). Number and percentage of occupational fatalities by accident class at underground mining locations, stone operators, 2011 2019 (N=5).
 Retrieved from https://wwwn.cdc.gov/NIOSH-Mining/MMWC/Fatality/Count?StartYear=2011&EndYear=2019&SelectedMineType=1&SelectedCommodity=4 (accessed June 25, 2022)
- National Institute for Occupational Safety and Health. (2021, 5 20). Number of active underground stone mines by year, 2000 - 2019. Retrieved from https://wwwn.cdc.gov/NIOSH-Mining/MMWC/Mine?StartYear=2000&EndYear=2019&SelectedMineType=1&SelectedCommodity=4#
- National Institute for Occupational Safety and Health. (2021, 5 20). Surface mine operator and independent contractor employees by sector, 2000 - 2019. Retrieved from https://wwwn.cdc.gov/NIOSH-
 - Mining/MMWC/Employee/Count?StartYear=2000&EndYear=2019&SelectedMineType=0#

- Süner, M C, (2021), The Effect of Natural Fractures on the Mechanical Behavior of Limestone Pillars: A Synthetic Rock Mass Approach Application. MS Thesis, West Virginia University, https://researchrepository.wvu.edu/etd/8254
- Wagner, H. (1992). Pillar design in South African collieries. In Proceedings of the workshop on coal pillar mechanics and design. U.S. Bureau of Mines. Report IC 9315, pp. 283-301.

9 Appendix A: Stone Mine Literature Review

In this task, field data collected by VT and WVU teams were processed to extract the datasets of parameters that were used to generate parameter grids in the statistical analysis and the development of the design guidelines. There are five companies that openly supported the autonomous UAV and robotic system inspections proposal by WVU and VT by providing mine access: Argos USA, Carmeuse Americas, Lhoist North America, Vulcan Materials, and Nyrstar. During the mine visits, the following data was collected for use in this project:

3D point cloud data from LIDAR and/or photogrammetry scans: There were two different point cloud data sets available for the autonomous robotic scans. The first set was lower resolution LIDAR data collected by a Unmanned Aerial Vehicle (UAV) using autonomous navigation (Figure 33 - Left). This lower resolution data was used to compute the dimensions of the surveyed rooms and pillars (Figure 33 - Middle), roof spans, and bolting patterns (Figure 33 - Right).

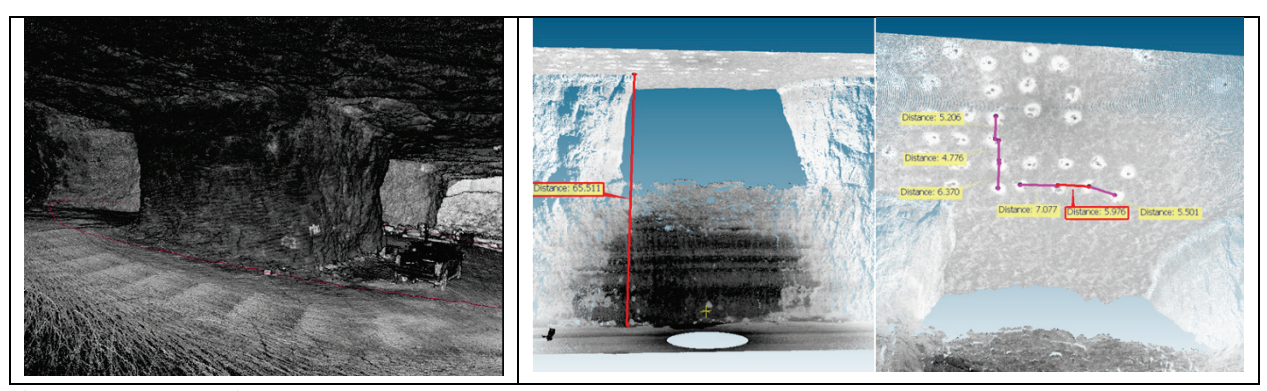


Figure 33: Low resolution LIDAR data.

The second set of point cloud data was a high-resolution data set as shown in Figure 34 and Figure 35. This data was used to evaluate the rock mass by extracting the discontinuity sets on the roof and pillar. The following information was gathered from the field surveys: orientation, spacing, persistence, roughness, aperture or filling (if applicable) of the discontinuities, and number of discontinuity sets. During the field visits, if water flow or free moisture was visible, this information was noted separately. In this study, since the full three-dimensional view of the rooms and pillars was available, 2D and/or 3D (number of fractures in an area or volume) discontinuity measures were used to characterize the rock mass of the formation. In addition to the underground surveys, high-resolution point cloud data of the outcrops was available from the UAV surveys.

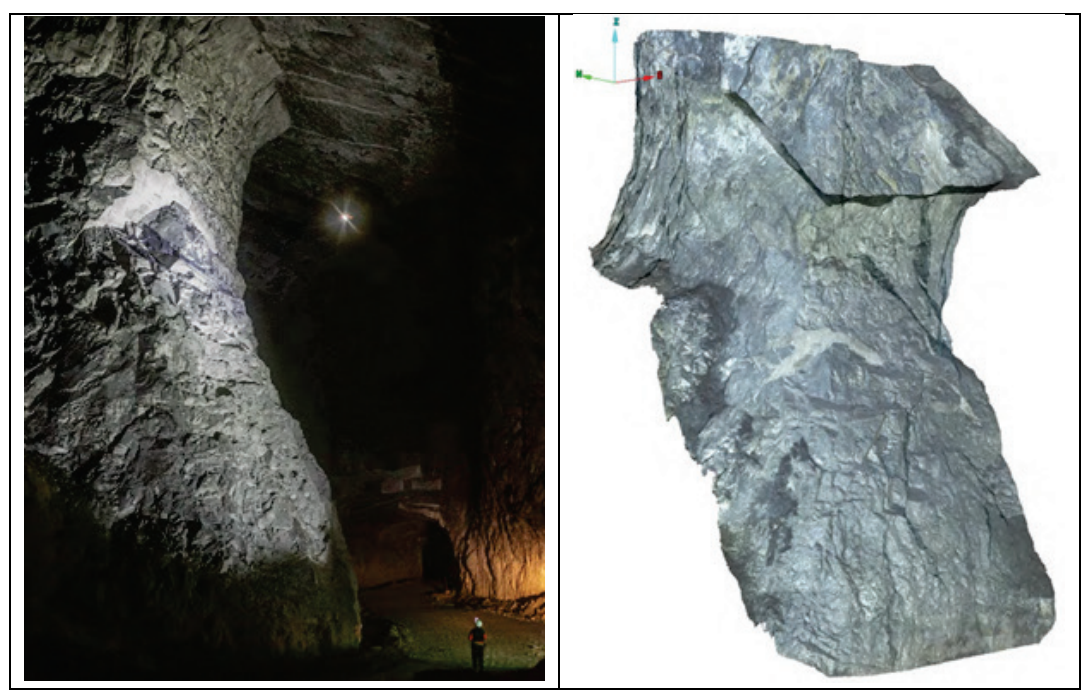


Figure 34: High resolution point cloud data of a pillar (after Bishop, 2022).

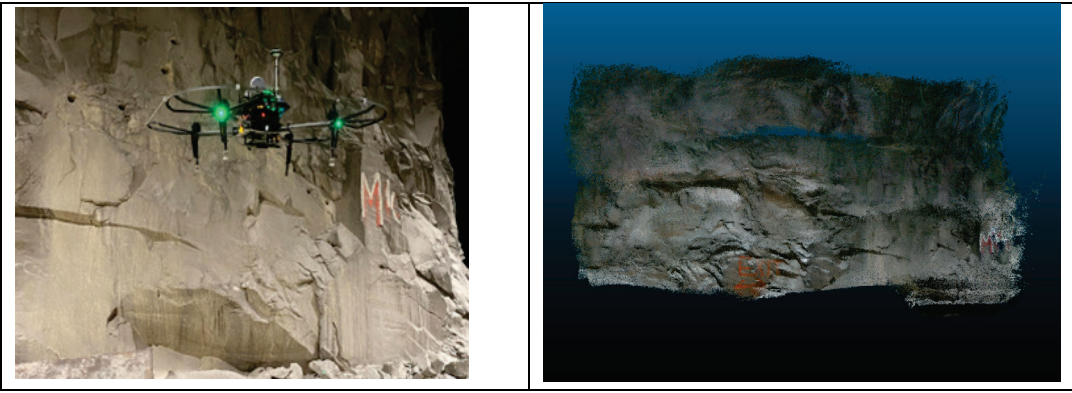


Figure 35: High resolution point cloud data of a pillar wall (after Bendezu, 2021).

Intact rock mechanical properties: From each mine, in addition to the point-cloud data, rock samples were collected and tested to characterize the intact rock properties. Therefore, the mechanical properties of the intact rock portion of the rock mass were identified for each mine.

Roof profile, pillar and room condition: From low resolution 3D maps, the research team qualitatively rated the conditions of the pillars, rooms, and entry roof. For pillar condition assessment, the rating system proposed by Esterhuizen et al. (2011) for stress and geological setting was used (Figure 36). Roof profile was rated as proposed by lannacchione et al. (2007): smooth, intermediate, or rough. Any significant rock debris on the floor was easily visible from the low-resolution 3D maps and was rated as proposed by lannacchione et al. (2007): none, slight, moderate, or significant.

Operational and design parameters: Mine pillar layout (CAD file), seam elevation, topographic elevation (CAD file), and other operational parameters were available from each mine.

Support practices and thickness of the roof beam: MSHA Handbook Number PH20–V–2, Roof Control Plan and Ground Support Review Procedures, states that inspection personnel may use the guidelines and procedures in the PH20–V–2 handbook to evaluate the suitability of ground support materials and rock burst control plan, but unless a mine is burst-prone, there are no federal regulations stating that M/NM mines have to submit a ground support plan (MSHA, 2020). Pillar and roof span dimensions and roof bolt application in the M/NM mines are largely based on experience, developed through trial and error. Therefore, during the field visits, mine personnel were interviewed for the application of the roof bolts. From the low resolution 3D maps (Figure 33 - Right), where roof bolts were applied within the mine were easily seen. The research team noted the reason for roof bolt application (i.e., weak immediate roof, discontinuity, or low roof beam thickness) and thickness of the roof beam. Core hole data can also give this information, however, in these mines core holes were generally widely spaced and it was difficult to observe any changes in roof beam thickness between working faces.

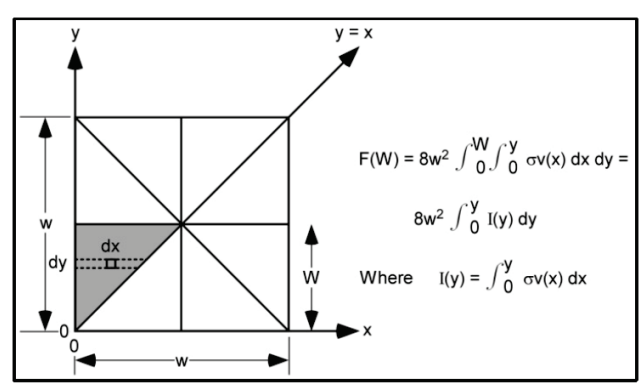
Horizontal stress related data: Regional horizontal stress directions was estimated from the publication of Mark and Gadde (2008). Direction of the horizontal stress was also be verified, if applicable, from the stress mapping. High resolution 3D maps allowed the mapping of the horizontal stress related damages (i.e., roof cutters) from the point cloud data. Direction of the horizontal stress with respect to mine plan was gathered from the survey data.

Pillar Stress Rating		Geolog	Geological Structure Rating				
Rating	Sketch	Description					
1	- aucorau	No stress related fracturing or	Rating	Sketch	Description		
None		spalling observed. Joint or blast related damage may exist.	1		Less than 0.3 m (1 ft) of joint related fallout during blasting.		
2	- Variable	Minor slabs or spalling, fractures through intact rock at corners,	None		Blast damage may exist.		
Minor	7.36	pillar corners and walls may be concave, does not typically deteriorate after initial mining and scaling.	2 Minor	7, 101	Pillar shape affected by 0.3- 1 m (1-3 ft). Some joint or bedding fallout during blasting, may form step at bedding planes. No or little		
3 Moderate	Juga	Slabbing, onion-skin, fractures more than 1m long, joints opened, corner damage, pillars may need re-scaling after initial development. Original square pillar shape maintained.			further fallout after initial scaling.		
	B. J.		3 Moderate	41.11	Pillar shape affected by 1-3 m (3- 10 ft). Joint or bedding controlled fallout. Fallout can continue after initial mining and scaling.		
4 Severe	Haih Haih	Spalling to hourglass shape. Open cracks in pillar more than Im long, debris around pillar, original square shape of pillar no longer visible, saw tooth slabs on ribs	4 Severe		Large block fallout >3 m (>10 ft). Pillar shape compromised by large block extrusion or block sliding on steep plane. Falls continue after initial mining and scaling.		
5 Very Severe	2500 mm	Formation of large open cracks, extreme hourglass. Pillar likely lost most of its residual strength.	5 Very Severe	3	Pillar bisected by through-going structure dipping at more than 35 degrees. Potential or actual loss of top half of pillar. Pillar strength depends on discontinuity strength.		

Figure 36: Pillar stress and geological ratings (after Esterhuizen et al. 2011).

Escobar and Tulu (2021) derived the gradient stress equation for stone mine pillars and the function of pillar width-to-height ratio from the empirically-based S-Pillar strength equation to extend the application of the

S-Pillar stone pillar strength equation to Boundary Element Method (BEM), LaModel. The integration of the empirical stone pillar strength equation in LaModel allows the empirical pillar stability analysis to be extended over complex mine geometries and variable topography. Escobar (2021) used approaches proposed by Mark et al. (1992) and Johnson et al. (2014) to derive stress gradient equations for rib and corner elements. Initially, Johnson et al. (2014) used four general assumptions to obtain the gradient stress equations that make this methodology valid for deriving gradient stress equations from empirical strength formulas: (i) The derivation of gradient stress equations is performed on square pillars. (ii) When the overall pillar strength reaches its maximum, all the "portions" of the pillar are at maximum strength. (iii) The variation of stress is a function of the distance to the nearest rib and is not dependent on the width of the pillar (Mark et al., 1992). (iv) The square pillar is divided into 8 symmetric pieces to simplify the calculations that relate the stress function to the failure force, which is a function of its width. Figure 37 shows their approach.



Variables are defined are follows:

Pillar half-width = W (Figure 4)
Pillar width = w = 2W
Pillar height = h

Total vertical force applied to pillar = F
Pillar load capacity = R
Strength coefficient = σ_0 Average pillar strength = σ_P Horizontal location within pillar = x
Local strength = $\sigma_v(x)$ Pillar rib at x = 0
Pillar centerline at x = W

Figure 37: Pillar stress and geological ratings (after Johnson et al., 2014).

It was proposed to expand the application of the Johnson et al. method to derive the stress gradient equations of the semi-benched pillars (Figure 38). The last assumption of the work by Johnson et al. was be replaced with "the square pillar which will be divided into 8 pieces (not necessarily symmetric depending on benching stage) and failure force will be applied as a function of its width and height." Therefore, the following general equation was used in the calculations where vertices of each triangular piece were used to linearly interpolate vertical height (z) within the pillar:

$$\frac{F(W,h)}{W^2} = \sum_{i=1}^{8} \int_0^h \int_0^w \int_0^y \sigma v(x) \, dx dy dz$$
 (Eq. 1)

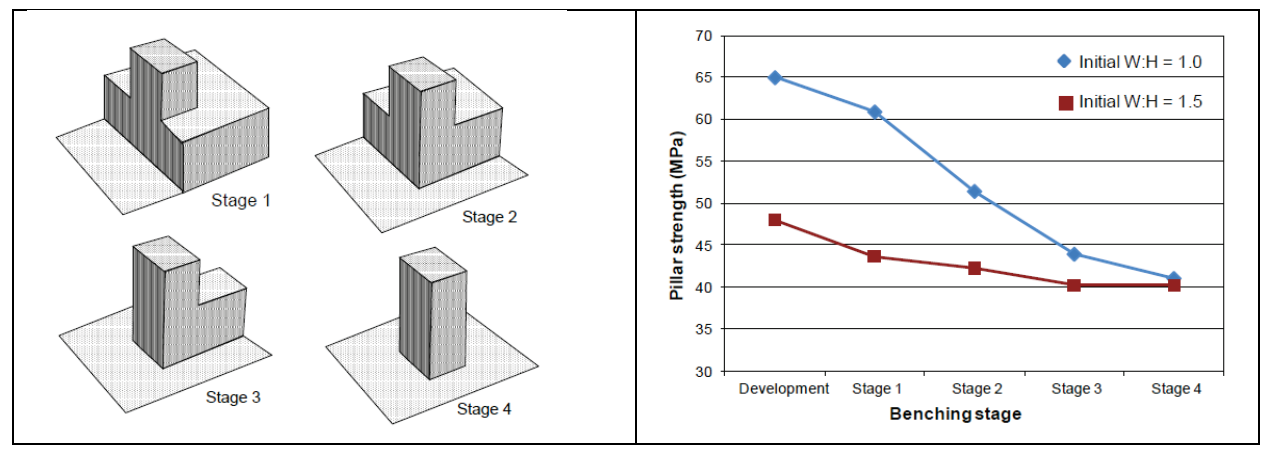


Figure 38: Benching stages and pillar strength (after Esterhuizen et al., 2011).

Since the response of the overburden strata in LaModel is the function of the seam convergence, and seam elements are one-dimensional spring elements, Escobar (2021) simulated the benched pillars with a reduced stiffness to simulate the stress distribution between the benched and development pillars realistically, such that benched pillars in the lower areas of the mine have higher stresses with reduced stiffness. This application also increased the stresses on the parameter pillars as observed in the field (Figure 39). As shown in Figure 3a, some of the recent pillar failures occurred when benching was in progress nearby the collapsed area. Therefore, accurate calculation of the stresses in stone mines is critical.

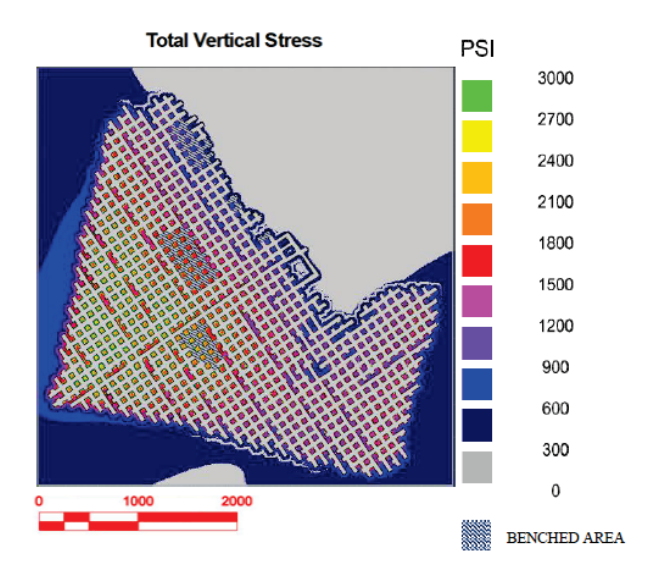


Figure 39: Total vertical stress with reduced stiffness in benched pillars (after, Escobar, 2021).

In this approach, it was proposed to use the stress mapping approach use by Heasley (1998) for calibrating the model inputs in multiple seam coal mining operations. Heasley maps the stress damage on the ribs and overlays the vertical stress grid on the rib condition rating grid to evaluate total stress distribution on the pillar system and if necessary, calibrate the lamination thickness parameter. For the stone mining

operations, a similar approach was proposed. In stone mines however, pillar or rib conditions are greatly influenced by the discontinuities. Since the field data used in this project allowed the project team to characterize the geological structures on each surveyed pillar, it was determined whether the damage on the pillar is attributed to stress or geology. Then a similar comparison and calibration was performed as proposed by Heasley (1998).

Laboratory test and discontinuity data were used to compute the rock mass rating of the formation. Suner (2021) demonstrated that stone mine rock masses, within the range of the S-Pillar database, can be represented as blocky (Figure 40). In Figure 40, the yellow area represents the range of GSI values of the stone mines in the S-Pillar database. For each case study mine, rock mass rating values were computed for each surveyed pillar. GSI rating of each pillar was used as an interpolation point and used to generate the GSI grid file. This approach was already included in the Integrated Stability Mapping software (Nandula et al., 2018) for Coal Mine Roof Rating (Figure 41). Similar to CMRR, a GSI grid was developed in this project.

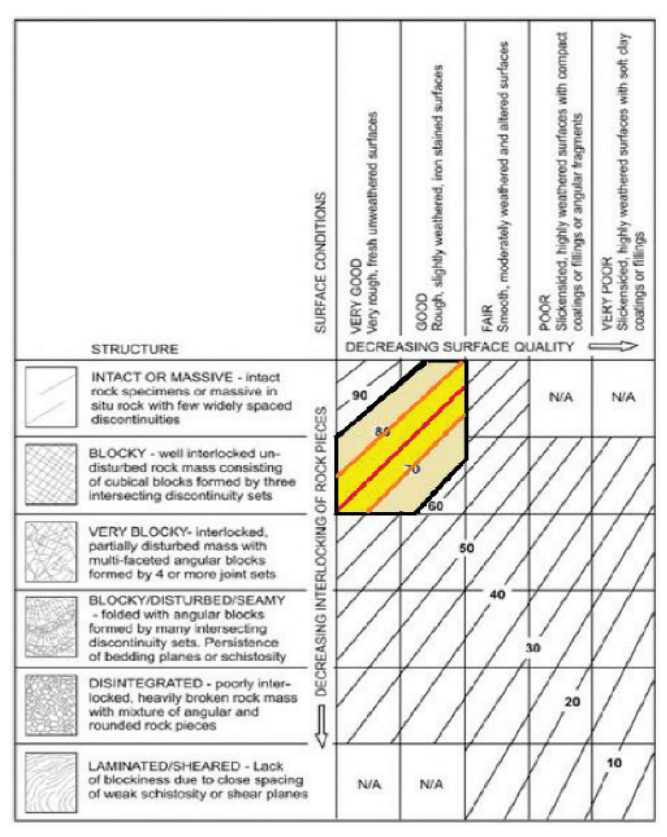


Figure 40: S-Pillar Database GSI Representation.

In addition to the GSI grid, large discontinuity sets that would affect the pillar and roof stability were gridded to a discontinuity factor grid. Ates (2022) demonstrated the application of this approach to pillar stability by finding the intersection of the large discontinuity set with pillars on a mine layout and reducing the load-bearing capacity of the pillar with a discontinuity factor (Figure 42). In this project, we applied the same approach for the entry and intersection roof spans.

The stress and safety factor analyses were performed using the mine plan, topography map, and operational parameters collected from the mine. LaModel and methods published by Escobar (2021) and Ates (2022), and the new methods that were developed were used during the analysis. A horizontal stress grid was developed by generating a pseudo-depth grid as demonstrated by Nandula et al., (2018) and using the equations proposed by Mark and Gadde (2008).

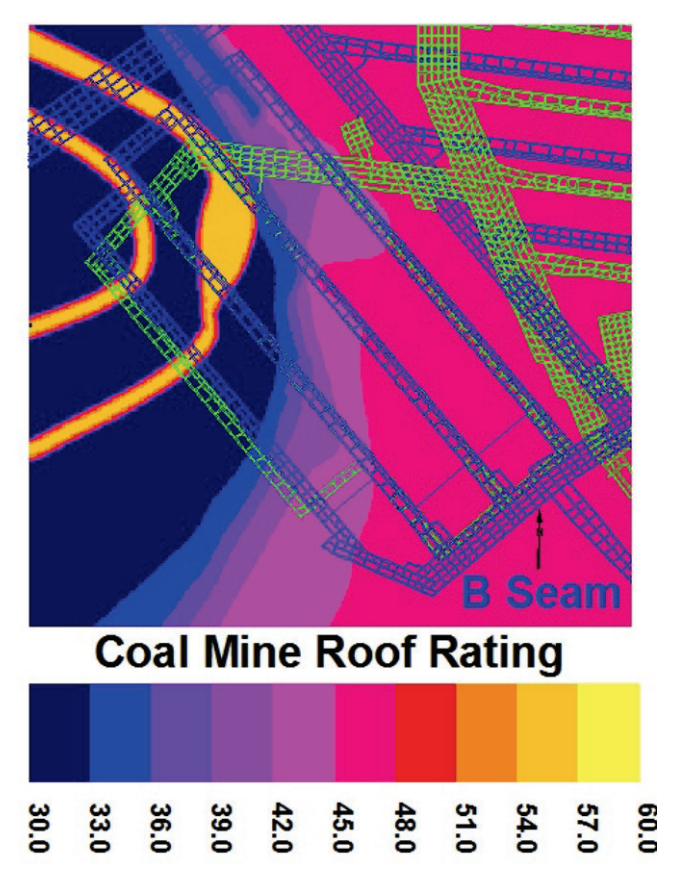


Figure 41: CMRR application with stability mapping software.

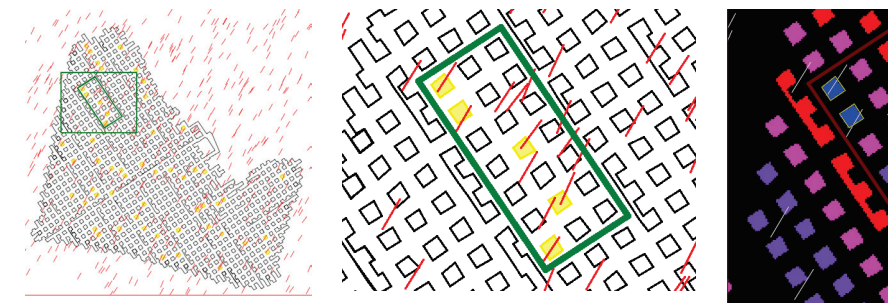


Figure 42: Application of the local large discontinuity factor.

Like the Analysis of Mine Roof Support (AMRS) approach (Mark et al., 2020), primary roof support rating (PSUP) for the bolted sections was computed. This rating was converted to the grid file using an approach like Ates (2022) applied for the pillars. In his approach, Ates assigned a discontinuity factor to the pillars by using the step function method of the stability mapping software. A similar approach was used to assign a PSUP rating to the bolted entry and intersection spans.

In addition, entry and intersection roof parameters (dimensions, GSI rating, roof beam thickness), stress parameters (overburden stress grid, horizontal stress grid, pillar safety factor grid), rock mass strength parameters (GSI grid), roof support parameters (PSUP grid), and large discontinuity distribution grid were overlaid on the mine layout and compared with the roof, rib, and pillar condition ratings. For each case study mine, the mine layout was divided into sub-sections (Figure 43). Relationships between the dependent parameters (condition ratings) and independent parameters were derived using the logistic regression analysis by finding the separation between different condition ratings to derive the hazard index.

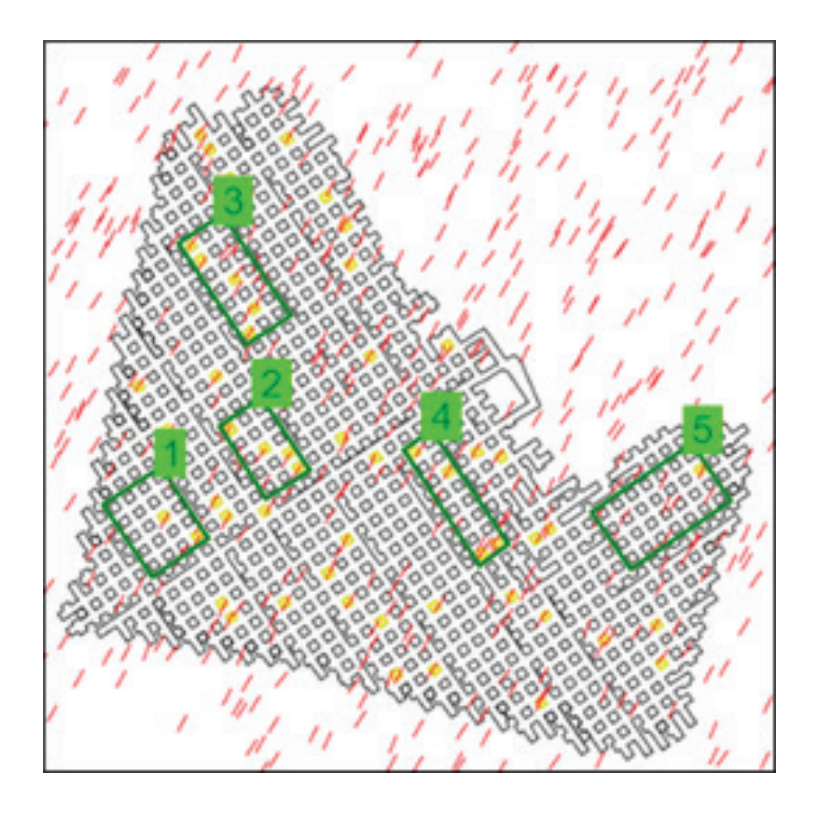


Figure 43: Mine layout is divided in sub-sections.

10 Appendix B: Stabmap Installation

The following screenshots display the installation process.

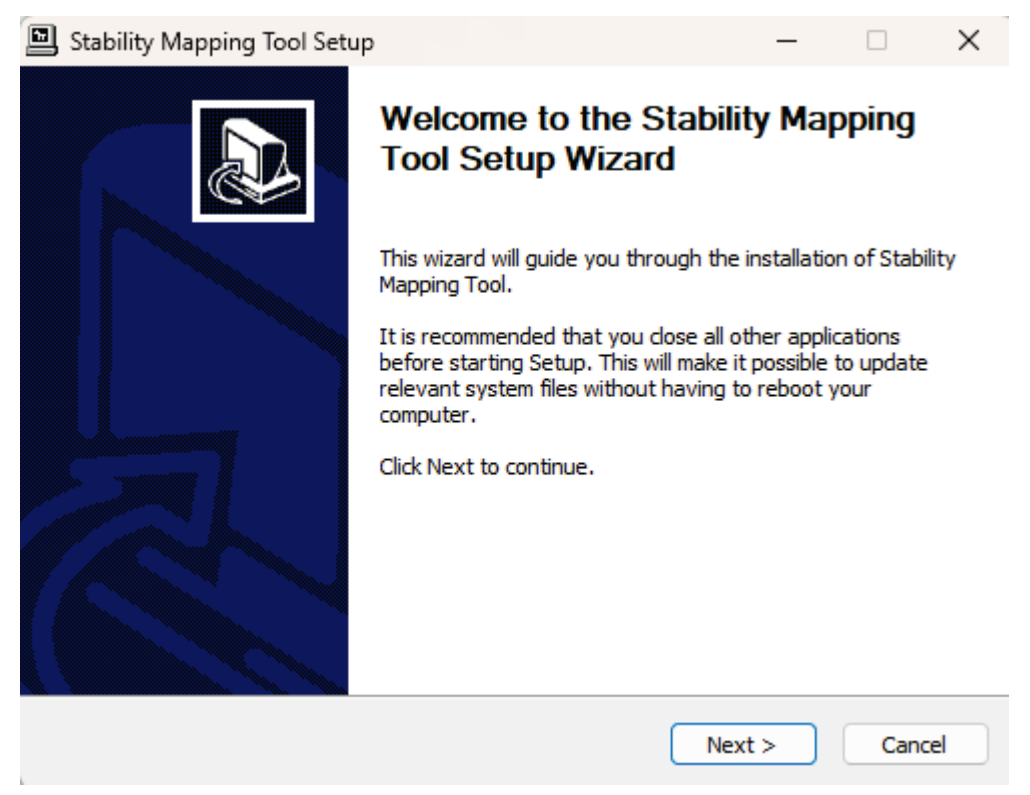


Figure 44: StabMap Setup Wizard

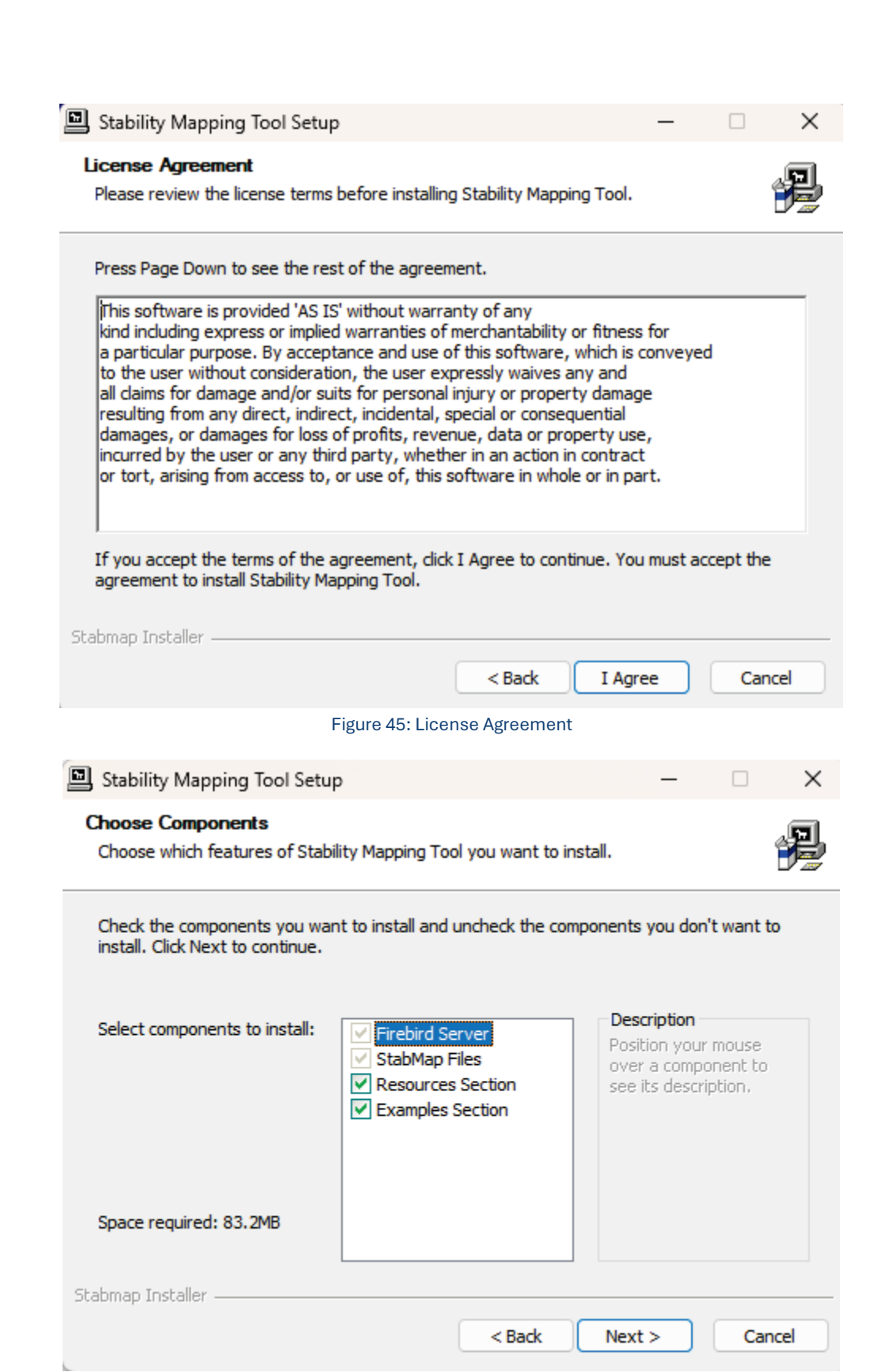


Figure 46: Component Selection

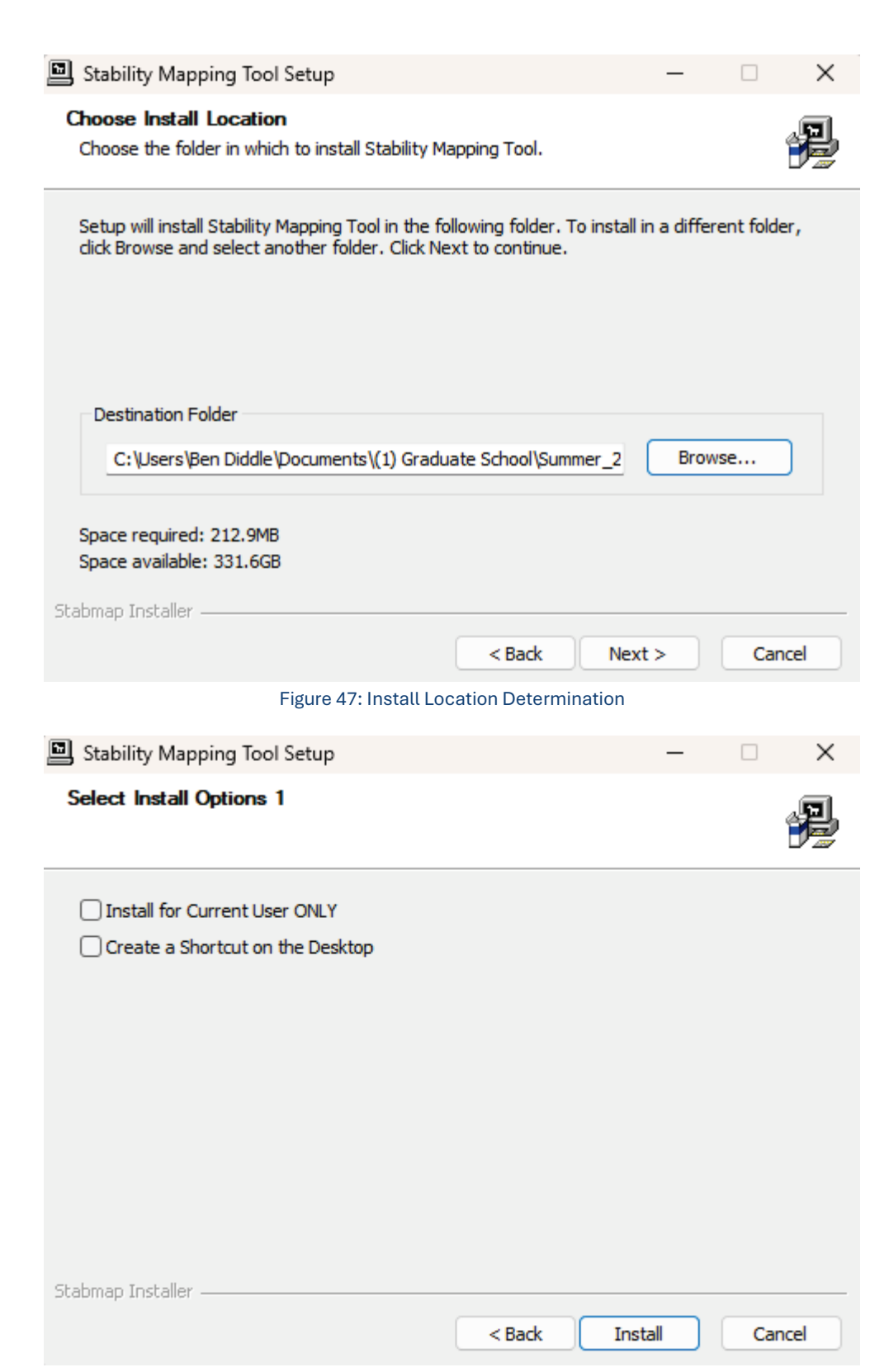


Figure 48: Selecting Install Options

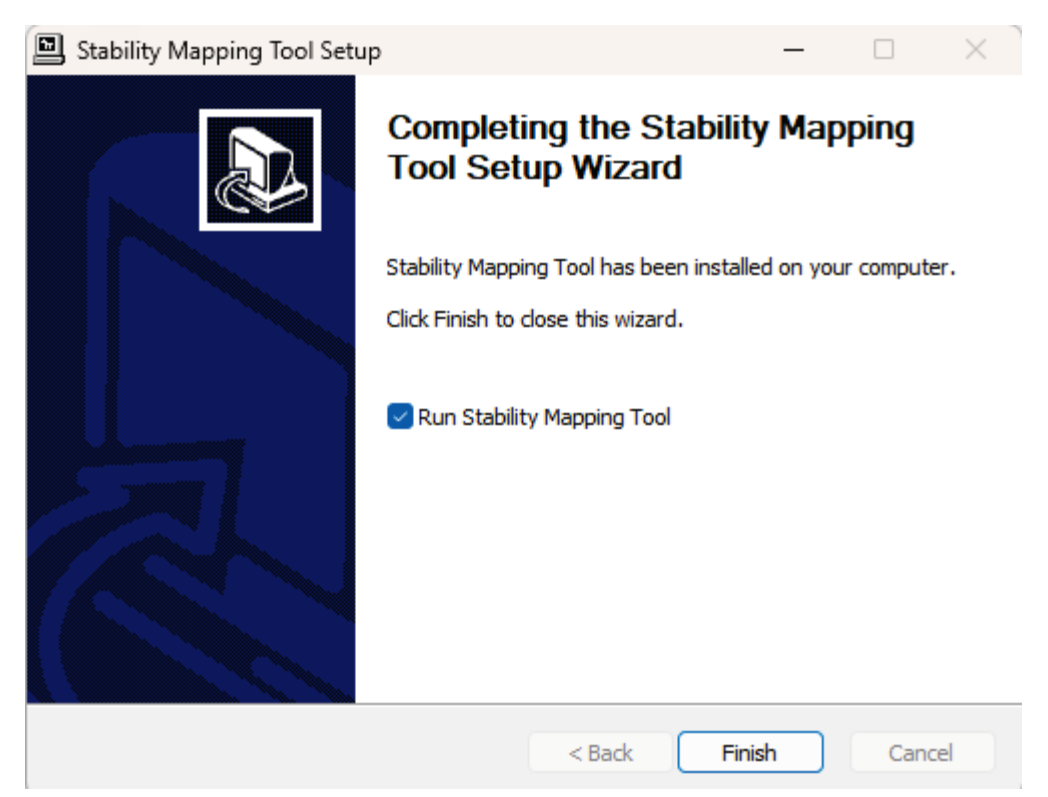


Figure 49: Completion and Commencement

11Appendix C: Stability Mapping Application Help File

Attached is a PDF file, which was generated by the help authoring system that was used to develop the context-sensitive help subsystem of the StabMap application.

StabMap Manual

Print Version of Online Help

Monday, October 27, 2025

This page is intentionally left blank. Remove this text from the manual template if you want it completely blank.

1. I	ntroduct	tion to StabMap	5
2. 6	General \	Workflow and Layout	7
3. N	Main Me	nu	9
3.1	Projec	cts	10
3.1	1 M	lanage Projects	11
3	3.1.1.1	Common Buttons	
3	3.1.1.2	General	12
3	3.1.1.3	Scenarios in Project	14
3	3.1.1.4	Project Summary	14
3.1	2 M	lanage Scenarios	15
3	3.1.2.1	General	
3	3.1.2.2	Input Parameters	17
	3.1.2.2.1	General Model Information	17
	3.1.2.2.2	Seams	20
	3.1.2.2.3	Lamination Thickness	21
	3.1.2.2.4	Materials	23
	3.1.2.2.	4.1 Coal Materials	23
	3.1.2.2.	4.2 Stone Materials	25
3	3.1.2.3	Mine Map	27
	3.1.2.3.1	Manage Mine Map and Import Polylines	27
	3.1.2.3.	1.1 Coal	27
	3.1.2.3.	1.2 Stone	29
	3.1.2.3.2	Generate Grid from Imported Polylines	30
	3.1.2.3.	2.1 Coal	30
	3.1.2.3.	2.2 Stone	32
	3.1.2.3.	2.3 Core Grid Characters	33
	3.1.2.3.3	Manage Imported Grids	
3	3.1.2.4	LaModel Grids	35
	3.1.2.4.1	Manage Grids	35
	3.1.2.4.2	Color Grid	
	3.1.2.5	La Model F1 Output File	
3	3.1.2.6	LaModel F1 Output Charts	
	3.1.2.6.1	Grid	
	3.1.2.6.2	Charts	
	3.1.2.6.3	Contours	
	3.1.2.6.4	Colored Square Plot	
	3.1.2.7	Summary	
	3.1.2.8	Progress Logs	
3.1		elect Project	
3.1	4 Ex	kit Program	43
3.2	Tools		43
3.2	1 Co	onvert a Carlson Grid File to TOP Grid File	43

3.2	.1.1 Carlson Grid	43
3.2	.1.2 LaModel Overburden Grid	44
3.2	.1.3 Help	
3.2	.1.4 Debug	47
3.3	Options	47
3.3.1	Settings	47
3.3	.1.1 General	48
3.3	.1.2 LaModel Program	49
3.3	.1.3 Backup	
3.3	.1.4 Updates	
	.1.5 Update Database Structure	
3.3	.1.6 Setup a New Database	
3.3.2	Backup / Restore Database	52
3.4	Help	54
3.4.1	Context Sensitive Help File	54
3.4.2	StabMap Users Manual (PDF)	54
3.4.3	Resource Files	54
3.4.4	Program Updates	54
3.4.5	Disclaimer	54
3.4.6	About	56
4. Us	ing Carlson Grids in StabMap	59
5. La	mination Thickness Calculation	61
6. Ma	aterial Model Generation	65
6.1	Coal Properties Generation	66
6.2	Gob Properties Generation	68
6.3	Stone Properties Generation	
1 m al a		
Index		71

1

Introduction to StabMap

1 Introduction to StabMap

The purpose of StabMap is to provide an efficient pre- and post-processor to LaModel that is independent of the AutoCAD package which allows mine operators to assess both coal and stone mine pillar stability to identify potential hazard zones in the mine. It is designed to be a significant improvement over the current LamPre and LamPlt platforms. In addition to the workflow improvements to existing features, StabMap contains several novel components.

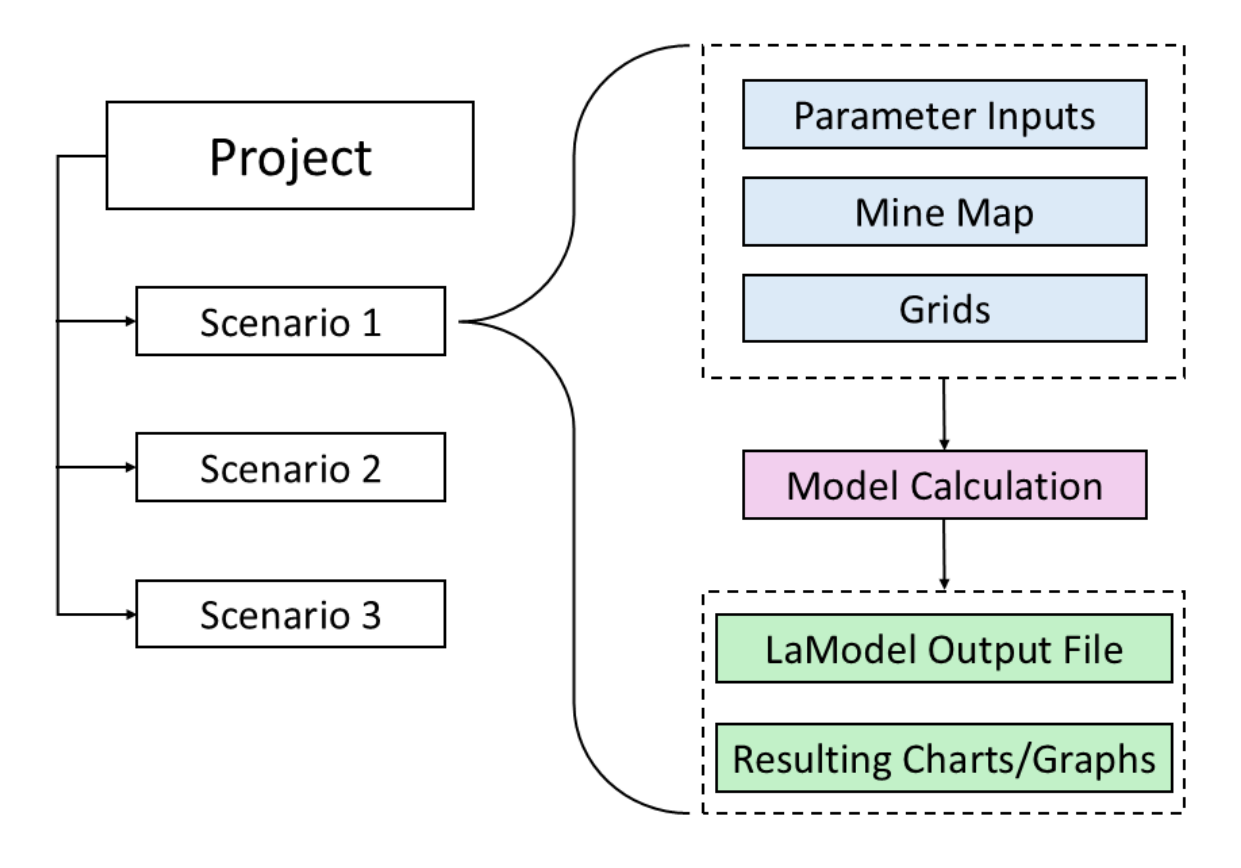
- StabMap is database driven, meaning all files are saved inside the program. This greatly eases file management and streamlines workflow.
- It combines the functionality of LamPre and the Stability Mapper AutoCAD plugin into a single platform.
- It extends the 2000 x 2000 grid dimension limit in LamPre.
- It allows more than four steps and four seams to be analyzed simultaneously.
- Operators may now employ the laminated overburden model in LaModel for stone mine analysis.
- StabMap incorporates the elasto-plastic analysis conducted by Escobar (2021) to generate material properties for both developed and benched stone pillars.

General Workflow and Layout

2 General Workflow and Layout

Using the LaModel program involves three distinct components: pre-processing, model computation, and result analysis. Historically, pre-processing was completed using LamPre, computation was completed in LaModel, and analysis was completed in LamPlt. One of the purposes of StabMap is to consolidate these functions into a single unit. The entire workflow may be completed in StabMap, though LaModel is still be utilized for computation.

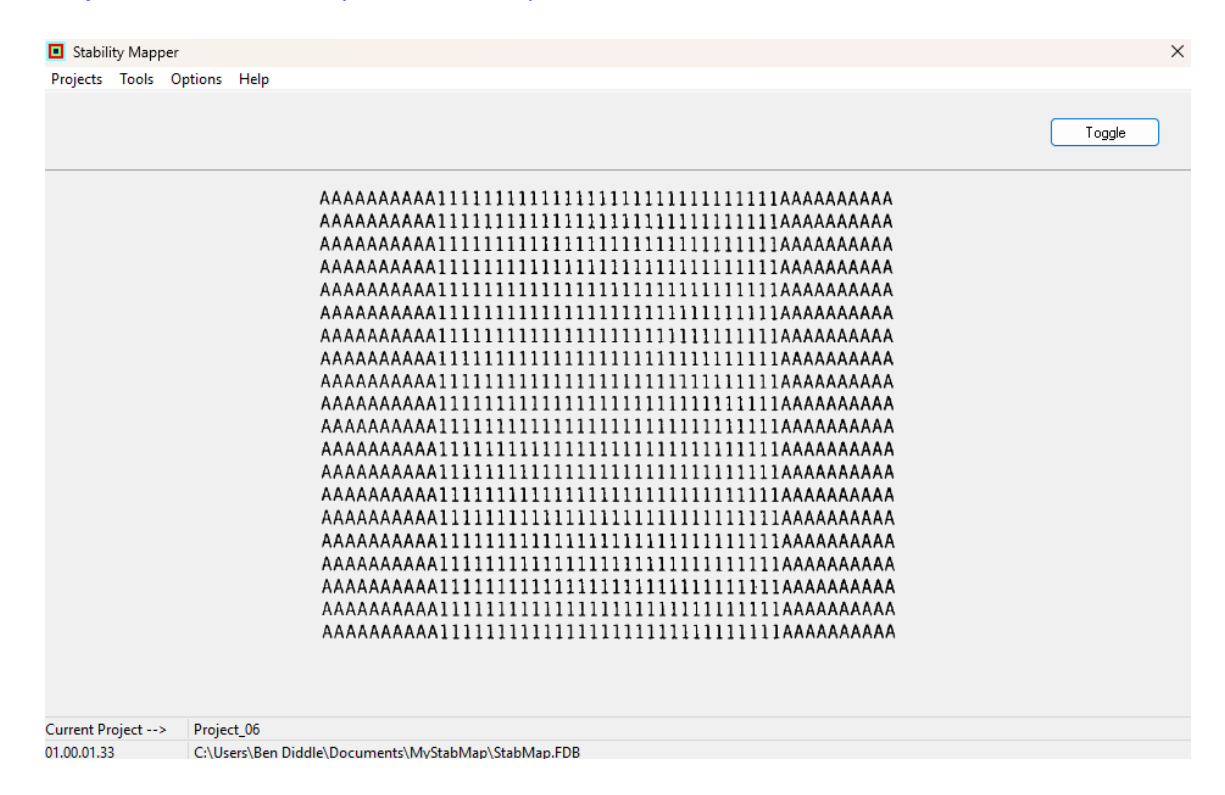
The file management system is composed of projects and scenarios, as shown in the scheme in the figure below. All inputs are <u>saved into a INP (.inp) file</u>, which can be loaded into LaModel. LaModel results are stored in F1 (.f1) files, which can be <u>loaded back into StabMap</u> for processing and analysis.



Main Menu

3 Main Menu

The StabMap main menu allows the user to access all program functions through four tabs: Projects, Parameters, Options, and Help.

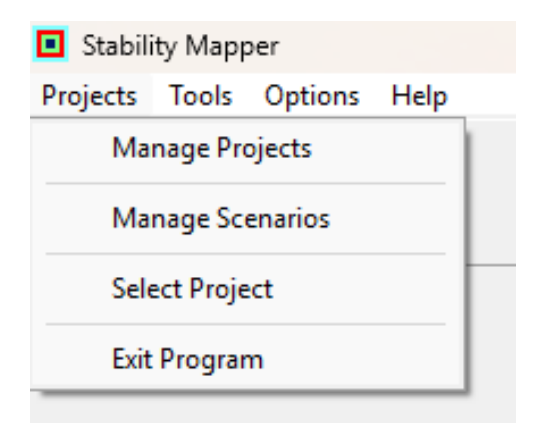


The bottom left corner of the page displays the active project, the specific version of the program, and the file location of the database file.

Depending on the selected <u>settings</u>, a Toggle button will appear in the upper right corner. This allows the user to toggle between the main and alternative databases.

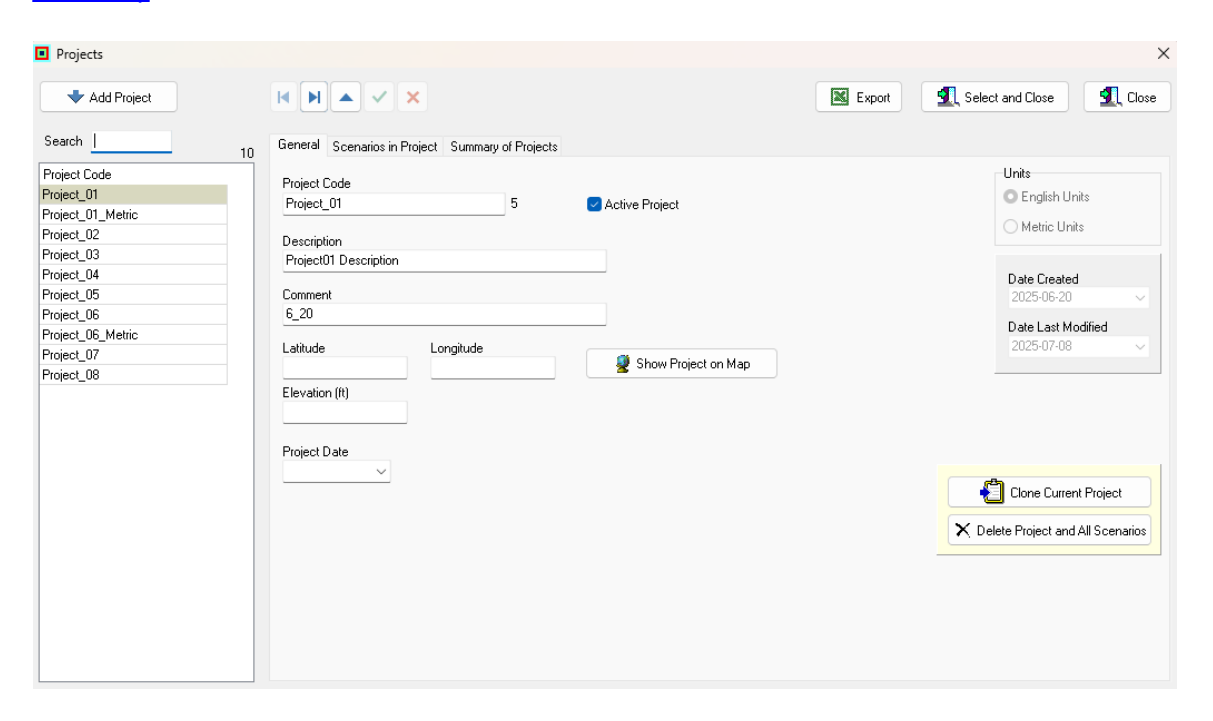
3.1 Projects

The Projects tab allows the user to access four windows: <u>Manage Projects</u>, <u>Manage Scenarios</u>, <u>Select a Project</u>, and <u>Exit the Program</u>.



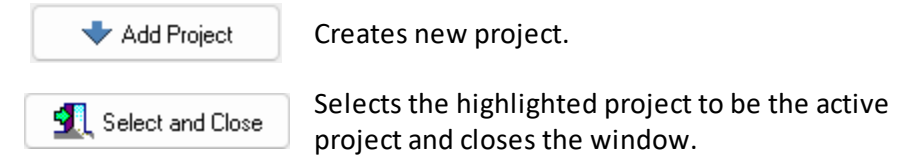
3.1.1 Manage Projects

The Manage Projects window comprises three tabs: <u>General</u>, <u>Scenarios in Project</u>, and <u>Project</u> <u>Summary</u>.



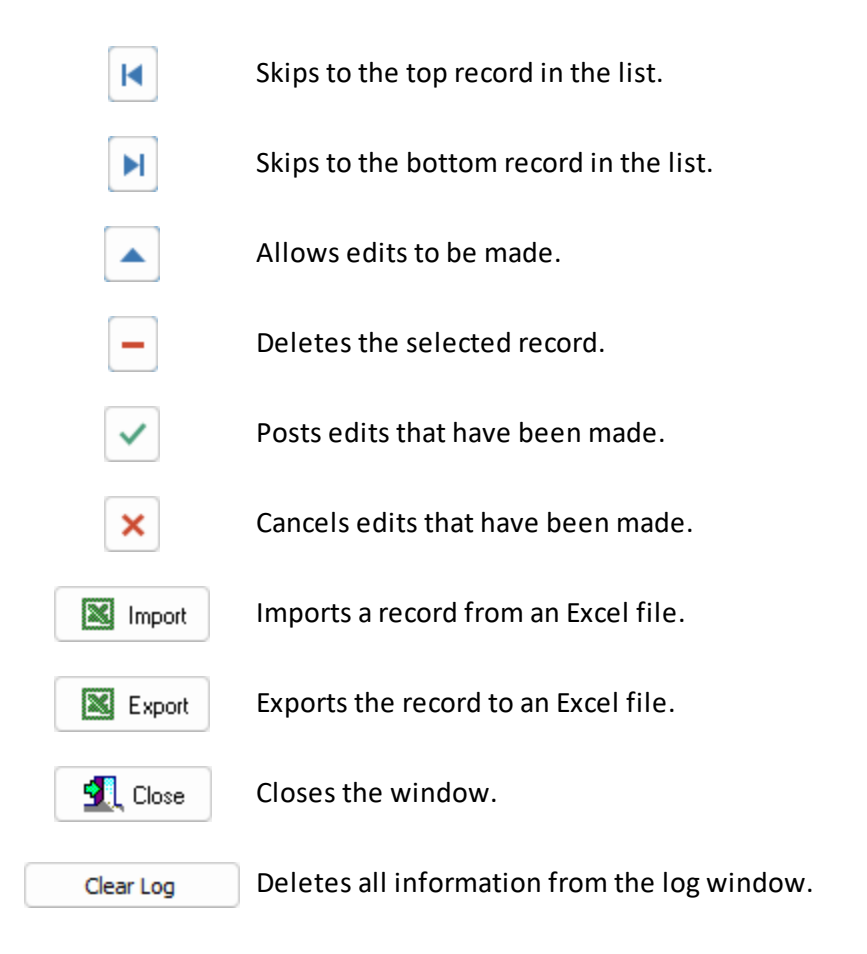
In each tab, the upper bar and left bar remain available. The left bar lists all projects in the program's database. Searching letter combinations will bring matching projects codes to the top of the list.

Button Functions



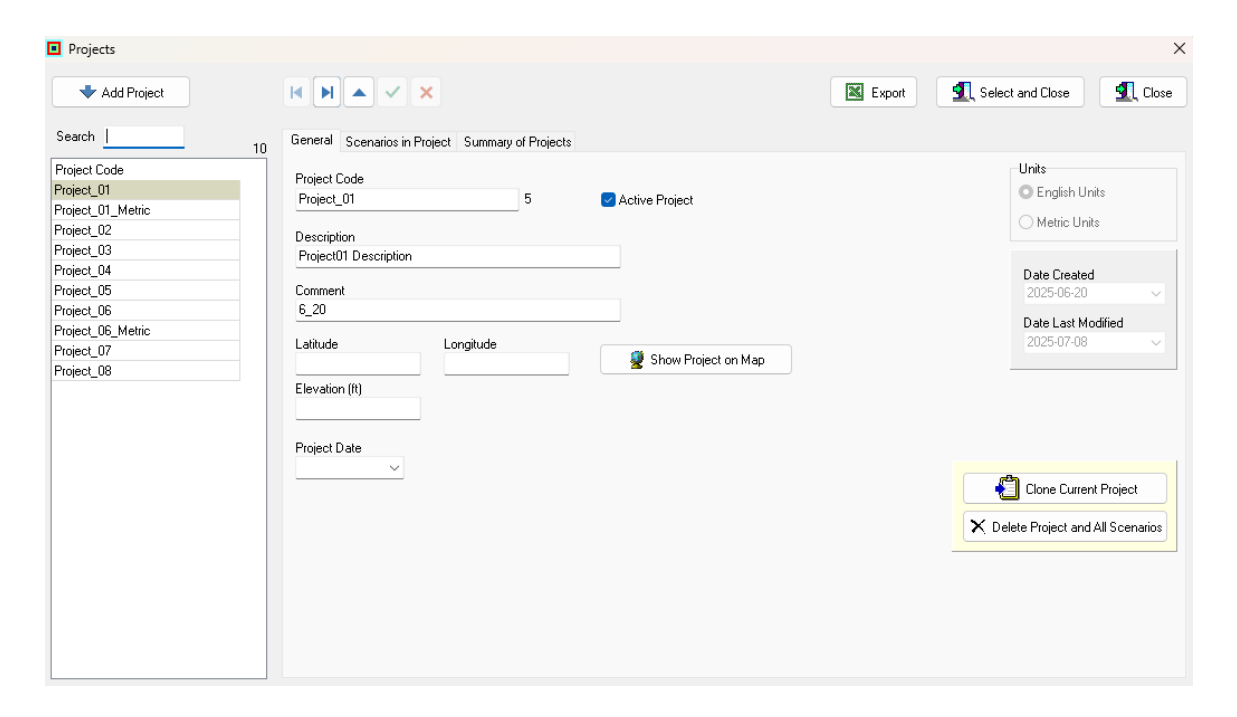
3.1.1.1 Common Buttons

The following table lists the functions of several buttons used in many parts of the program.



3.1.1.2 **General**

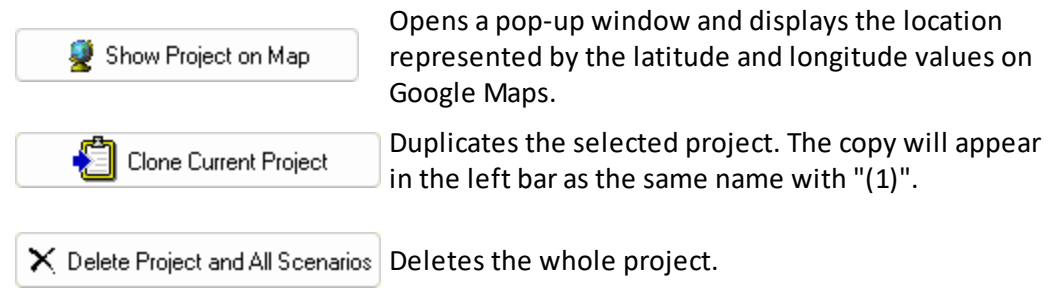
The General tab displays the general characteristics of the selected project.



The utility of each of the fields in the general tab are explained below:

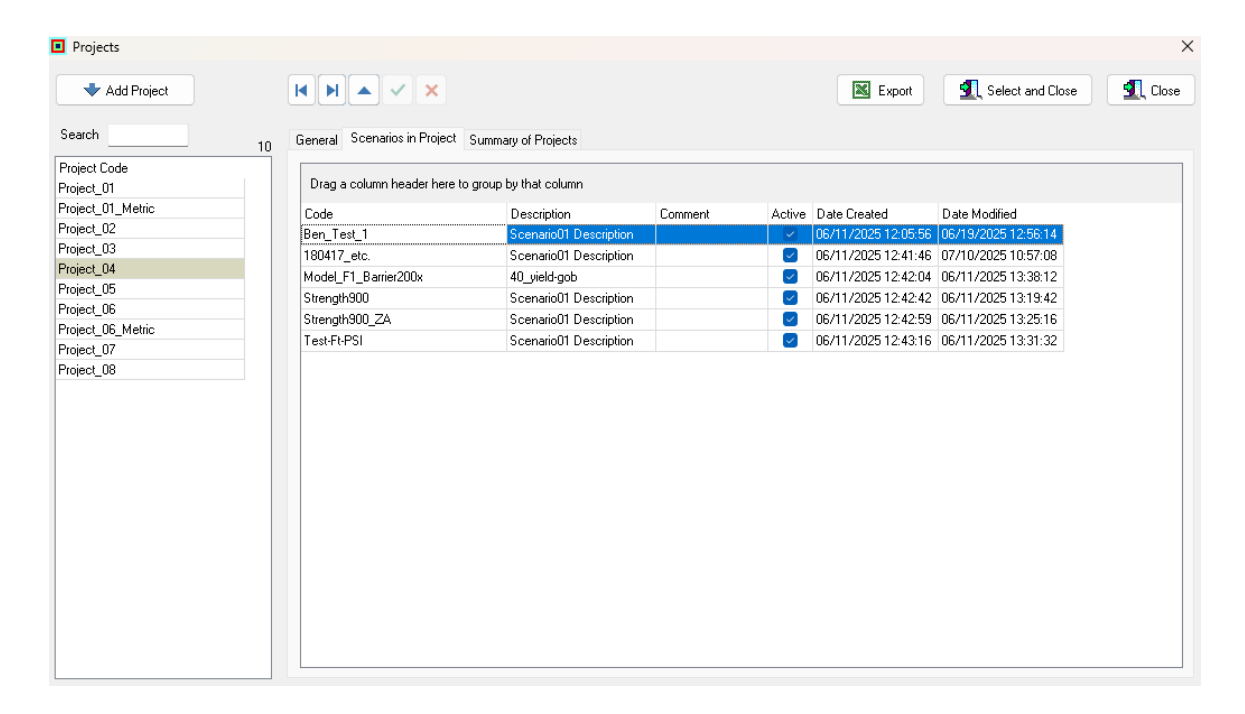
- 1. The Project Code bar is where the user may create a name for the project. To the right of the entry, a unique number is created for each item in the program.
- 2. The project may be selected as active using the "Active Project "check-box."
- 3. The Description bar allows the user to write a short characterization of the project.
- 4. Latitude and Longitude may be input in each respective bar. In the United States, latitude values will be positive and longitude values will be negative.
- 5. An average Elevation for the project may be input. Note that this is not used in any formulations elsewhere in the program, it is only for the user's reference.
- 6. A Project Date may be selected using the drop-down calendar. This may be changed anytime throughout the project.
- 7. The Comment box may be used for any notes concerning the project.
- 8. The project's units are displayed in the upper right-hand corner of the tab. They are not editable once the project is created.
- 9. The project creation date and date of last project modification are displayed, both are uneditable.

Button Functions



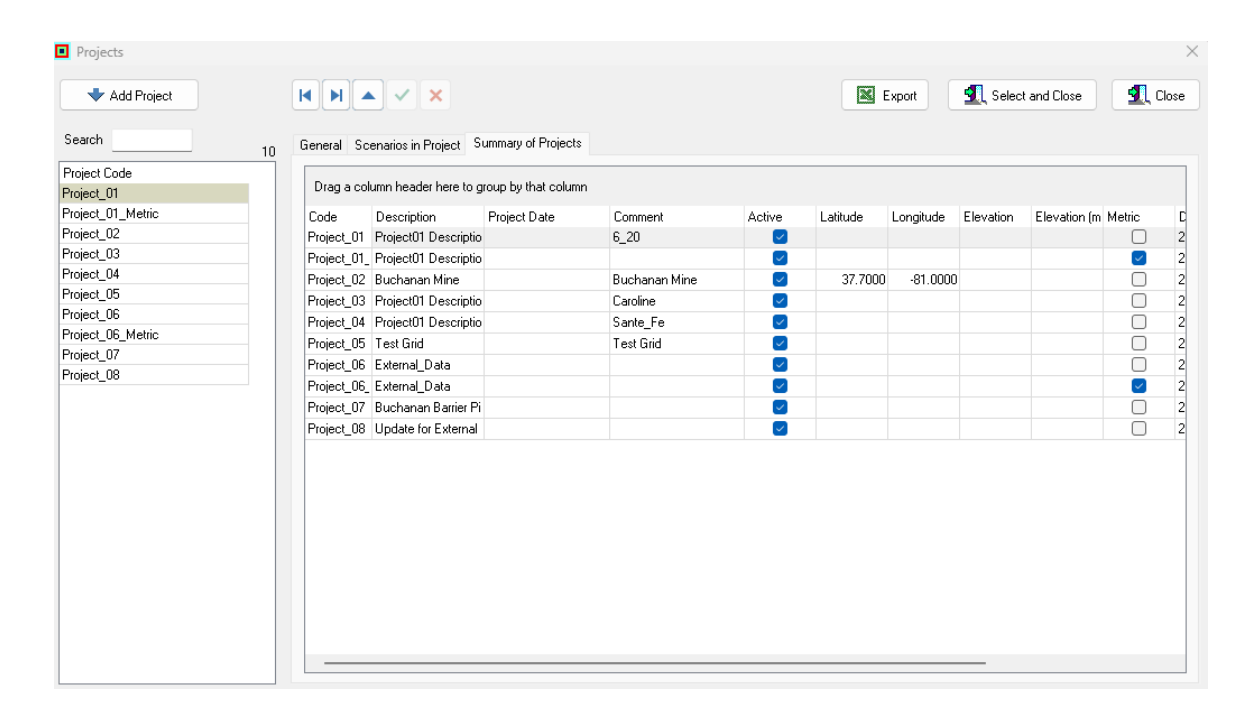
3.1.1.3 Scenarios in Project

This tab displays a list of all the scenarios in the selected project. They may be sorted by any of their general characteristics: Code, Description, Comments, Active Status, Date Created, or Date Modified.



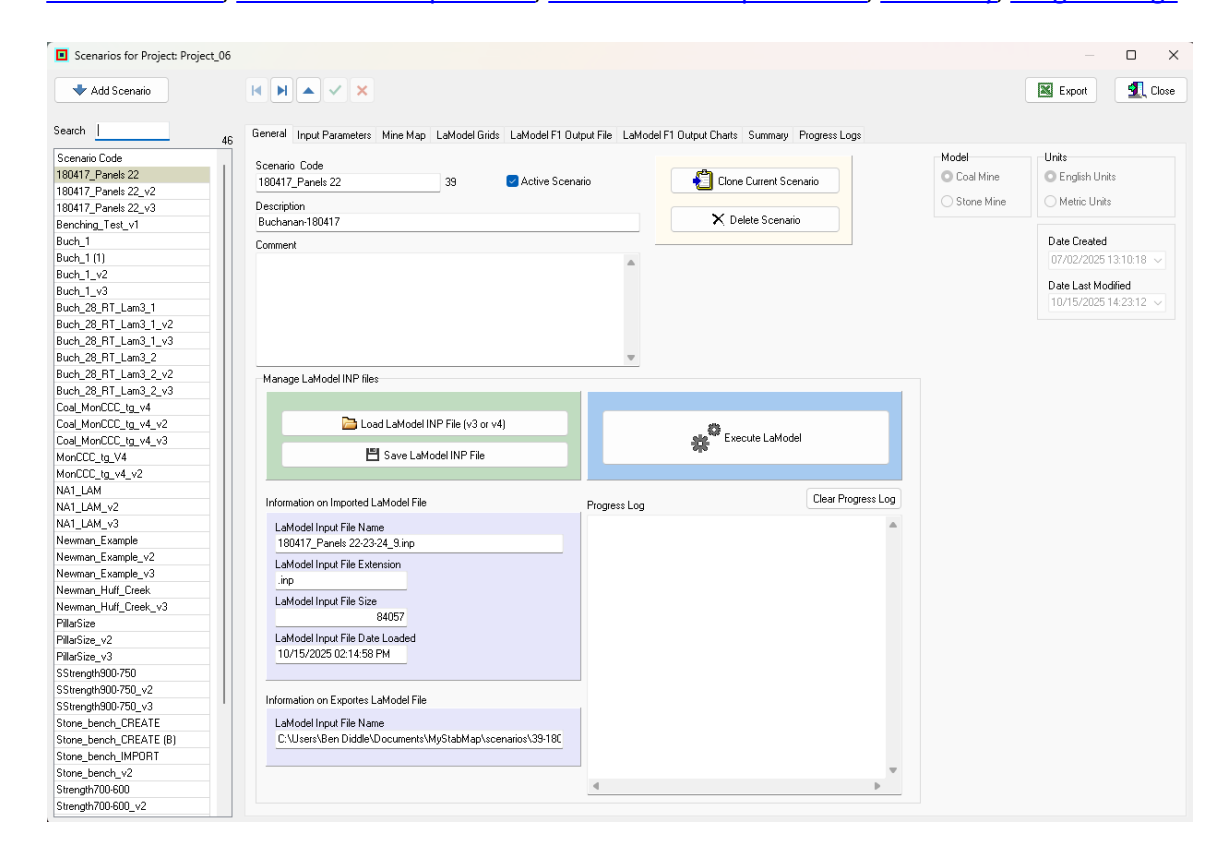
3.1.1.4 Project Summary

This tab displays a list of all the projects in the user's database. They may be sorted by any of their general characteristics: Code, Description, Project Date, Comments, Active Status, Latitude, Longitude, Elevation, Units, Date Created, or Date Modified.



3.1.2 Manage Scenarios

The Manage Scenarios window comprises eight tabs: <u>General,Input Parameters</u>, <u>Mine Map</u>, LaModel Grids, <u>LaModel F1 Output Files</u>, <u>LaModel F1 Output Charts</u>, <u>Summary</u>, <u>Progress Logs</u>.



In each tab, the upper bar and left bar remain available. The left bar lists all scenario in the selected project. Searching letter combinations will bring matching scenario codes to the top of the list.

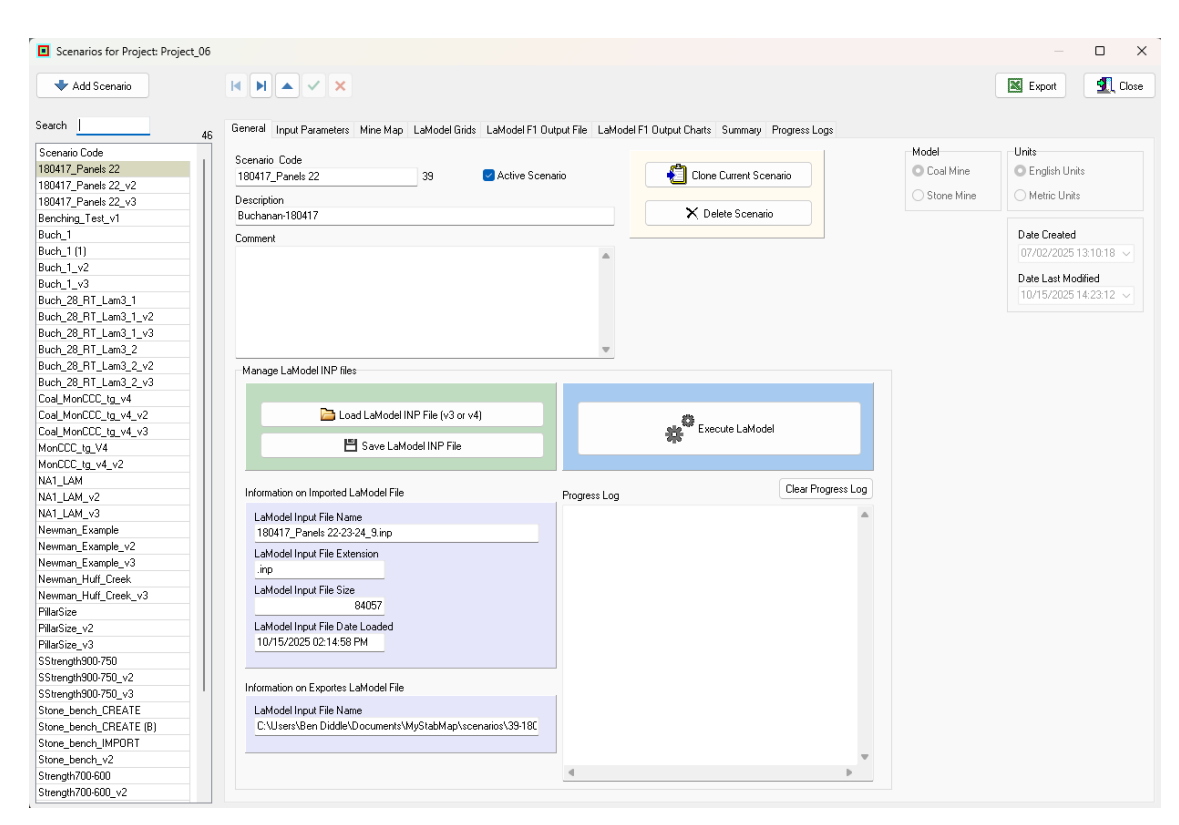
Button Functions



Creates new scenario. Once selected, a window will display that allows the user to designated permanently the scenario as coal or stone.

3.1.2.1 General

The General tab displays the general characteristics of the selected scenario.

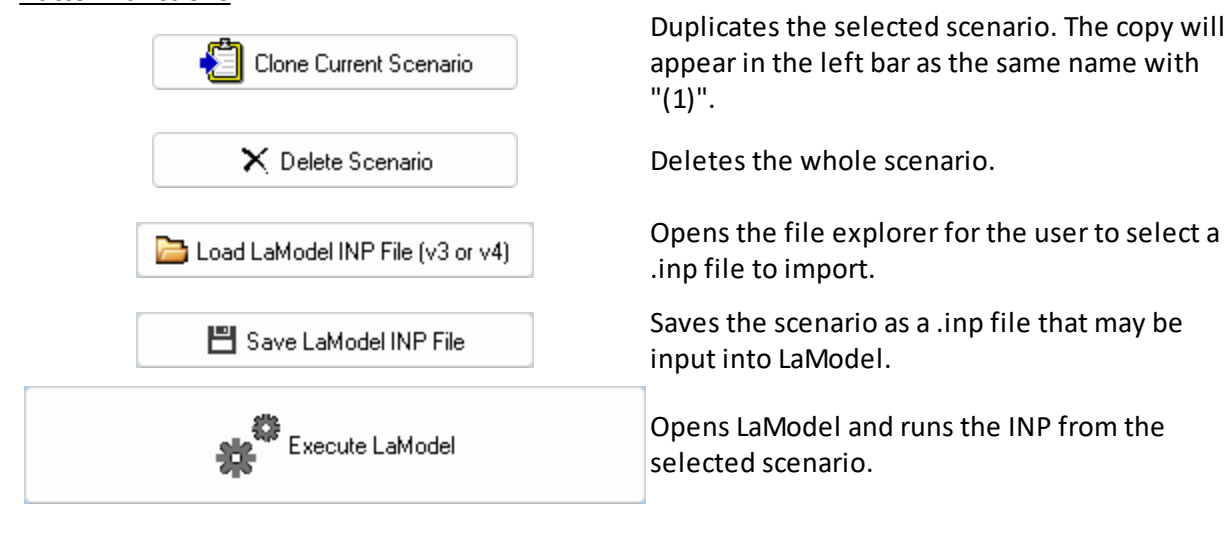


The utility of each of the fields in the general tab are explained below:

- 1. The Scenario Code bar is where the user may create a name for the project. To the right of the entry, a unique number is created for each item in the program.
- 2. The project may be selected as active using the "Active Scenario "check-box.
- 3. The Description bar allows the user to write a short characterization of the project.
- 4. The Comment box may be used for any notes concerning the scenario.
- 5. The LaModel Input File Name bar, LaModel Input File Extension bar, LaModel Input File Size bar and LaModel Input File Date Loaded bar each display information about the .inp file loaded into the scenario.
- 6. The scenario's units and model type are displayed in the upper right-hand corner of the tab. They are not editable once the project is created.

7. The scenario creation date and date of last project modification are displayed in the upper right-hand corner of the tab.

Button Functions



3.1.2.2 Input Parameters

The Input Parameter tab is composed of four sub-tabs: <u>General Model Information</u>, <u>Seams</u>, <u>Lamination Thickness</u>, and <u>Materials</u>.

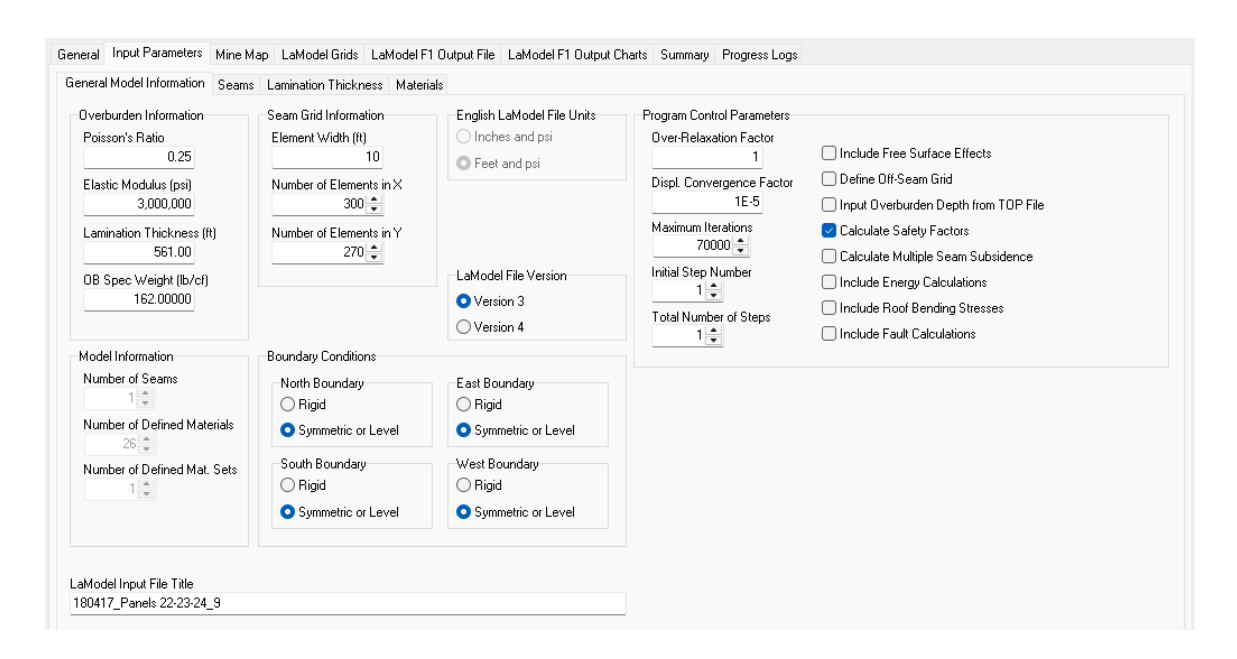
These tabs allow the user to input the desired values in each of these categories. If a .inp file is loaded, these tabs will populate based on the files data.

3.1.2.2.1 General Model Information

The Overburden Information region allows the user to input values for Poisson's Ratio, Elastic (Young's) Modulus, Lamination Thickness, and Overburden Density.

For coal scenarios, the Lamination Thickness may be determined using the tools under the Lamination Thickness sub-tab.

For stone scenarios, the only the option is for the user to define a lamination thickness. There is no accepted method for determining the lamination thickness. Based on collected industry experience, a reasonable default is 50ft.



The utility of each of the fields in the general model information tab are explained below:

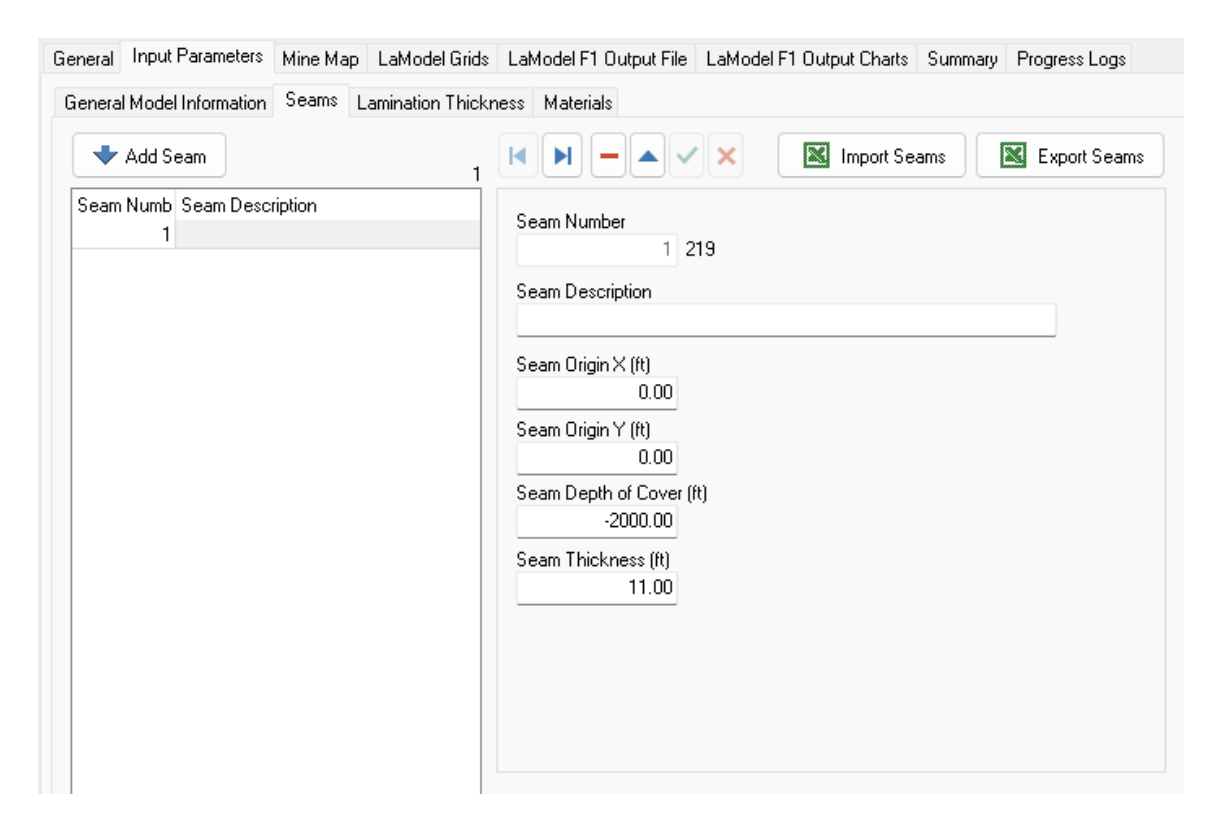
- 1. The Seam Grid Information region allows the user to input values for Element Width, Number of Elements in the X-Direction, and Number of Elements in the Y-Direction.
- 2. The LaModel File Units region displays the units for the loaded .inp file.
- 3. The LaModel File Version region displays the version from which the .inp file was created.
- 4. The Model Information region allows the user to alter the number of seams, materials, and material sets.
- 5. The Boundary Conditions region allows the user to select either rigid or symmetric/level conditions for each boundary. Rigid boundaries mean that there will be no displacement at the model's edge. Selecting
- 6. this boundary condition can result in large edge effects along the model's border. Symmetric boundaries mean that the slope of the displacement curve is zero at the edge of the grid.
- 7. The LaModel Input File Title bar displays the name of the loaded .inp file. This may be altered by the user. If loaded, all values will populate in this page automatically.
- 8. The Program Control Parameters region allows the user to alter several LaModel settings.
- 9. The Over-Relaxation Factor defines the rate of convergence in the LaModel solution algorithm. Essentially, it is a numerical factor used to overestimate the calculated displacement in an attempt to derive a solution in fewer iterations. The Over-Relaxation Factor can range from one to two. A user input parameter of 1 provides no over estimation in the central difference solution method, while an input of 2 will double the estimate causing the solution to diverge. Understanding this, it is recommended that users define this parameter within the range of 1.35 to 1.8. Please recognize that the default parameter of 1.65 has been found to be the optimal value for most models.
- 10. The Displacement Convergence Factor determines the precision of the results generated by the LaModel solution algorithm. Decreasing the input value increases the models precision and vice versa. The program default parameter is 0.00001, which provides adequate precision for all models and therefore should not be modified by the user.
- 11. The Maximum Iterations value refers to the number of iterations to be run by LaModel. If the maximum iteration number is reached, then the program will close without fully converging. The default value provided will be adequate for basic models. However when the user

- increases the number of seams to be analyzed, the iteration value should be increased. The user should be aware the that number of interactions defined only allows the solution algorithm a larger iteration set if needed
- 12. The Initial Step Number allows users to break down a large input file into multiple runs. This is achieved by inputting a step value that corresponds to the analysis start point of the model. For example, if there was a ten step model and one wanted to separate the model into two separate program runs, the user would begin the first run with an initial step of 1 and then a second run with an initial step of 6.
- 13. The Total Number of Steps refers to the amount of steps to be run by LaModel.
- 14. Selecting the "Include Free Surface Effects" check-box allows users to take into consideration the existence of a surface effect stresses. The Surface Effect accounts for in accuracies of the laminated model through the implementation of a mirror image seam(s) centered about the surface; elevation of zero. From extensive case studies it is suggested that Surface Effect be taken into consideration when the panel width to depth ratio is greater than 1.80. This increases the required number of computations due to the element interactions between the real and mirror imaged seams.
- 15. Selecting the "Input Topography from File" check-box direct LaModel to search for a .top file before running. This file can be easily converted from a Carlson grid (.grd) file. Note that this grid should represent the overburden depth, not the actual elevation. For the best results, these grid files should have elements of equal or lesser size than 10 times the seam element. To be used by LaModel, the .top file should be share the name of the .inp file and be placed in the same folder.
- 16. Assuming a 21 degree abutment angle, the overburden grid should always be larger than the seam grid by a minimum of Depth*tan(21). As a rule of thumb, the dimensions of this file should be greater than those of the seam grid file by one overburden depth. For example, if the seam grid is 100ft by 100ft with an average overburden depth of 50ft, the overburden grid should 200ft x 200ft, an additional 50ft in each direction.
- 17. Selecting the "Calculate Safety Factors" check-box directs LaModel to calculate both stress and strain safety factors for all pillars.
- 18. Selecting the "Calculate Multiple Seam Subsidence" check-box allows users to calculate inseam subsidence caused by multiple seam mining geometries for each seam analyzed. Using this information in conjunction with the LamPlt post processor, users can determine the Remote Displacements as well as strains in both the X & Y directions with respect to multiple seam mining activity.
- 19. Selecting the "Include Energy Calculations" check-box allows users to calculate the energy stored and energy released with respect to inseam mining activity. Using this information in conjunction with the <u>processed results</u>, users can determine the bump potential through the analysis of the element energy input and the rate of energy release from a given element.
- 20. Selecting the "Include Roof Beam Bending Stresses" check-box allows users to calculate the compression and tension stresses in the modeled roof. Using this information in conjunction with the processed results, users can anticipate roof behaviors with respect to mining geometries in an attempt to be proactive in their roof control system.
- 21. Selecting the "Include Fault Calculations" check-box will display the Fault Information region, which allows the user to incorporate a frictionless vertical fault within the grid. There will be no stress transfer along the fault.
- 22. Selecting the "Include an Off-Seam Plane" check-box will display the Off Seam Plane region. Here the user is able to define an off-seam location and geometry such that surface subsidence can be calculated with respect to the defined underground geometries and

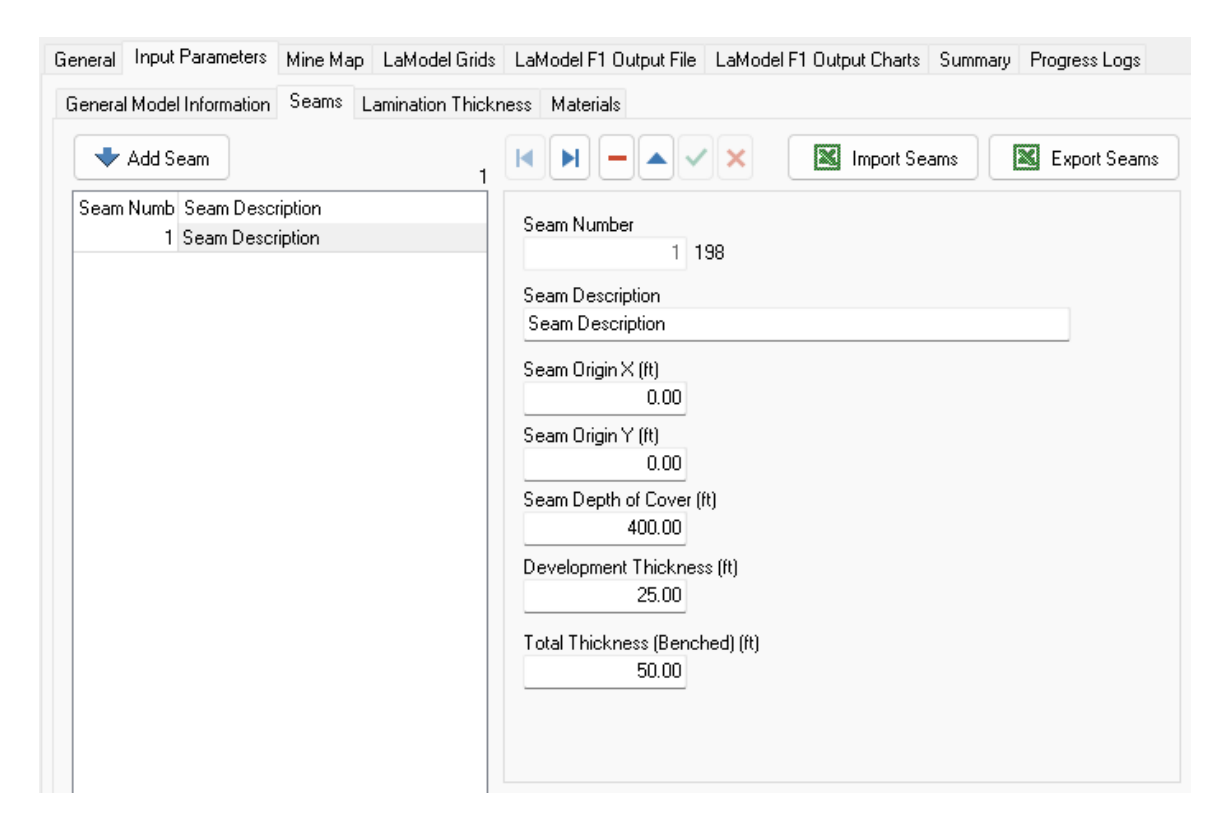
material properties. The accepted grid block size for the plane is between 5ft and 50ft. A smaller block size causes a large increase in program run time, while a large block size can cause numerical instability in the model and produce in accurate results. The program allows a maximum of 2000 elements in both the x and y directions such that the grid will completely encompass the area in which surface subsidence is to be calculated.

3.1.2.2.2 Seams

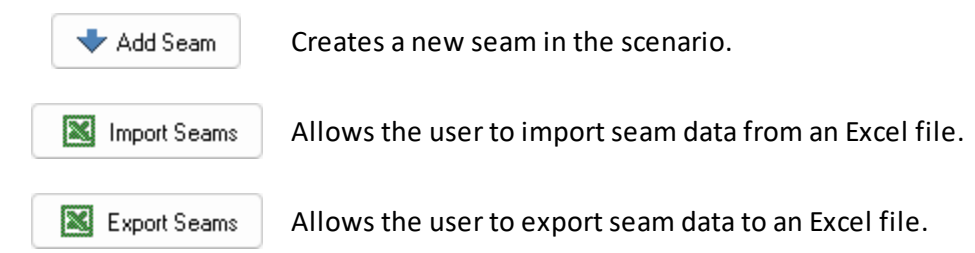
For Coal scenarios, the Seams tab displays each seam in the selected scenario, including name, origin points, depth of cover, and thickness.



For Stone scenarios, the Seams tab displays each seam in the selected, including name, origin points, depth of cover, development pillar height and total benched pillar height.



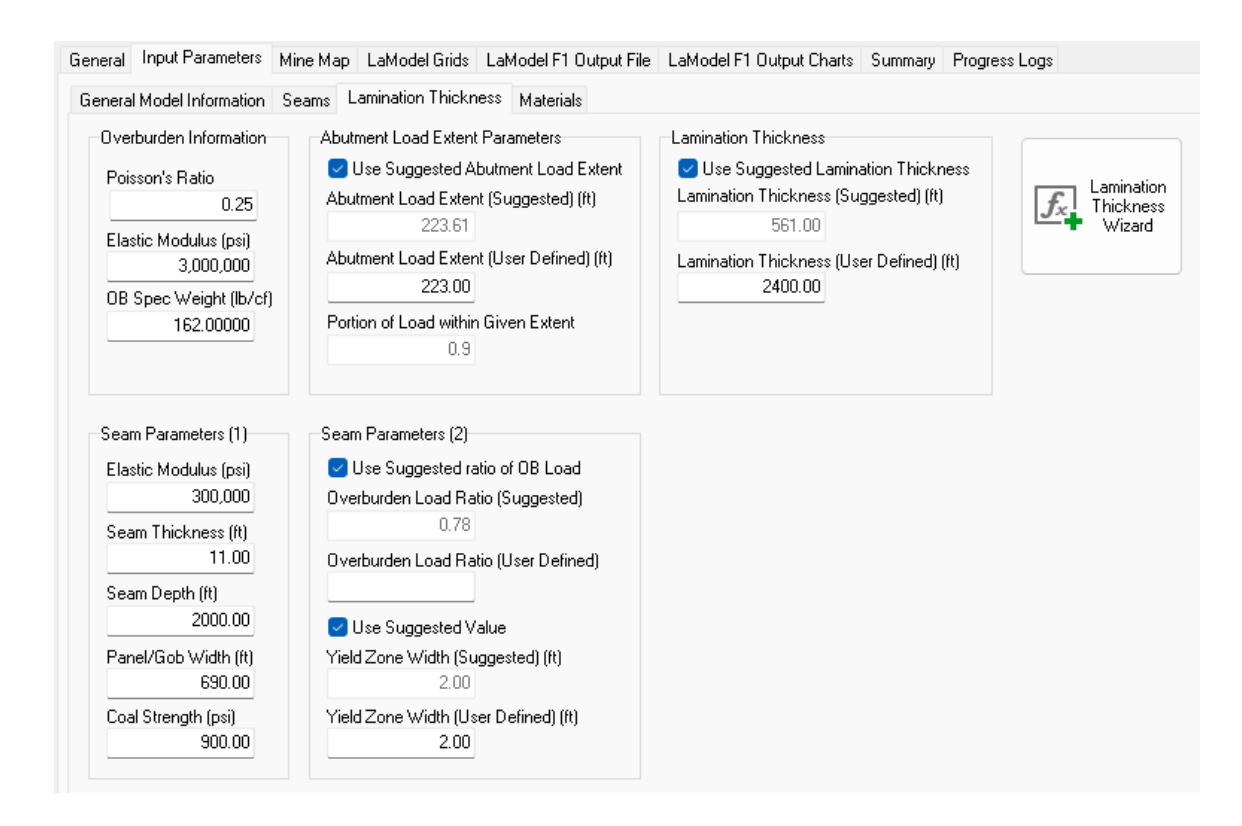
Button Functions



3.1.2.2.3 Lamination Thickness

The lamination thickness represents an average vertical distance between major geological discontinuities in the overburden or the interburden between two seams. It has a mathematical effect on the stiffness and behavior of the overburden. In general cases, a thinner lamination thickness creates a less rigid overburden and tends to generate increased inseam convergences, interseam interactions, and steeper subsidence troughs. A thicker lamination thickness creates a more rigid overburden and tends to decrease inseam convergences over gob areas and distributes stresses caused by interseam interactions over a larger area. It should be noted that a Lamination Thickness less than 2 or 3 times the element size will produce numerical instability in the solution algorithm for the laminated model.

For Coal scenarios, this tab allows the user to calculate the optimal lamination thickness based on a calibration of loading at the abutment load extent to values suggested by the Mark-Bieniawski empirical equations. The mathematical procedure is detailed here.



All parameters in the Overburden Information and Seam Parameters (1) regions must be input for the wizard to run. If Abutment Load Extent, Overburden Load Ratio on the Abutment and/or Yield Zone Width estimates are known, simply deselect each respective check-box and enter the estimate.

Button Functions



This icon will run the Lamination Thickness calculation.

Coal Default Values

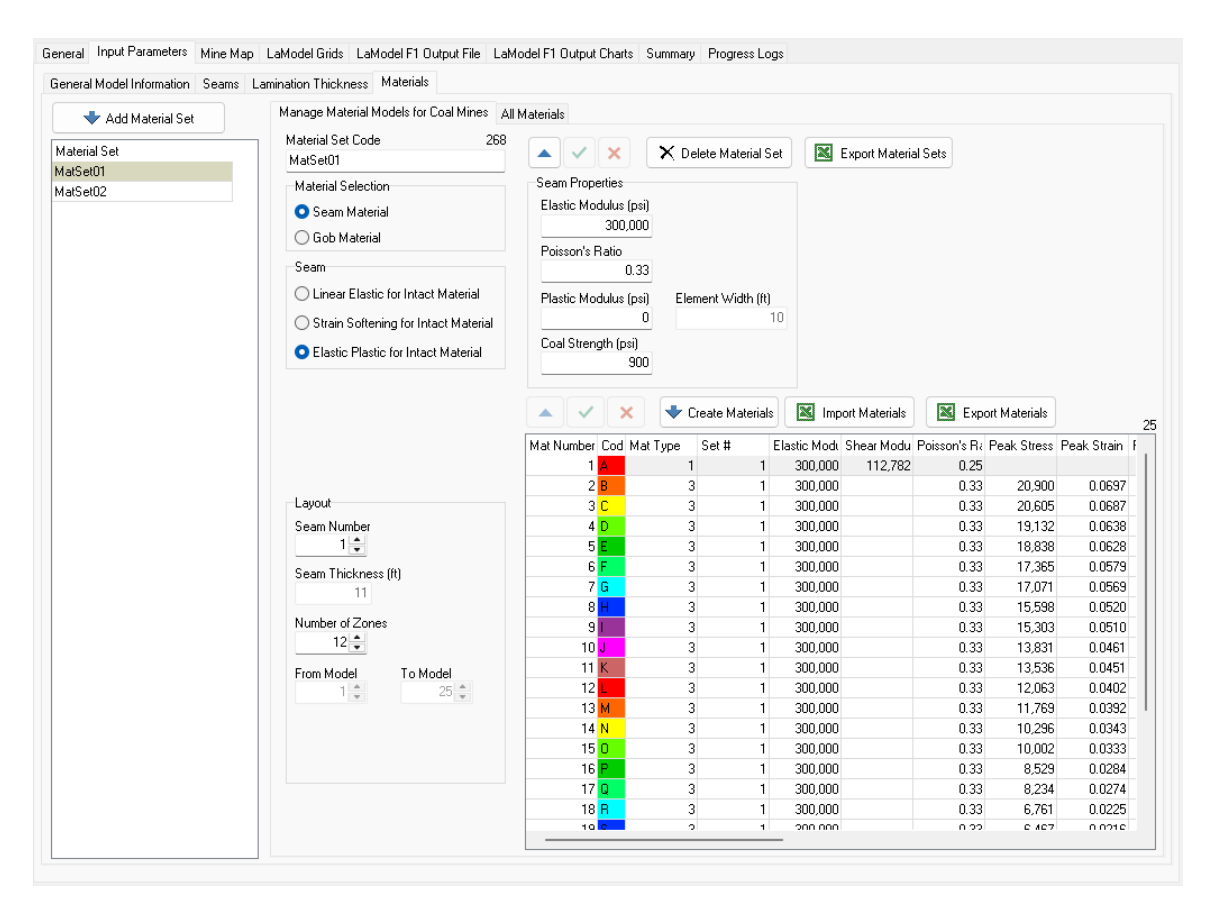
Parameter	English	Metric	
Poisson's Ratio (OB)	0.25		
Elastic Modulus (OB)	3,000,000 psi	20,680 MPa	
Specific Weight (OB)	162 lbs/ft ³	2600 kg/m³	
Elastic Modulus (Seam)	300,000 psi	2,068 MPa	
Seam Thickness	6 ft	1.8 m	
Seam Depth	1000 ft	305 m	
Panel/Gob Width	1000 ft	305 m	
Seam Strength	900 psi	6.2 MPa	

3.1.2.2.4 Materials

The process of material definition is different for <u>coal</u> and <u>stone</u> materials. The mathematical theory behind each be found <u>here</u>.

3.1.2.2.4.1 Coal Materials

Once a material set is added, designation of the material as either seam or gob is made. There are three seam material model types: Linear Elastic, Strain Softening, and Elastic Plastic. There are three gob material model types: Bi-Linear Hardening, Strain Hardening, and Linear Elastic.



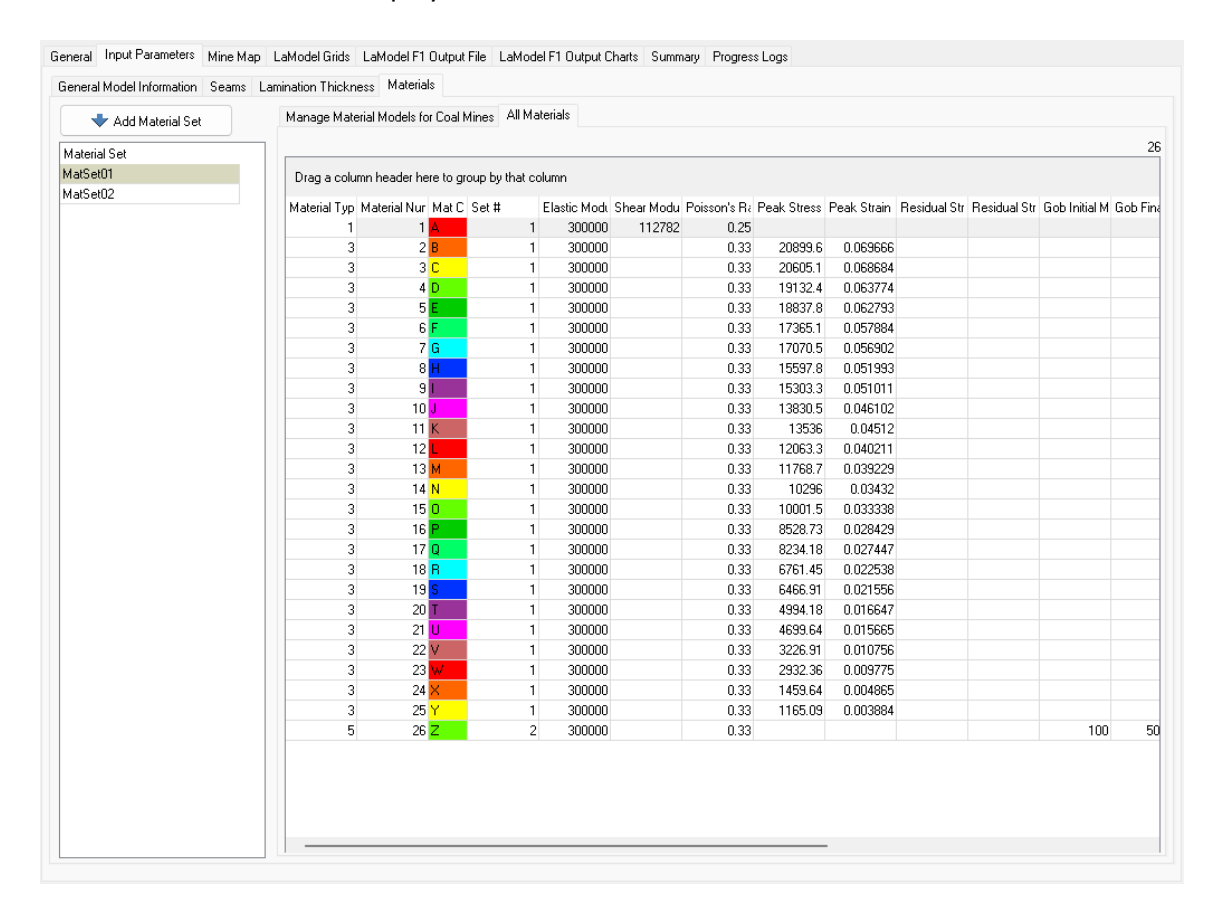
Seam Properties Required for Each Model Type

	Linear Elastic (1)	Strain Softening (2)	Elastic Plastic (3)
Elastic Modulus	~	~	~
Poisson's Ratio	~	✓	~
Element Width	✓	✓	✓
Coal Strength	✓	✓	✓
Plastic Modulus			~
Residual Stress Factor		✓	
Residual Strain Factor		✓	

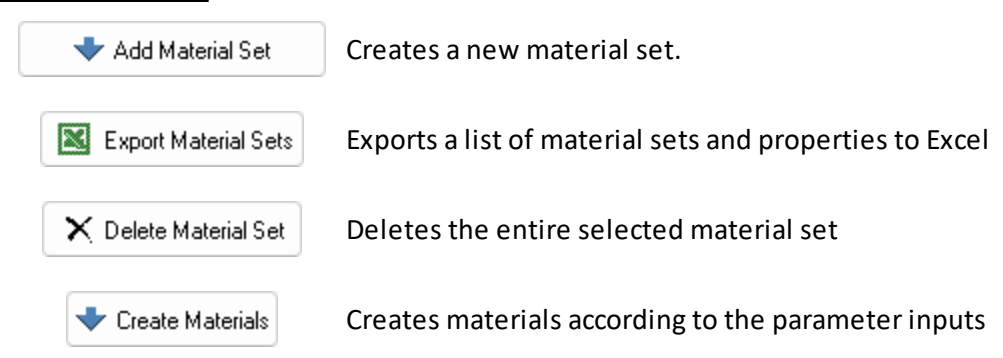
In the Layout region, seam number and number of zones must be input. Each zone comprises two materials. Seam thickness will populate based on the <u>Seams</u> tab. From Model and To Model will populate once the materials are created.

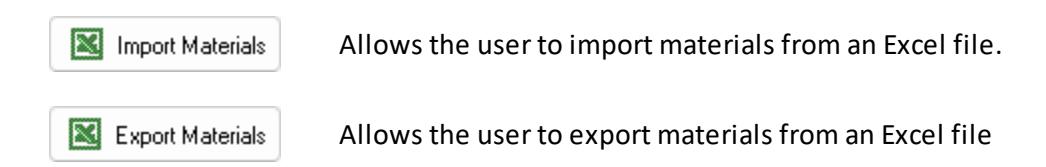
Once all inputs have been made, the materials may be created. Materials will populate in the table, with the first material will always linear elastic, regardless of model type, to represent the pillar core. Each material number is used only once in a single scenario. The code is how material will be identified in the grid. The material type value refers to the material model type.

The All Materials sub-tab displays all materials in the scenario in tabular form.



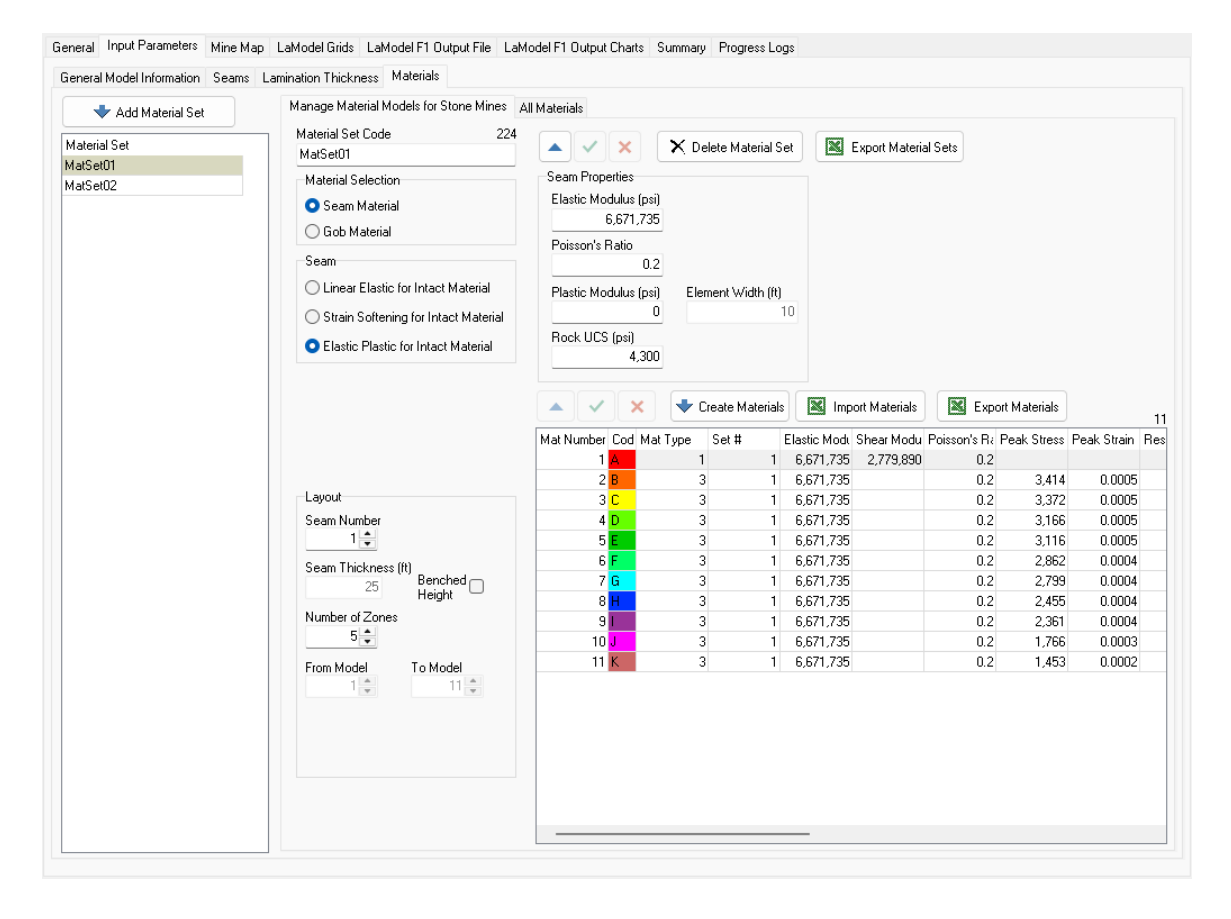
Button Functions





3.1.2.2.4.2 Stone Materials

There is one stone material model type, Elastic Plastic.



Properties Required for Stone Models

	Elastic Plastic
Elastic Modulus	~
Poisson's Ratio	~
Element Width	~
Rock UCS	~
Plastic Modulus	~

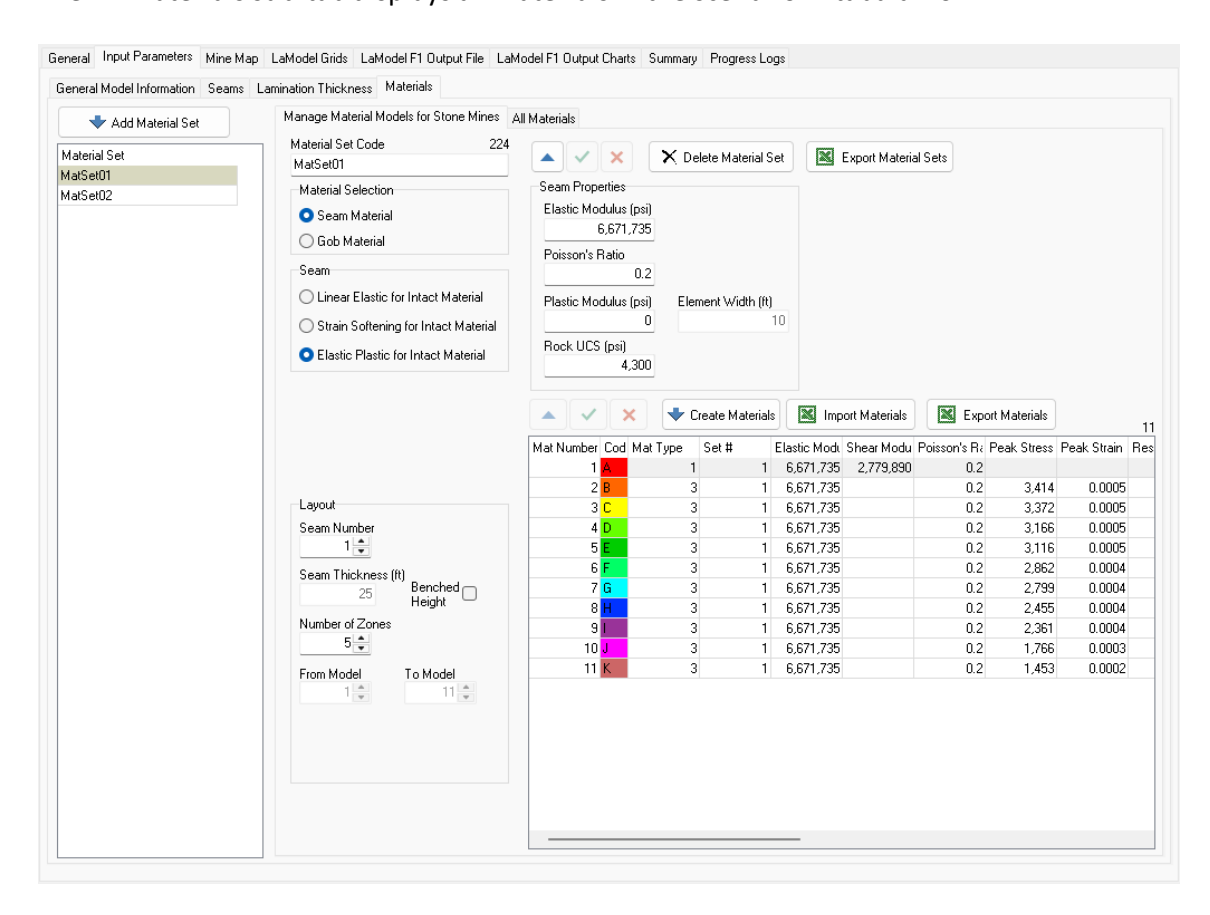
In the Layout region, the seam number and the number of zones must be input. Each zone comprises two materials. The seam thickness will populate based on the information in the Seams tab. If "Benched Height" is selected, it too will populate based on the information in the Seams tab. From Model and To Model will populate once the materials are created.

Once all inputs have been made, the materials may be created. Materials will populate in the table. The first material will always be linear elastic, regardless of model type, to represent the pillar core. Each material number (material letter or code) is used only once in a single scenario. The material code is how material will be identified in the grid. The material type value refers to the material model type.

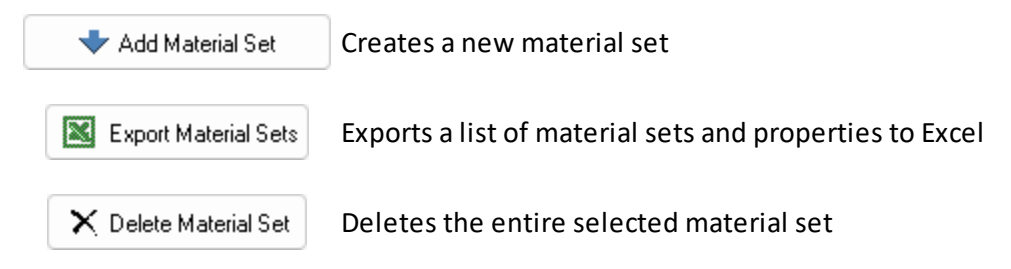
For benched materials, the user may note that the elastic modulus is reduced from the input value. This new value is determined using Equation 1 below.

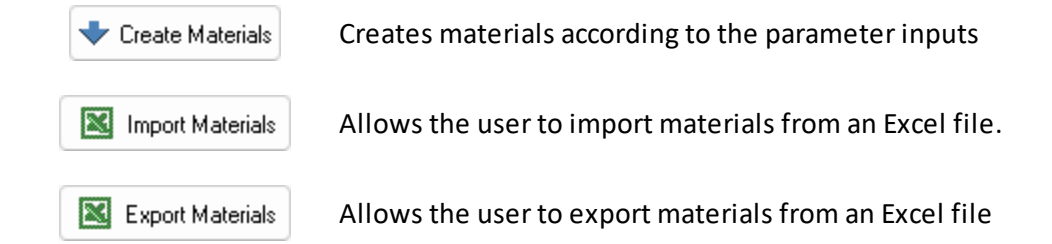
$$E_{bench} = E * \frac{DevelopmentHeight}{TotalHeight}$$
 (1)

The All Materials sub-tab displays all materials in the scenario in tabular form.



Button Functions





3.1.2.3 Mine Map

The Mine Map tab is composed of three sub-tabs: Manage Mine Map and Import Polylines, Generate Grid from Imported Polylines, & Manage Imported Grids.

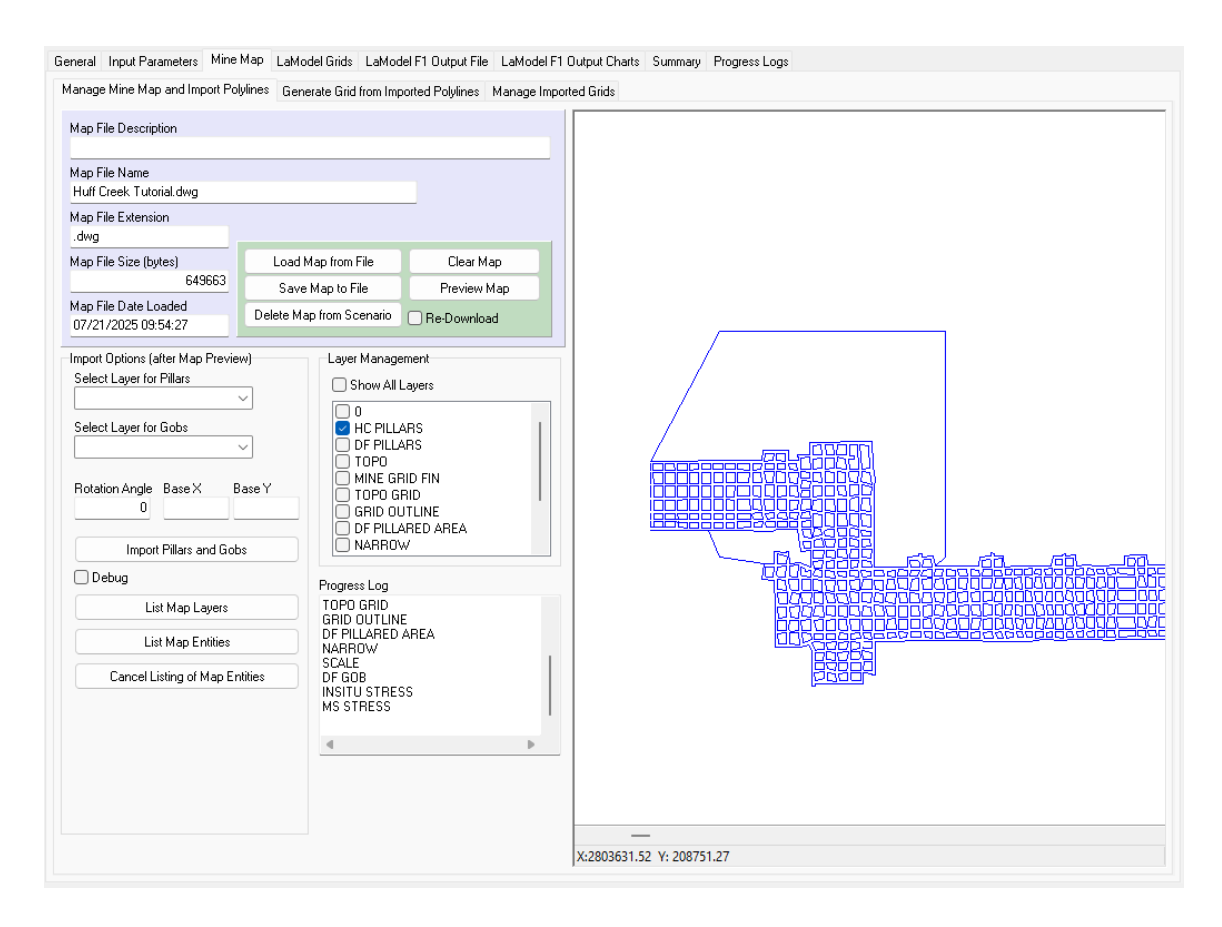
If implementing a multiple seam project, it is suggested that the user first review the video tutorials in the <u>resource files</u> window.

3.1.2.3.1 Manage Mine Map and Import Polylines

This tab will function differently for <u>coal</u> and <u>stone</u> scenarios.

3.1.2.3.1.1 Coal

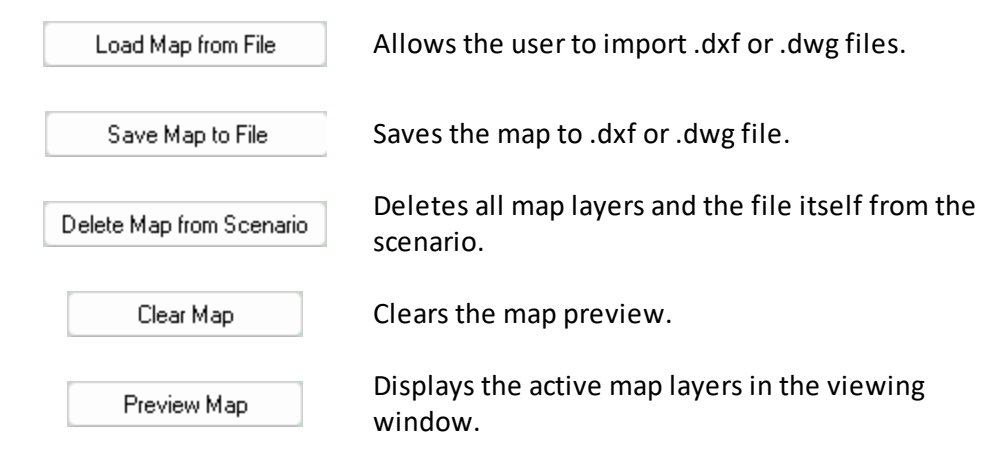
This sub-tab allows the user to load, save and delete maps from each scenario. The file details will populate when a map is loaded.

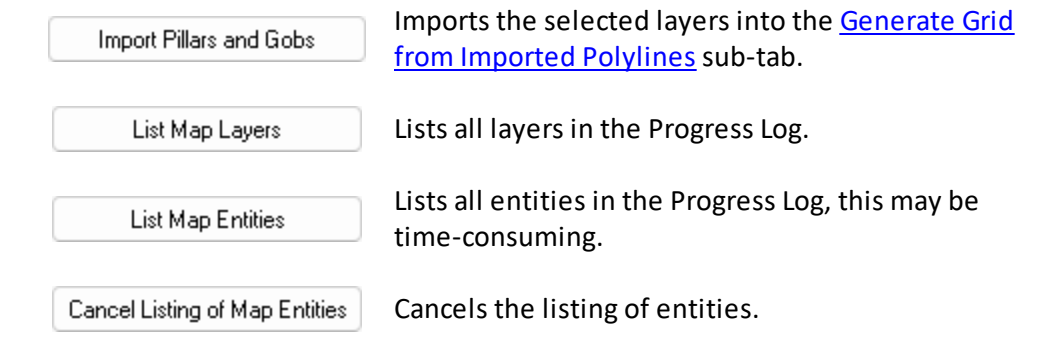


The Import Options region allows the user to select layers to import as pillars and gob. The map must be shown in the preview window before this can occur. The rotation feature allows the user to alter the map alignment. Generally, it is best to choose the alignment that allows for the greatest portion of the entries to be oriented vertically. This will lead to the most accurate grid generation. The rotation angle should be entered in degrees, and will rotate the map counterclockwise. The reference coordinates should be entered in the Base X and Base Y bars.

The Layer Management region allows the user to select active layers. The selected layers will appear in the right window when the map is previewed.

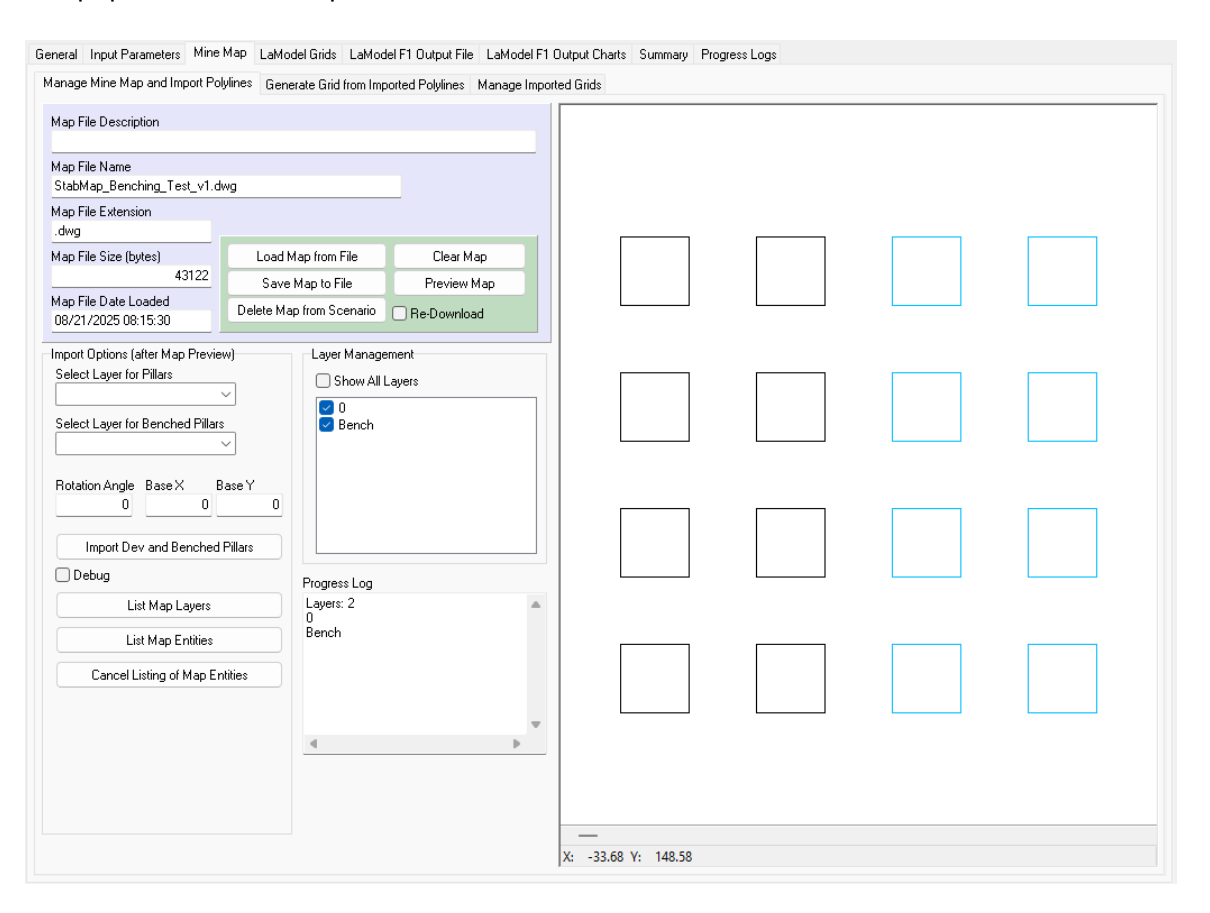
Button Functions





3.1.2.3.1.2 Stone

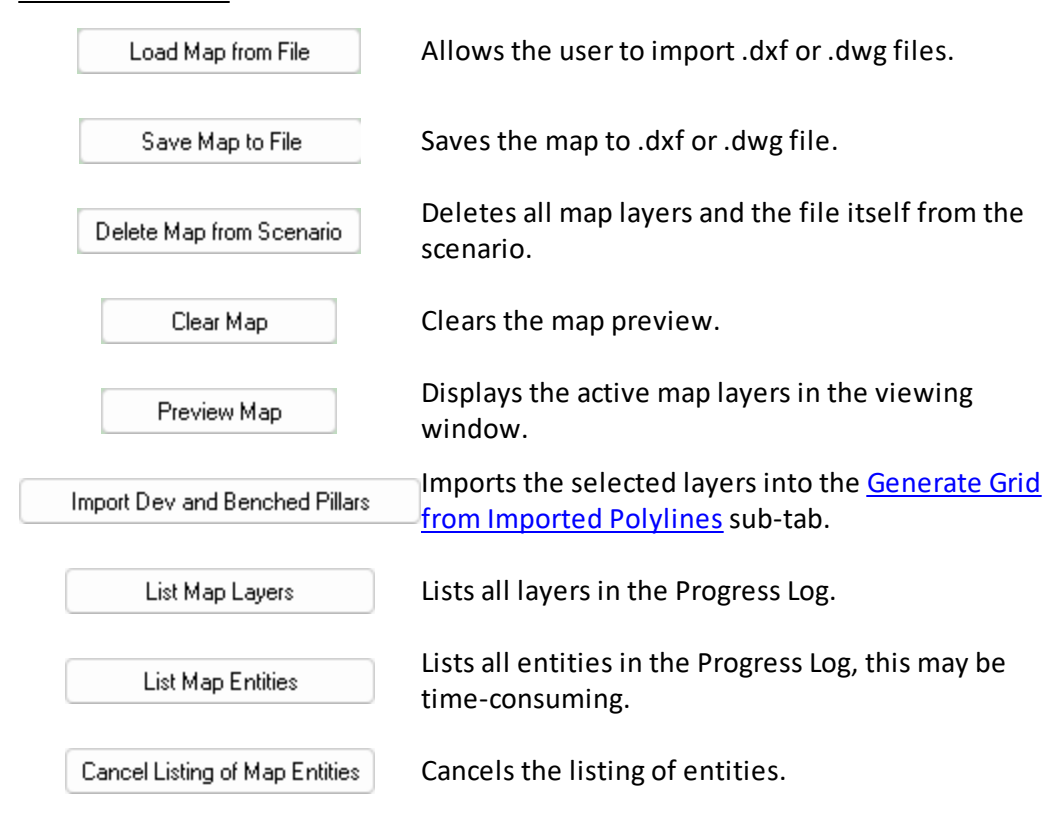
This sub-tab allows the user to load, save and delete maps from each scenario. The file details will populate when a map is loaded.



The Import Options region allows the user to select layers to import as development pillars and benched pillars. The map must be shown in the preview window before this can occur. The rotation feature allows the user to alter the map alignment. Generally, it is best to choose the alignment that allows for the greatest portion of the entries to be oriented vertically. This will lead to the most accurate grid generation. The rotation angle should be entered in degrees, and will rotate the map counter-clockwise. The reference coordinates should be entered in the Base X and Base Y bars.

The Layer Management region allows the user to select active layers. The selected layers will appear in the right window when the map is previewed.

Button Functions



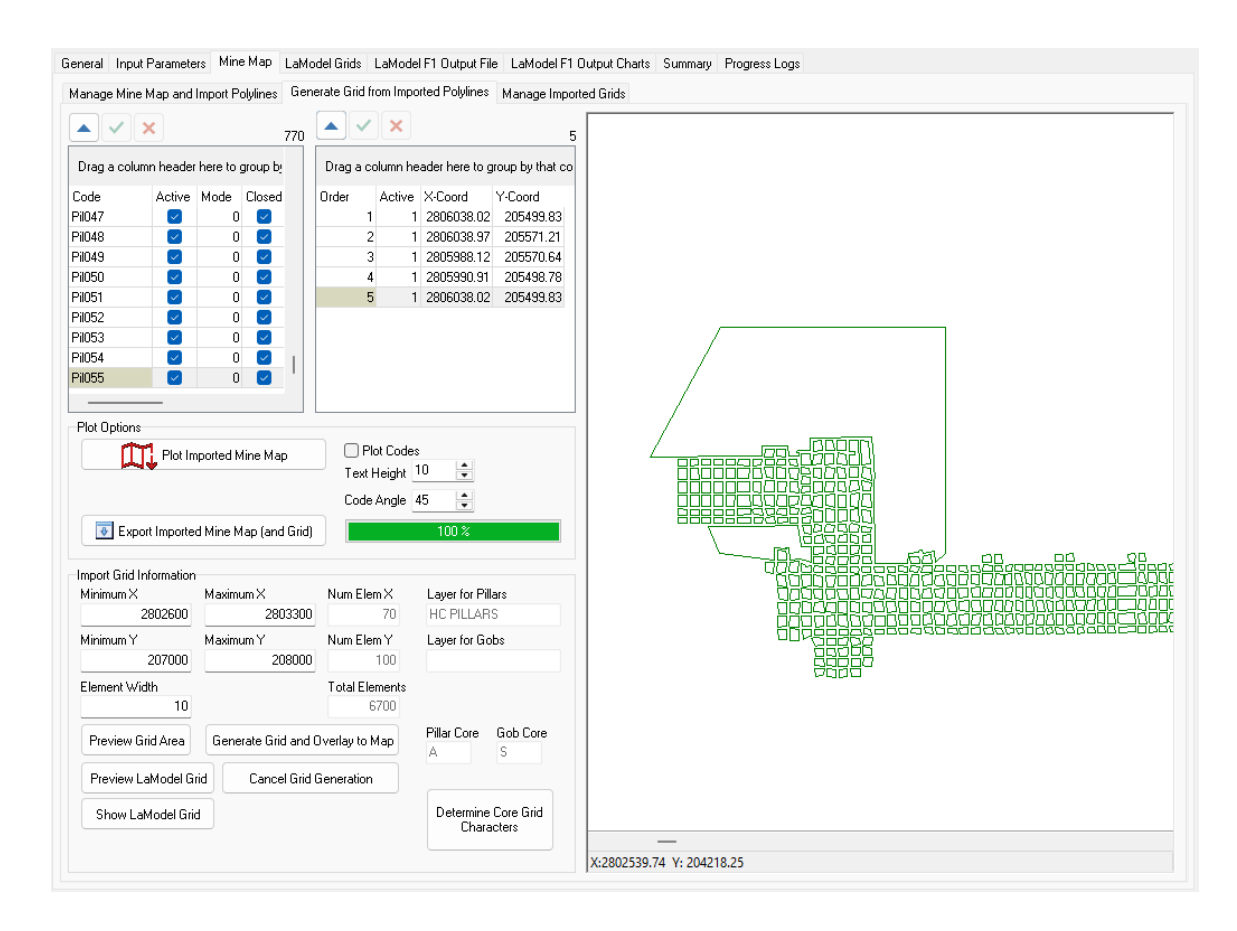
3.1.2.3.2 Generate Grid from Imported Polylines

This tab will function differently for <u>coal</u> and <u>stone</u> scenarios.

If implementing a multiple seam project, duplicate scenarios must be created to generate additional seam grids. These grids may be combined back into a single scenario in the <u>LaModel Grids</u> tab. It is suggested that the user first review the video tutorials in the <u>resource files</u> window.

3.1.2.3.2.1 Coal

The left table at the top of this sub-tab displays each entity (closed polylines). The right table displays the vertices for the selected entity.

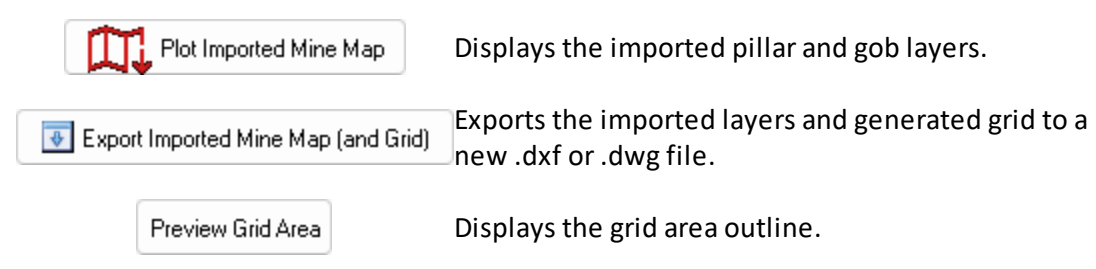


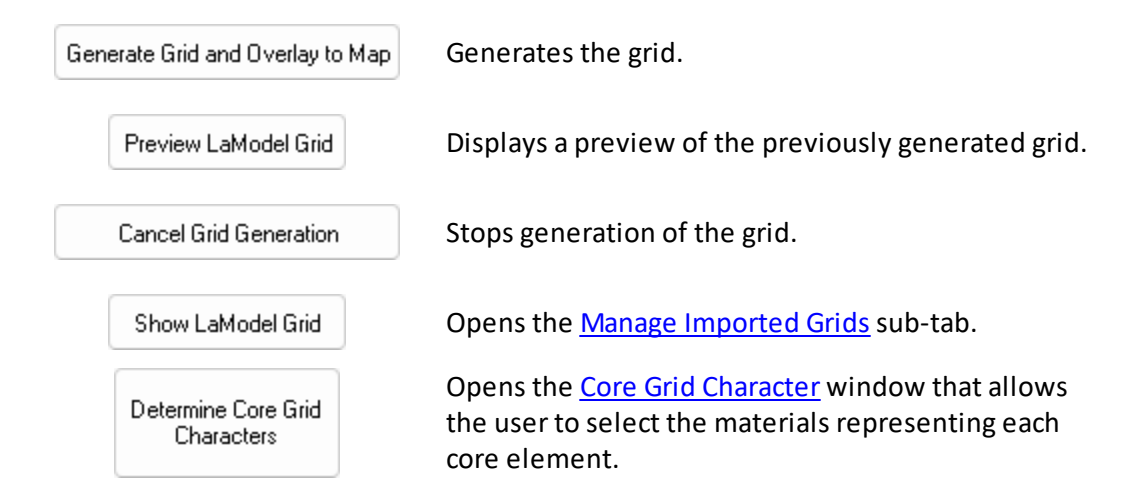
The Plot Options region allows the user to plot the layers imported from the <u>previous sub-tab</u>. The progress bar will activate once grid generation begins.

The Import Grid Information region allows the user to generate the grid. The user should first input the minimum and maximum X & Y coordinates in their respective bars. The element width should then be input in the Element Width bar. The Number of Elements in the X and Y directions will populate automatically, as will the number of Total Elements. Note that the number of elements in both dimensions must be divisible by 10. This is due to the nature of the LaModel processor.

The Layer for Pillars and Layer for Gobs will populate based on the <u>previous sub-tab</u>. The Pillar Character and Gob Character will populate based on the <u>material codes</u>. These refer to the core element for each material set.

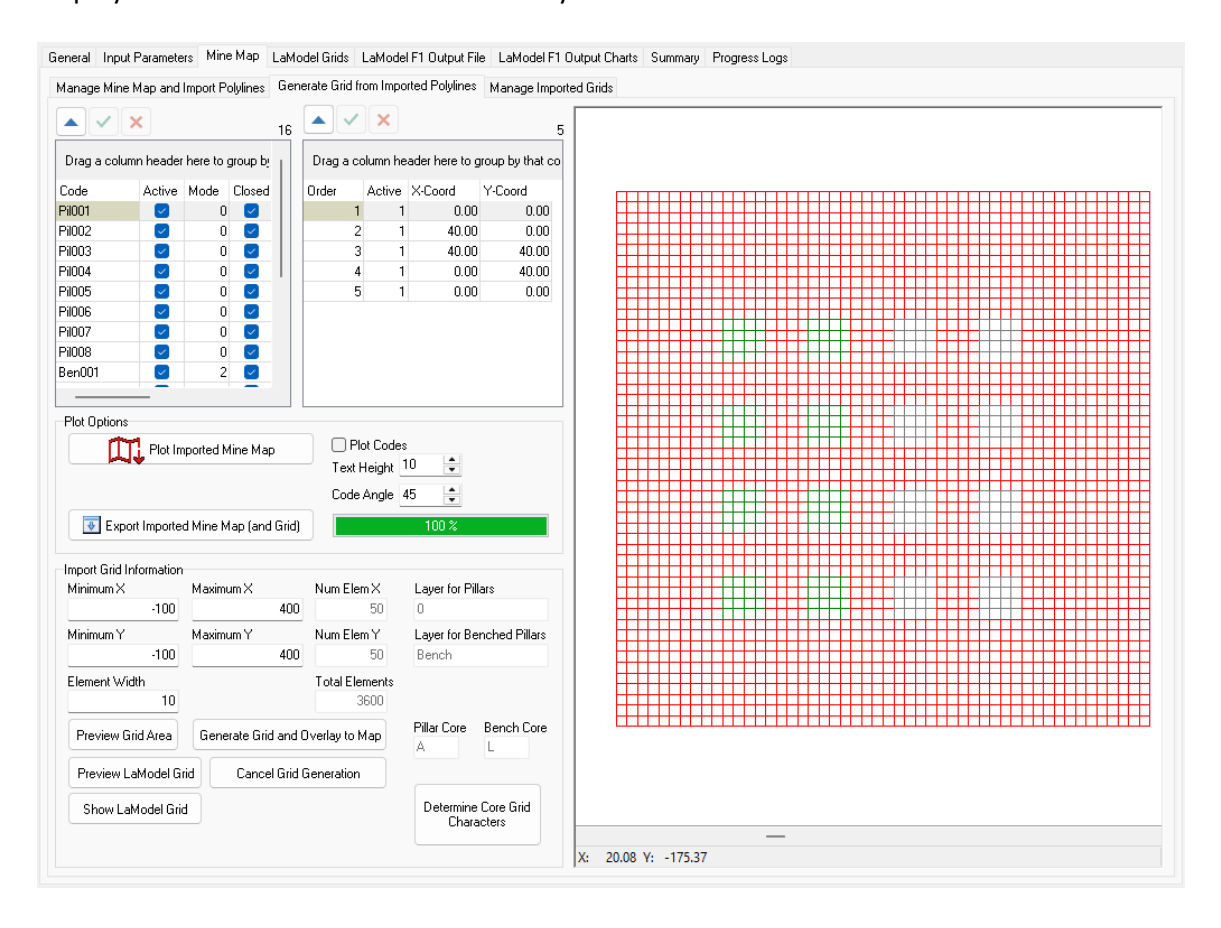
Button Functions





3.1.2.3.2.2 Stone

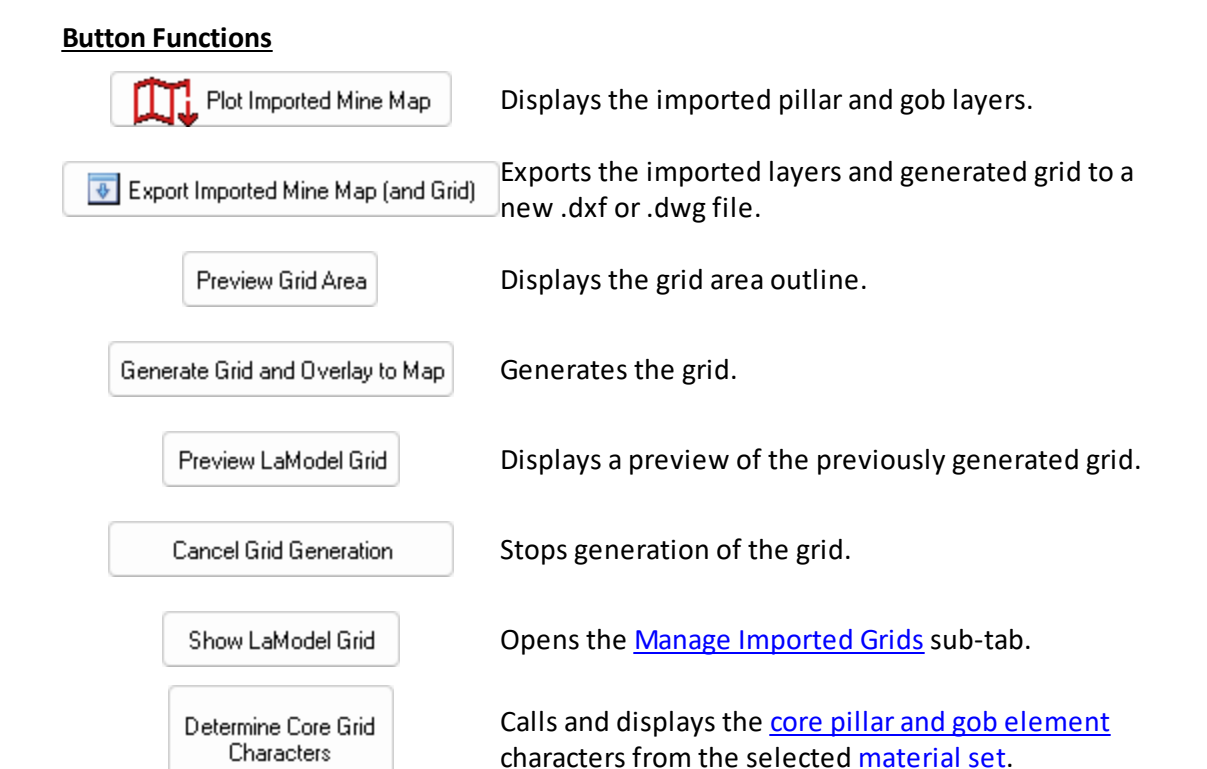
The left table at the top of this sub-tab displays each entity (closed polylines). The right table displays the vertices for the selected entity.



The Plot Options region allows the user to plot the layers imported from the <u>previous sub-tab</u>. The progress bar will activate once grid generation begins.

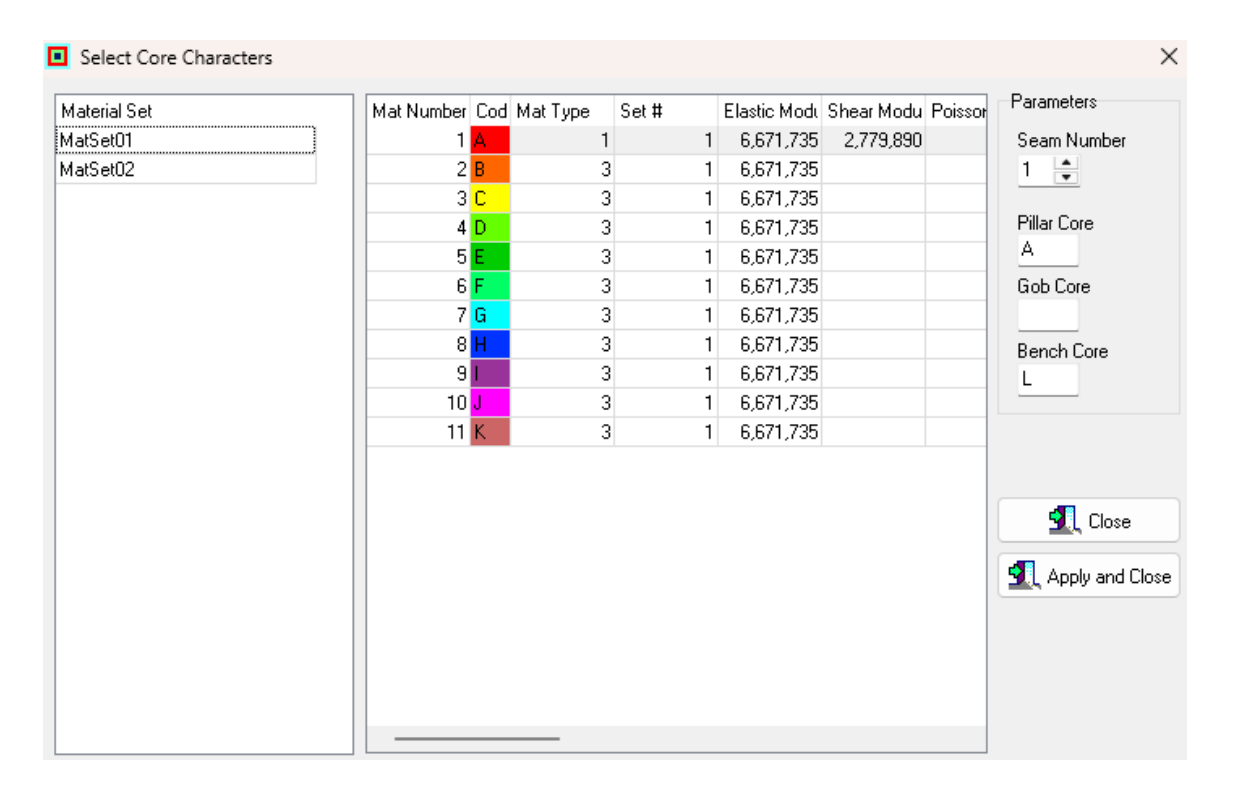
The Import Grid Information region allows the user to generate the grid. The user should first input the minimum and maximum X & Y coordinates in their respective bars. The element width should then be input in the Element Width bar. The Number of Elements in the X and Y directions will populate automatically, as will the number of Total Elements. Note that the number of elements in both dimensions must be divisible by 10. This is due to the nature of the LaModel processor.

The Layer for Pillars and Layer for Benched Pillars will populate based on the <u>previous sub-tab</u>. The Pillar Character and Benched Character will populate based on the <u>material codes</u>. These refer to the core element for each material set.

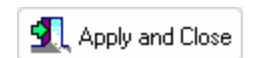


3.1.2.3.2.3 Core Grid Characters

This window allows the user to view a summary of all materials and select one to represent each core. The Parameters region displays input bars for the pillar, gob, and benched pillar core materials.



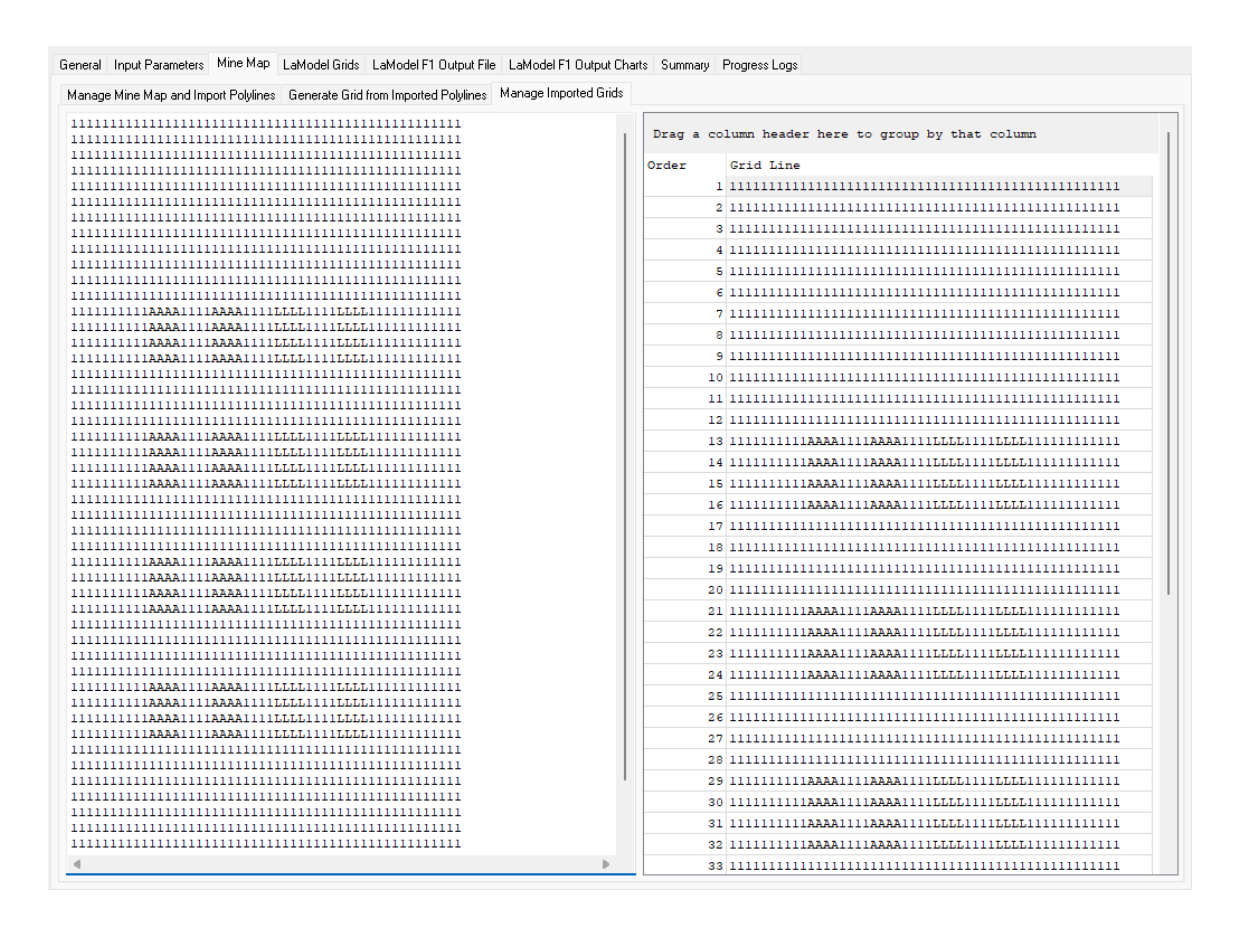
Button Functions



Applies the selected core characters and displays them in the appropriate bars.

3.1.2.3.3 Manage Imported Grids

This sub-tab displays the generated grid in text form, with only three characters displayed: one for entries, one for pillars, and one for gob (coal) or benched pillars (stone).

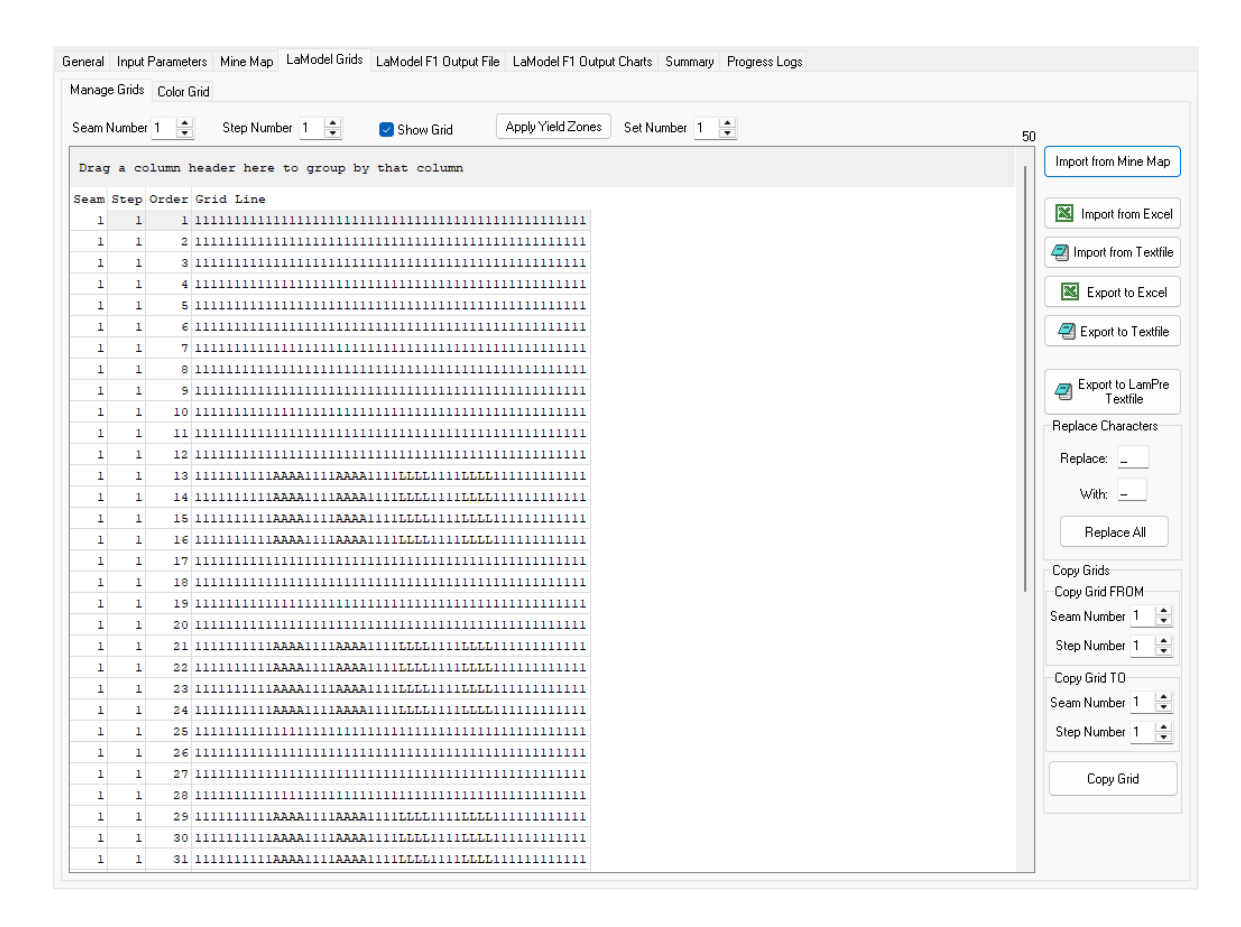


3.1.2.4 LaModel Grids

Grid work occurs in the Manage Grids sub-tab and is displayed in the Color Grid sub-tab.

3.1.2.4.1 Manage Grids

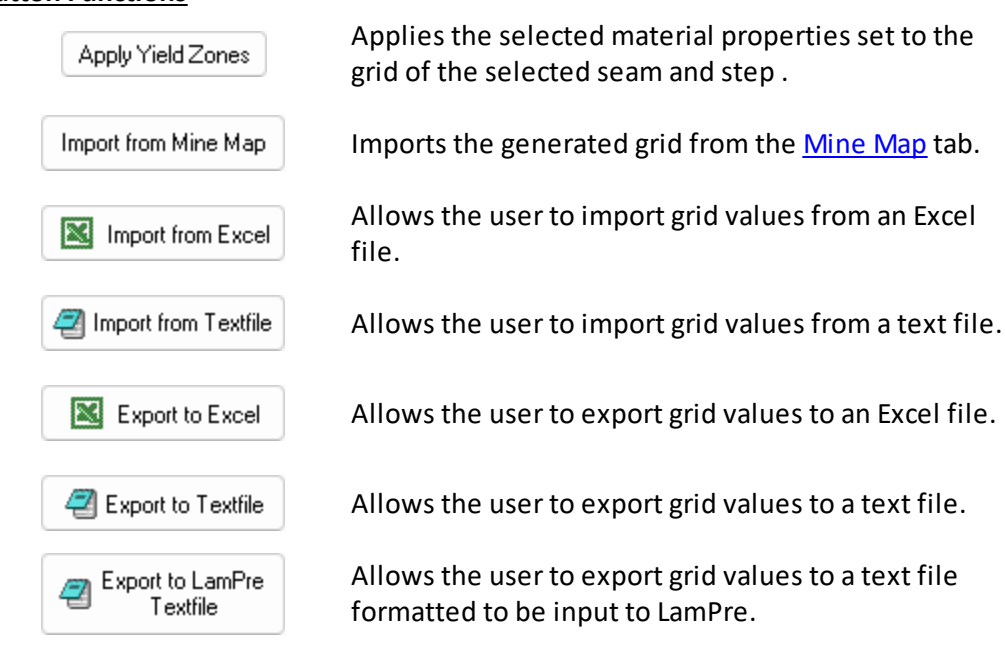
Grids may be imported and exported using the icons on the right of the tab. After import, "Show Grid" must be selected to display the grid. To apply yield zones (material properties), the correct Seam Number, Step Number, and Set Number values must be input. After applying the zones, the Color Grid sub-tab will activate.



At any point after import, values may be altered using the Replace Characters region.

Grids may also be copied from one seam and step to another using the Copy Grids region.

Button Functions



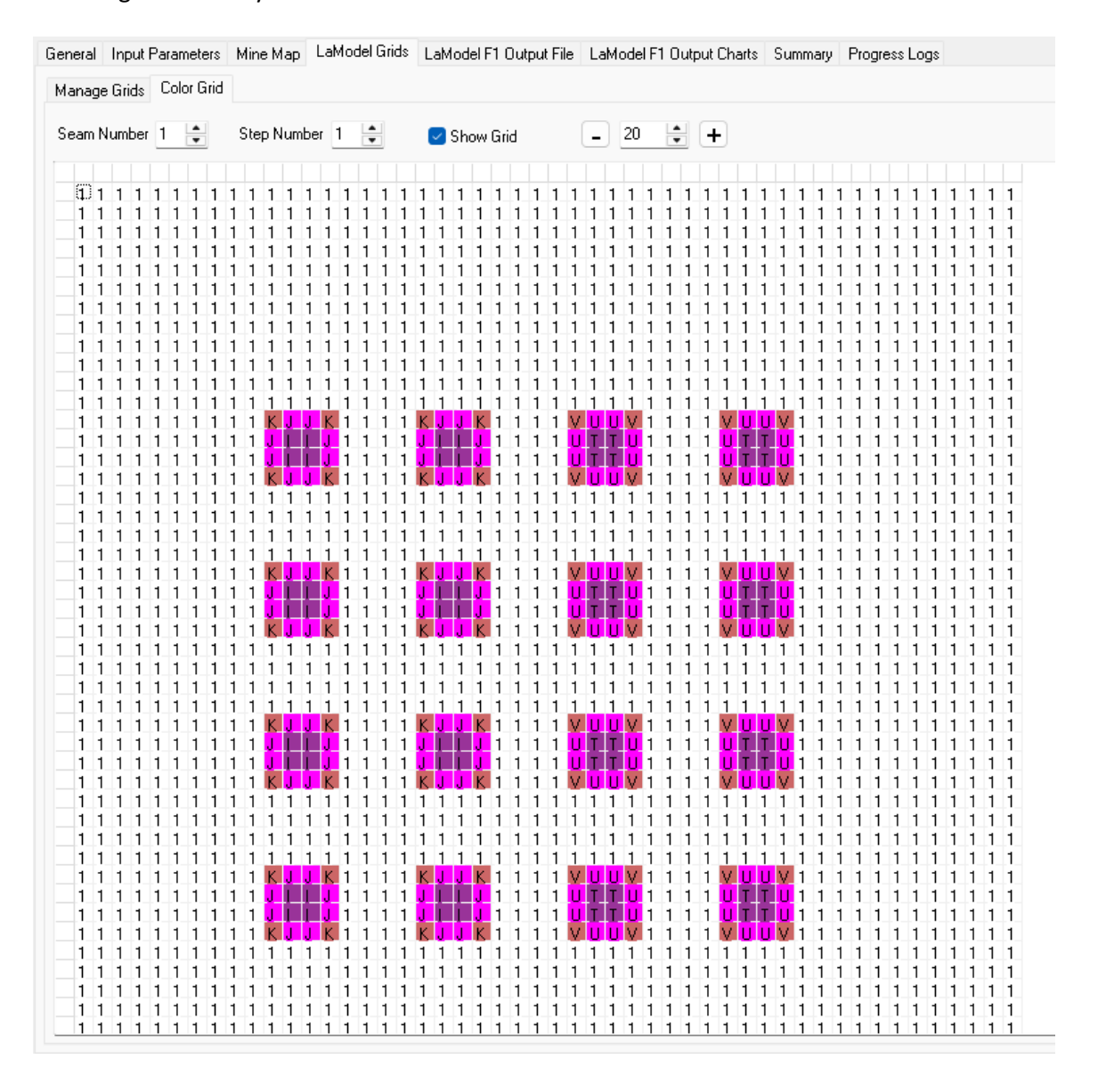


Replaces all instances of the input character with the new character.

Copies the active grid from the selected FROM location to the selected TO location.

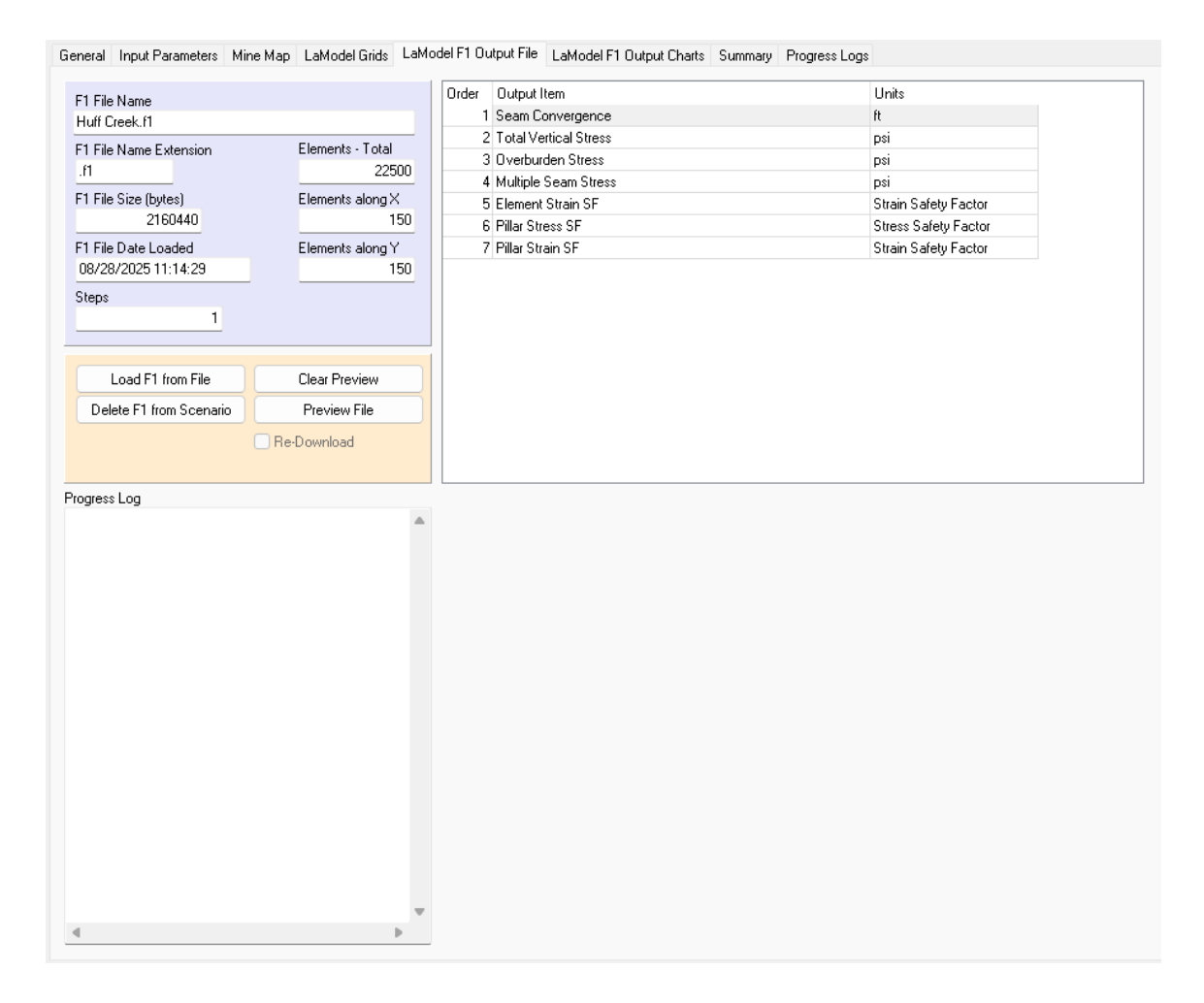
3.1.2.4.2 Color Grid

The Color Grid sub-tab displays a plan view of the grid with applied yield zones. Characters may be changed manually in this window.

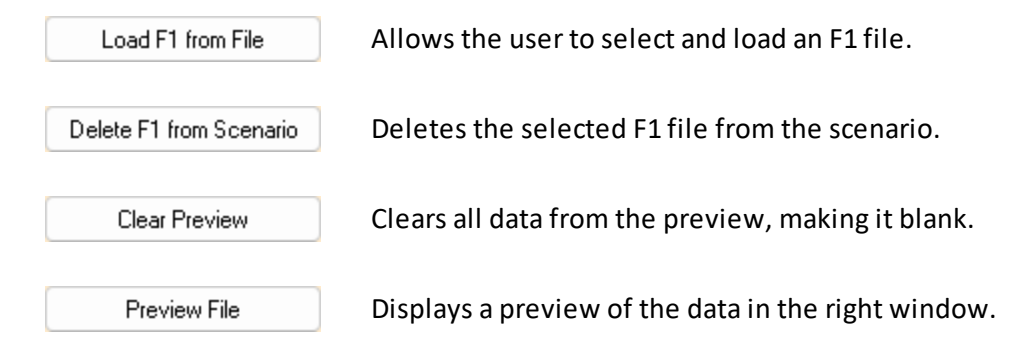


3.1.2.5 LaModel F1 Output File

The LaModel F1 File tab allows the user to load and save F1 files. It also allows for a preview of the file to be shown.



Button Functions

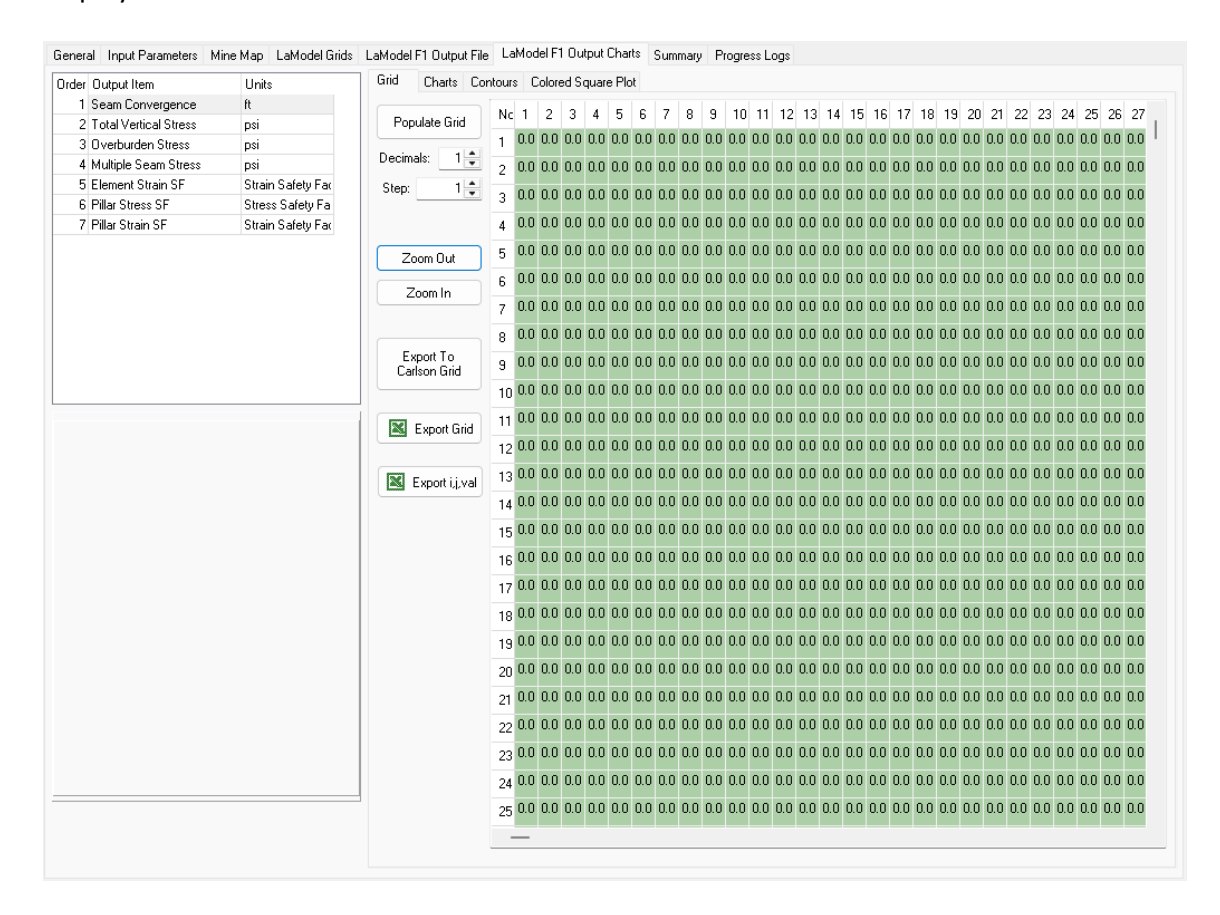


3.1.2.6 LaModel F1 Output Charts

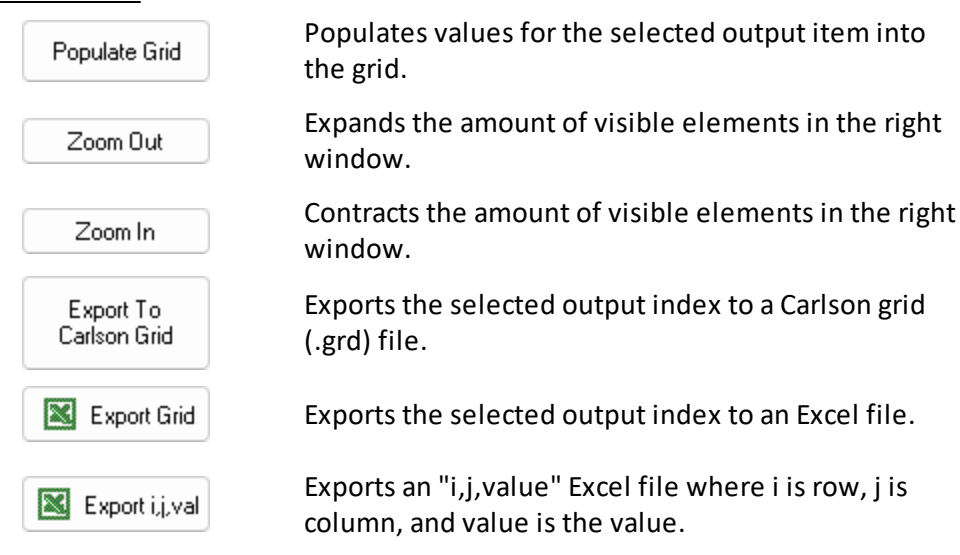
The LaModel F1 Output tab contains four sub-tabs; <u>Grid</u>, <u>Charts</u>, <u>Contours</u>, and <u>Colored Square</u> <u>Plot</u>.

3.1.2.6.1 Grid

The figure below shows a grid associated with the selected stress item in an F1 file. The grid is displayed as numeric values in the units shown in the stress item.

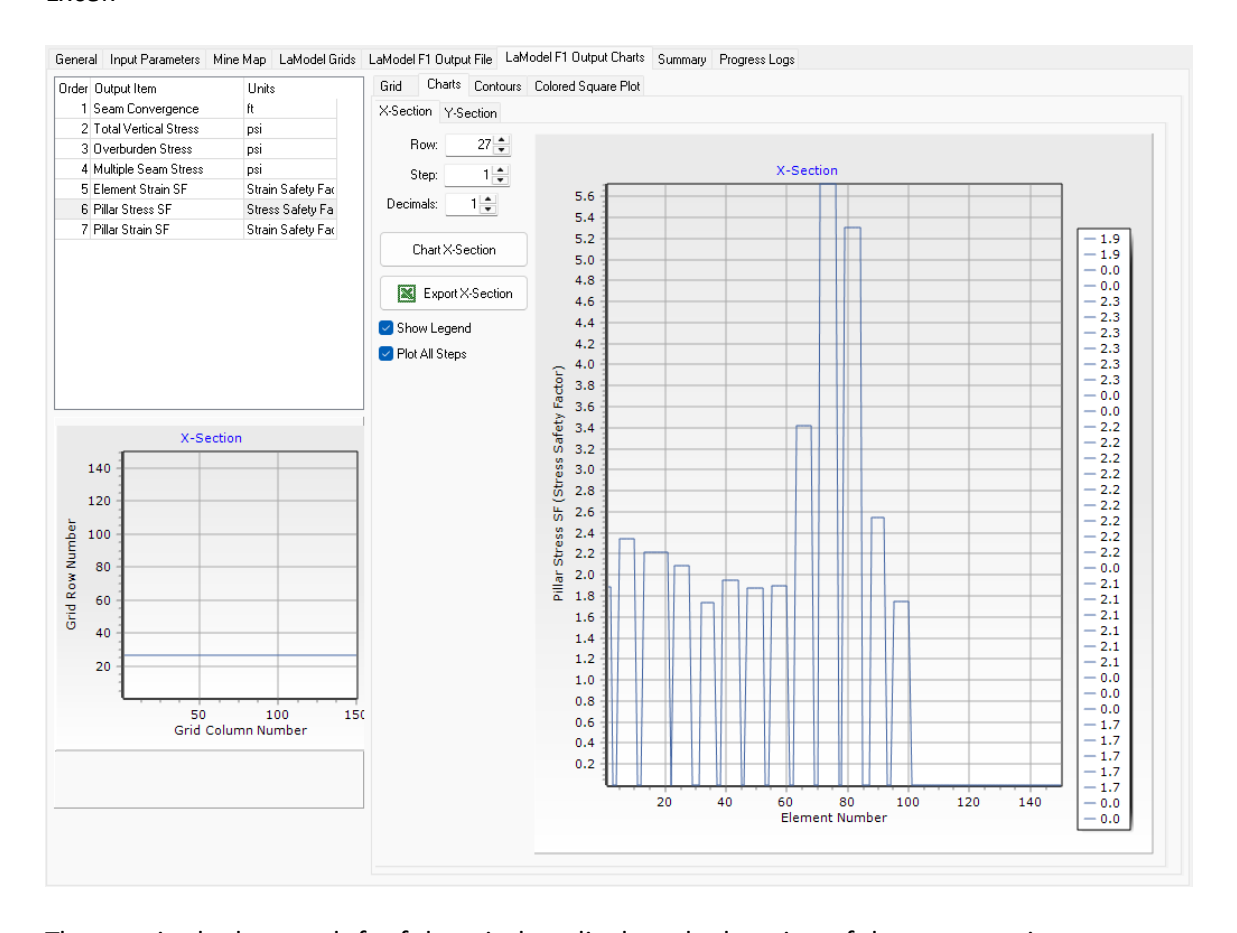


Button Functions



3.1.2.6.2 Charts

The Charts sub-tab allows the user to display cross sections along the X and Y profiles for the selected stress item. It also allows for the results for each section to be exported to Microsoft Excel.

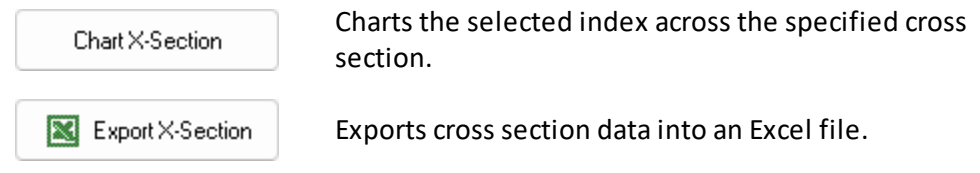


The map in the bottom left of the window displays the location of the cross section.

Selecting "Show Legend" will display the legend for the selected index.

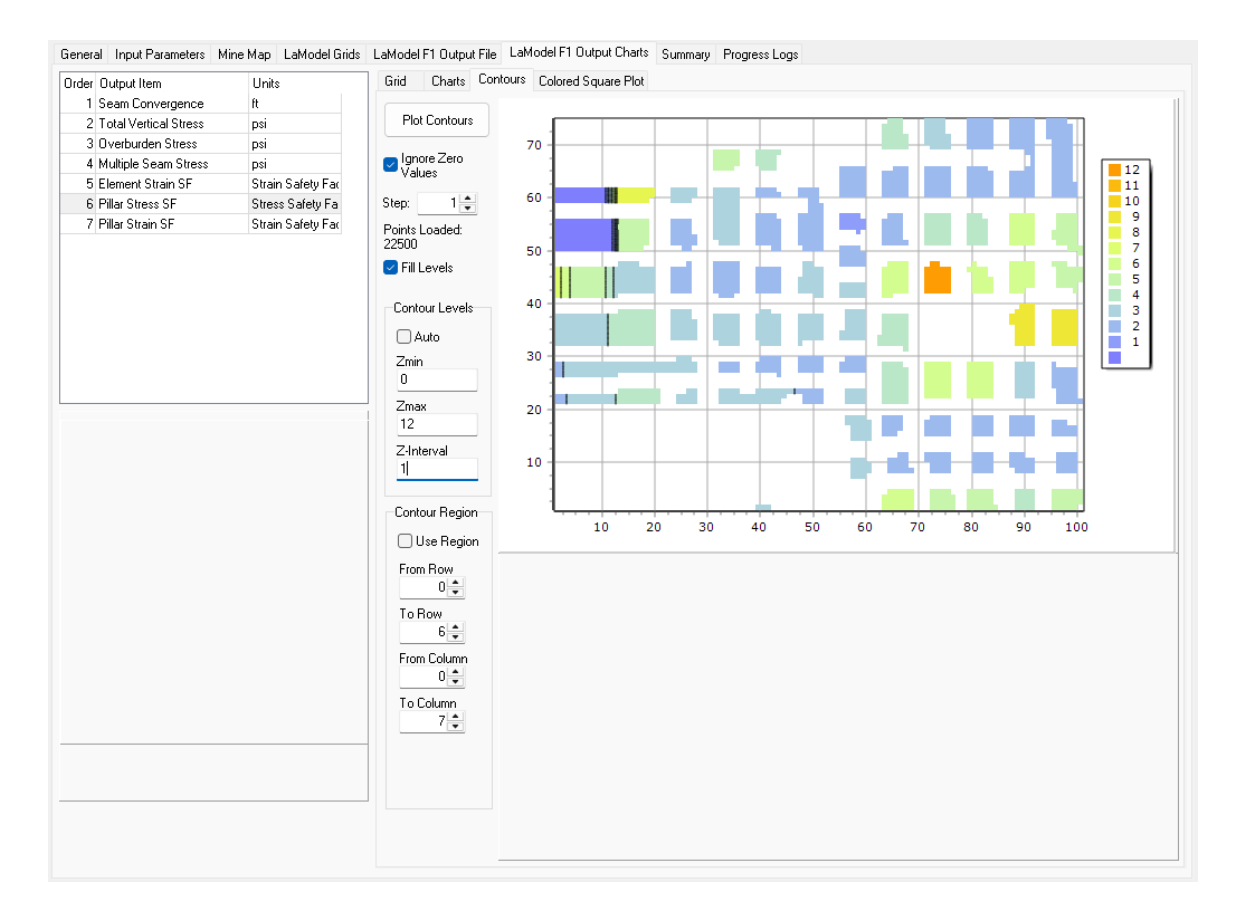
Selecting "Plot All Steps" will plot the cross section for each step on the same chart.

Button Functions



3.1.2.6.3 Contours

The Contours sub-tab allows the user to contour the results for the selected stress index.



In the Contour Levels region, deselecting "Auto" allows the user to customize the range and interval for color coding.

In the Contour Region region, selecting "Use Region" allows the user to zoom in on a smaller area of the map.

Button Functions

Plot Contours

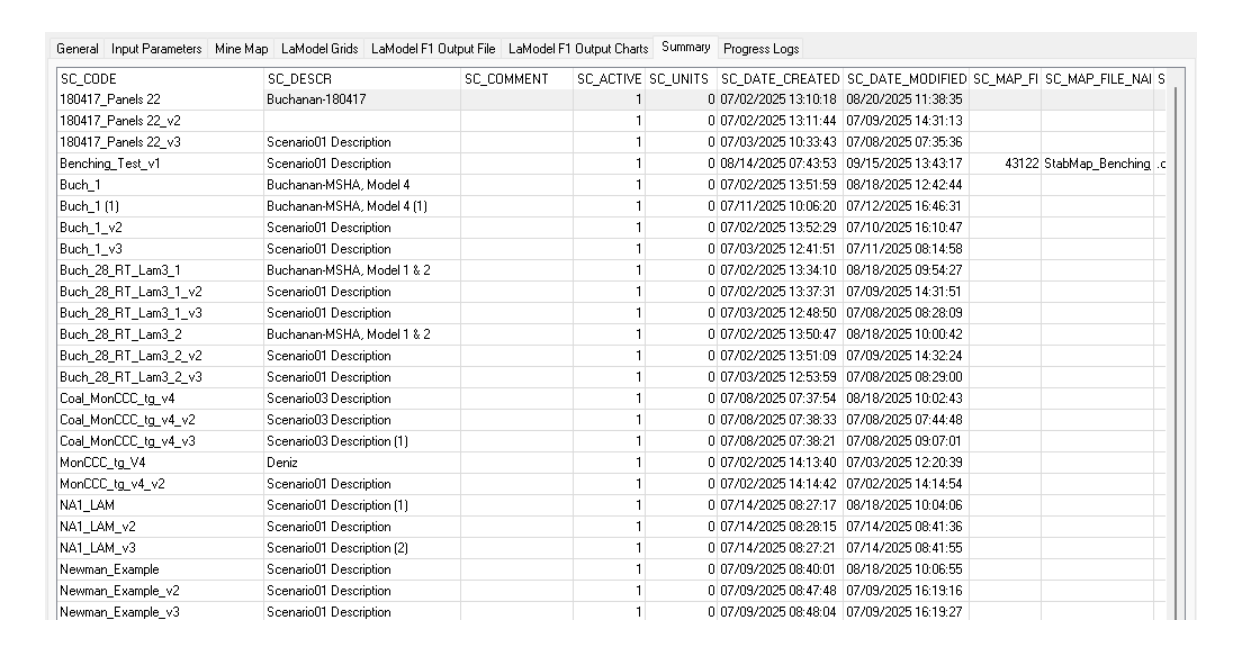
Plots contours for the selected index.

3.1.2.6.4 Colored Square Plot

This section still under development.

3.1.2.7 **Summary**

The Summary tab is displays information for all scenarios in the project.

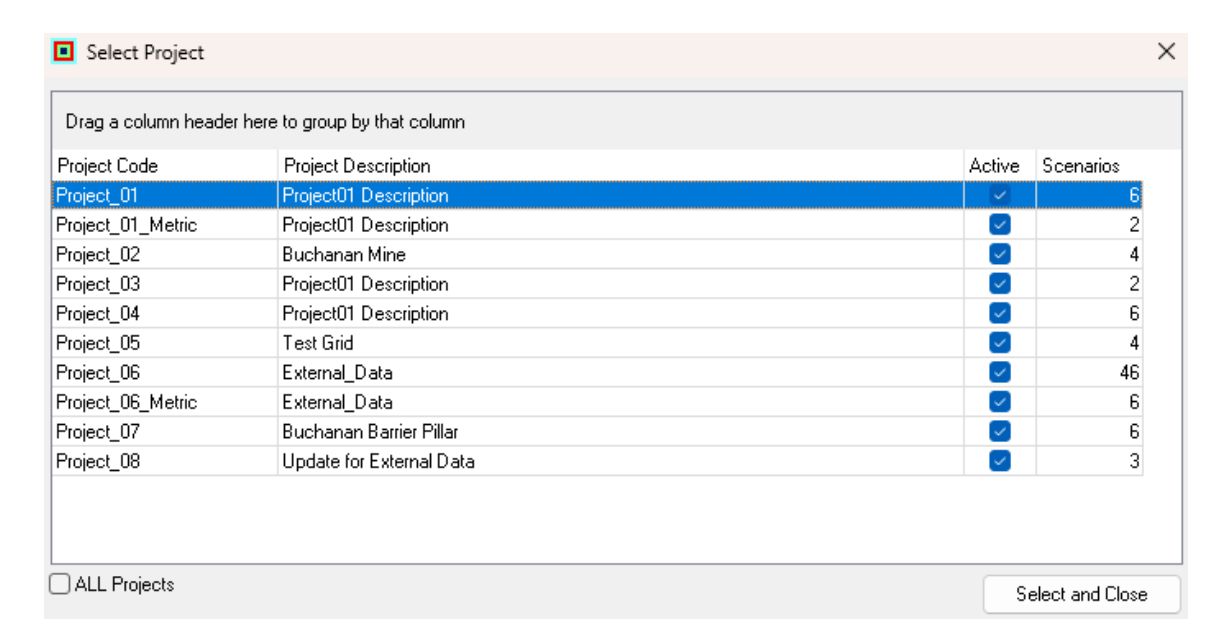


3.1.2.8 Progress Logs

The Progress Logs tab allows the user to see the progress of selected functions.

3.1.3 Select Project

The Select Projects window allows the user to choose the current project. The window initially displays all active projects, selecting the "ALL Projects" check-box in the bottom left will display all projects in the program. Once the desired project is selected, the user will be returned to the Main Menu and the selected project will be listed in the bottom left as the Current Project.



3.1.4 Exit Program

Selecting "Exit Program" under the Projects tab will close the program.

3.2 Tools

The Tools tab comprises one option: Converting Carlson Grids into TOP Grid File.

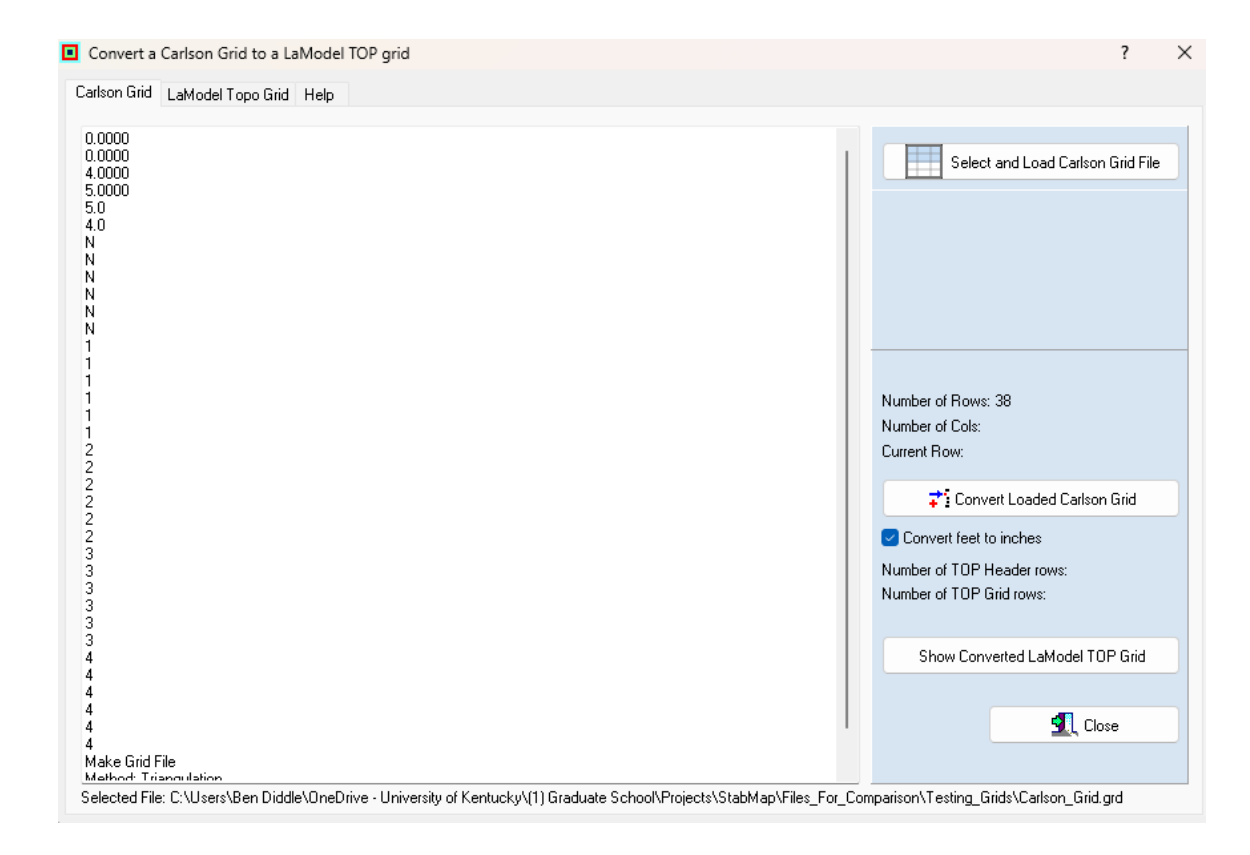
3.2.1 Convert a Carlson Grid File to TOP Grid File

LaModel utilizes a .top file to account for varying overburden depth. Though grid files (.grd) are nearly identical in form and function, they are unable to be read by the program. This tool allows the user to easily convert such grid files to the appropriate form, beginning in the <u>Carlson Grid</u> sub-tab.

To be used by LaModel, the .top file should be share the name of the .inp file and be placed in the same folder. LaModel will automatically read it when run with the "Input Overburden Depth from File" check-box is selected in Input Parameters. Note that this grid should represent the overburden depth, not the actual elevation.

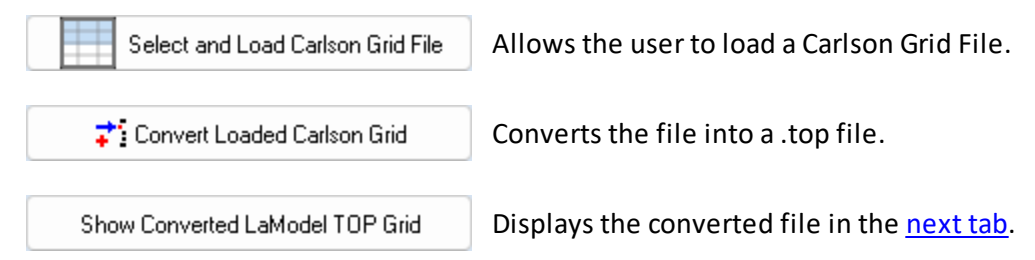
3.2.1.1 Carlson Grid

First, select the Carlson grid file to be converted. NOTE: grid files must be in ASCII format, not Binary. The default setting in Carlson produces binary files, so it is likely the <u>settings must be changed</u>.



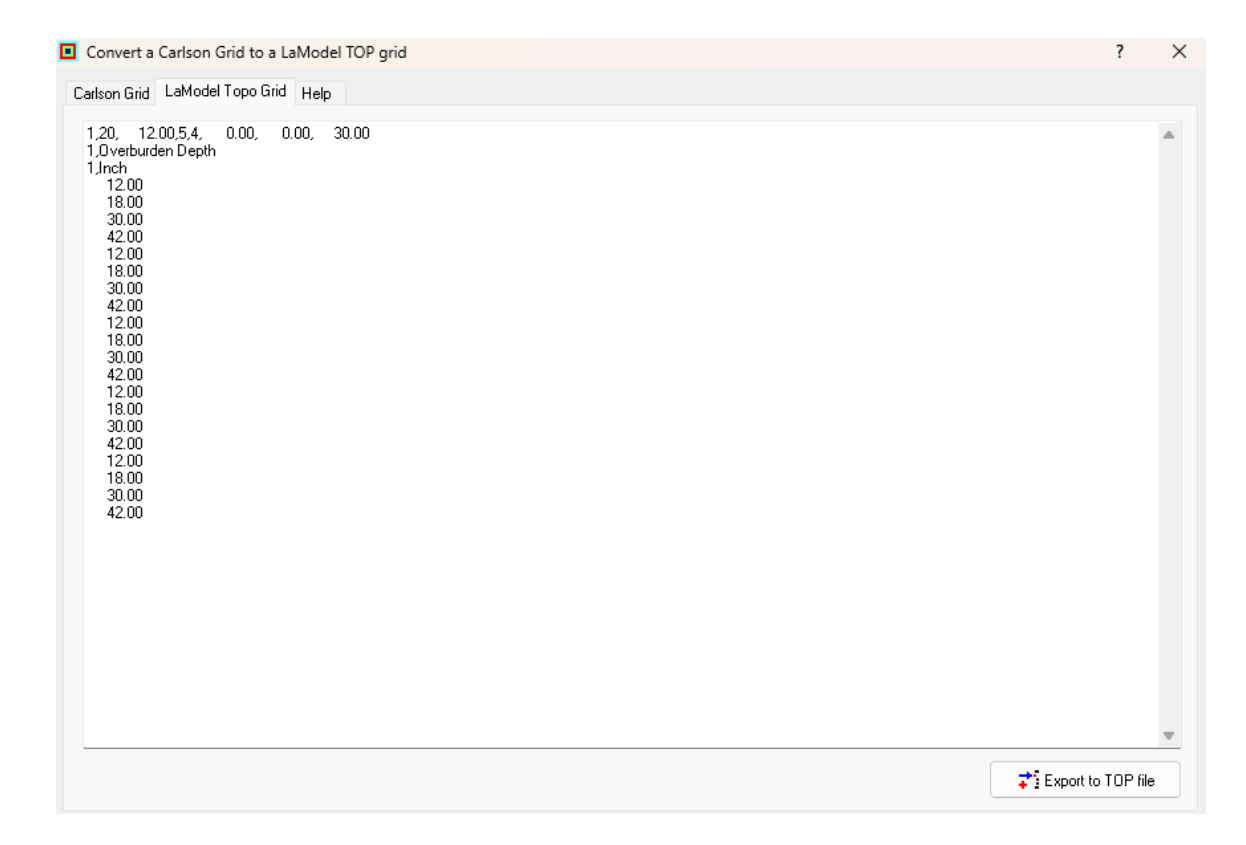
If the file is large, the user will be prompted to display only the header lines. This will not affect the conversion, only speed it up. Once loaded, the file may be converted. Ensure the "Convert feet to inches" check-box is selected.

Button Functions

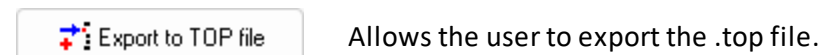


3.2.1.2 LaModel Overburden Grid

The converted file will be displayed here. If large, only the header will appear. The file may now be exported.



Button Functions



3.2.1.3 Help

This routine converts a Carlson Grid file to a LaModel TOP file.

- if the input is in feet it will convert to inches.
- if the input is in meters, it will keep it in meters

Notes1:

- A Carlson grid with 100x100 cells has 101x101 grid points
- A TOP grid with 100x100 cells has 100x100 grid points, which correspond to the center of each Carlson cell.

Notes2:

- The imported GRID file should be in ASCII format
- There are no other options to set before import as a Carlson Grid file has a well defined format.
- The name of the currently selected file for import is displayed below the grid.
- Upon conversion, feet are converted to inches and the header is changed to that of a TOP file.
- The TOP file can be exported as an ASCII (text) file
- Errors during data import are logged.

Notes on Carlson Software Grids and LaModel Grids:

A Carlson grid (.GRD) file has the following format:

- Line 1 is the lower left Y coordinate
- Line 2 is the lower left X coordinate
- Line 3 is the upper right Y coordinate
- Line 4 is the upper right X coordinate
- Line 5 is the number of grid cells along the X axis
- Line 6 is the number of grid cells along the Y axis

The grid generator generates a grid that has NX+1 nodes along the X axis and NY+1 nodes along the Y axis. All calculations are based on the grid notes.

The rest of the lines are the Z values of the grid intersects starting from the lower left moving in the left to right direction and ending at the upper right.

If the intersect has no value, the letter 'N' is saved instead of the Z value for Null values.

Annotated Example of Carlson Grid

337906.7268 (ymin)

1028543.4120 (xmin)

339086.7268 (ymax)

1030663.4120 (xmax)

106.0 (nx=number of cells along x; there are nx+1 points for nx cells)

59.0 (ny=number of cells along y; there are ny+1 points for ny cells)

2289.887 (elevation of first point; points are listed row by row, left to right and from the bottom up)

2292.6615 (elevation of second point)

A LaModel Grid is specified using

- The lower left X coordinate, the lower left Y coordinate
- Grid cell size (same for X and Y)
- Number of Grid Cells in the X Direction
- Number of Grid Cells in the Y Direction

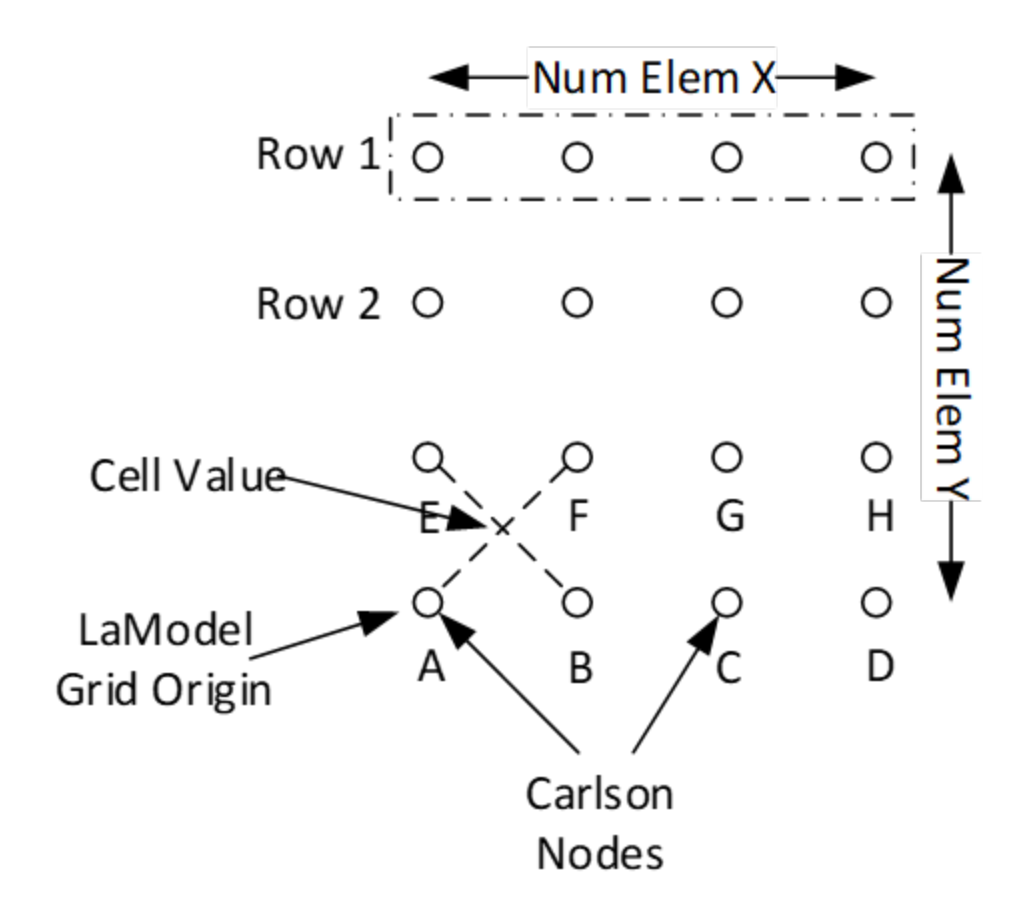
LaModel Grid calculations are performed at each element and they can conceptually be assigned to the center of each element ((e.g., the middle of ABFE).

When a LaModel grid is saved into an INP file, then it is saved row by row and the first row corresponds to the top row of the grid.

A LaModel TOP file, follows the same convention, i.e. it is specified using

- The lower left X coordinate, the lower left Y coordinate
- Grid cell size (same for X and Y)
- Number of Grid Cells in the X Direction
- Number of Grid Cells in the Y Direction

Note that LaModel grids and Carlson grids need to be aligned so that the seam and topo grids line up.



3.2.1.4 Debug

This tab is activated by a check-box under **Settings**.

3.3 Options

The Options tab allows the user to access two windows: <u>Settings</u> and <u>Backup / Restore Database</u>.

3.3.1 Settings

The Settings window comprises six tabs:

General

<u>LaModel Program</u>

Backup

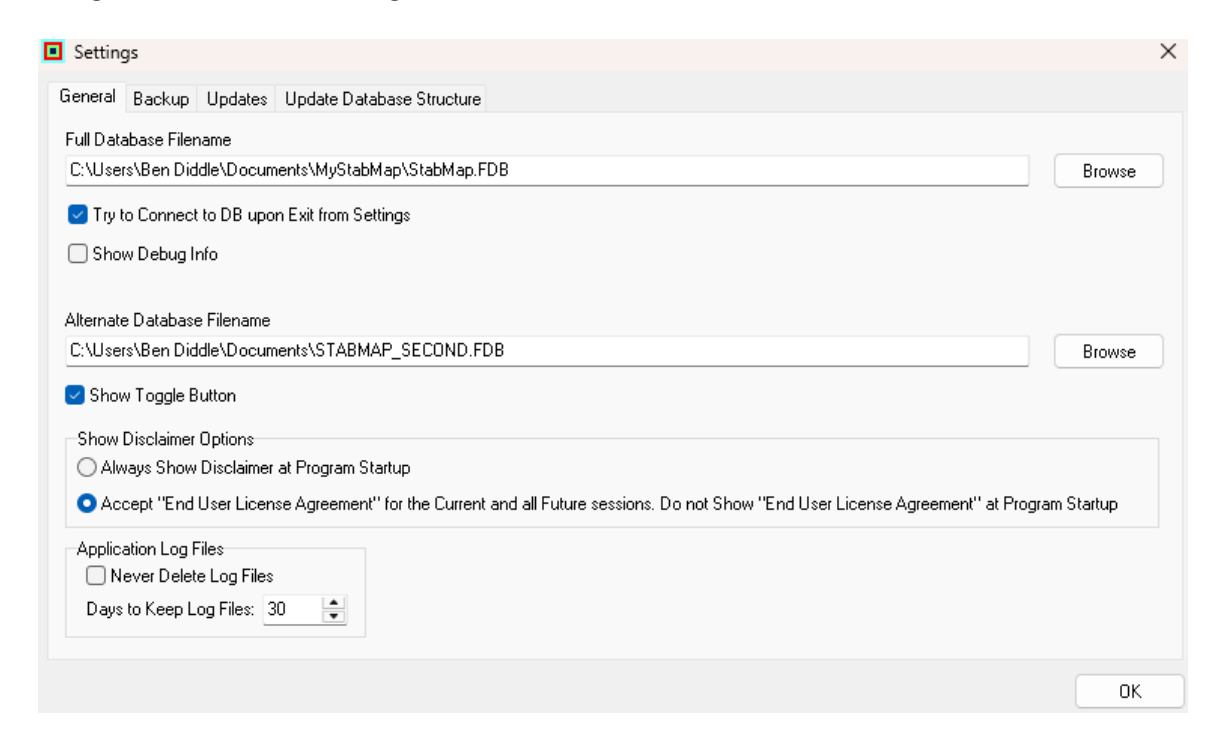
<u>Updates</u>

<u>Update Database Structure</u>

Setup a New Database

3.3.1.1 General

The general tab under settings is shown below.

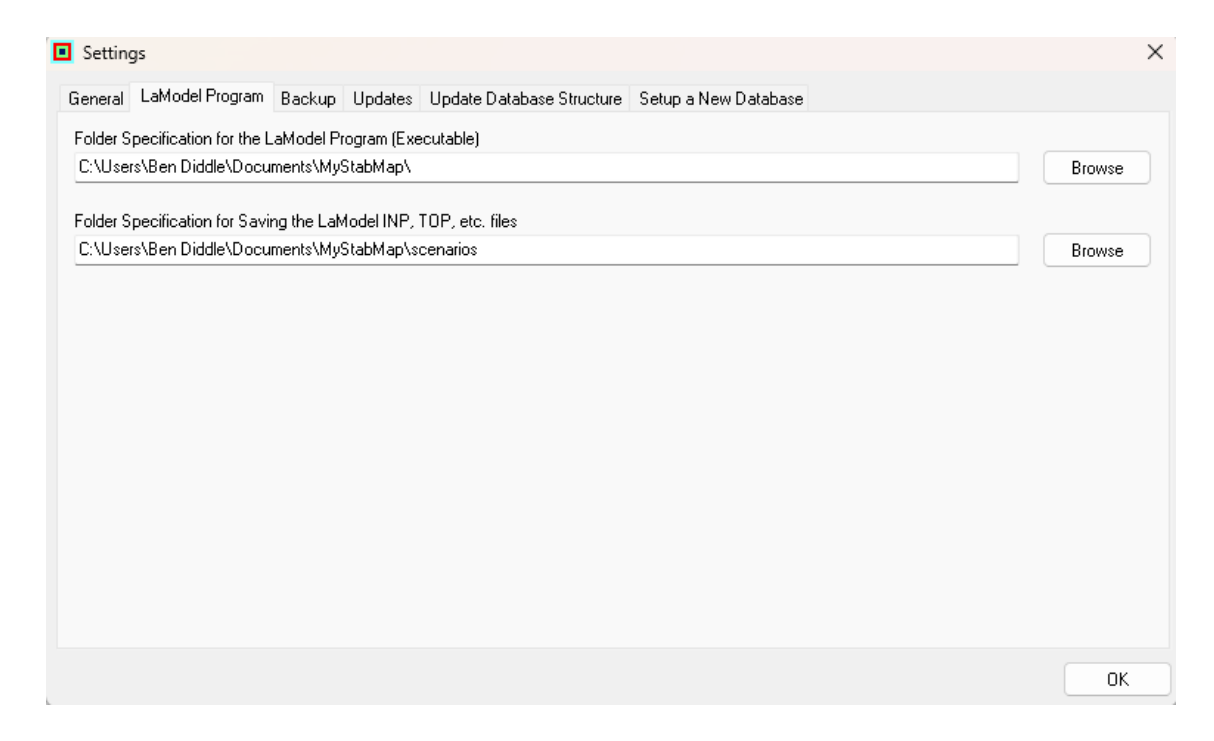


The utility of each of the fields in the general tab is explained below:

- 1. The Full Database Filename field displays the file location of the primary database file (.fdb). The user has the option to move the database file to any location and then specify that location in this field.
- 2. Selecting the "Try to connect to DB upon exit from Settings" check-box will prompt the program to connect to the selected database file when the settings window is closed.
- Selecting the "Show Debug Info" will allow for certain debug information to be displayed in progress logs and/or the program log file. To do so, several debug tabs throughout the program will be activated.
- 4. The Alternate Database Filename displays the file location of the secondary database file (.fdb). The user has the option to move the database file to any location and then specify that location in this field.
- 5. Selecting the "Show Toggle Button" check-box will generate a Toggle button on the Main Menu. This button can be used to switch the database file that the program is connected to immediately.
- 6. The Show Disclaimer Options region allows the user to determine whether the disclaimer will appear every time the program starts up.
- 7. The Application Log Files options allow the user to determine the amount of time that log files are kept on the hard drive. The default duration is 30 days.
- 8. Selecting the "Never Delete Log Files" check-box will retain the log files indefinitely. Log files are stored under Documents\MyStabmap\logs.

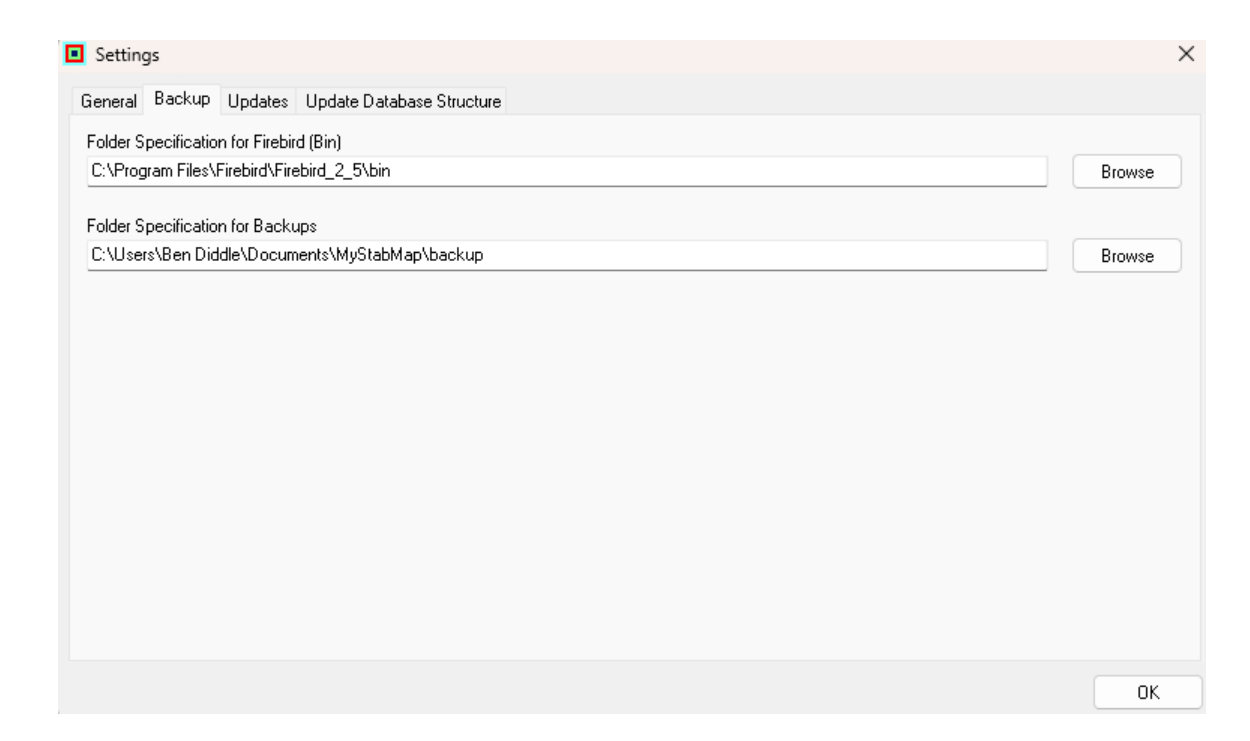
3.3.1.2 LaModel Program

The LaModel Program tab under settings is shown below. It allows the user to select the file location for both the LaModel executable file as the resulting INP, F1, etc. files. The executable file should be stored in the same location as the StabMap FDB file to allow functionality.



3.3.1.3 Backup

The backup tab under settings is shown below.

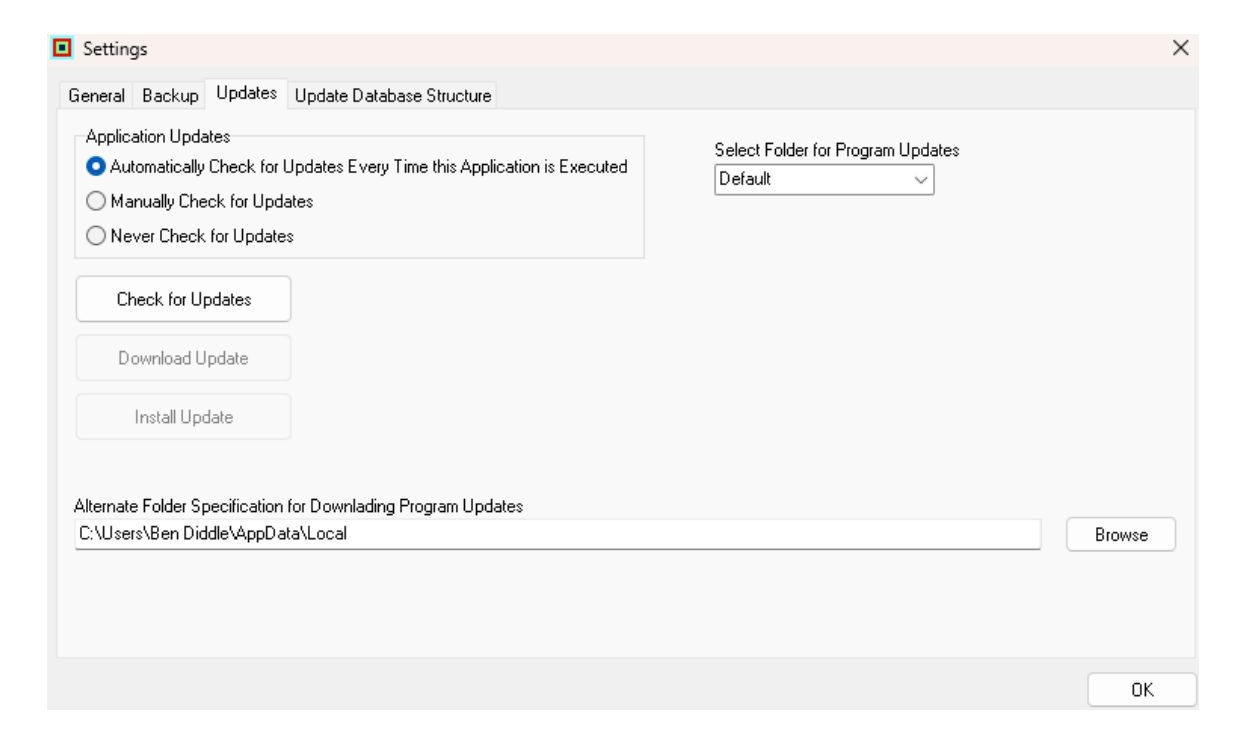


The utility of each of the fields in the backup tab is explained below:

- 1. The Folder Specification for Firebird (Bin) field displays the file location of Firebird Runtime.
- 2. The Folder Specification for Backups field displays the file location where database backup files are stored.

3.3.1.4 **Updates**

The updates tab under settings is shown below.

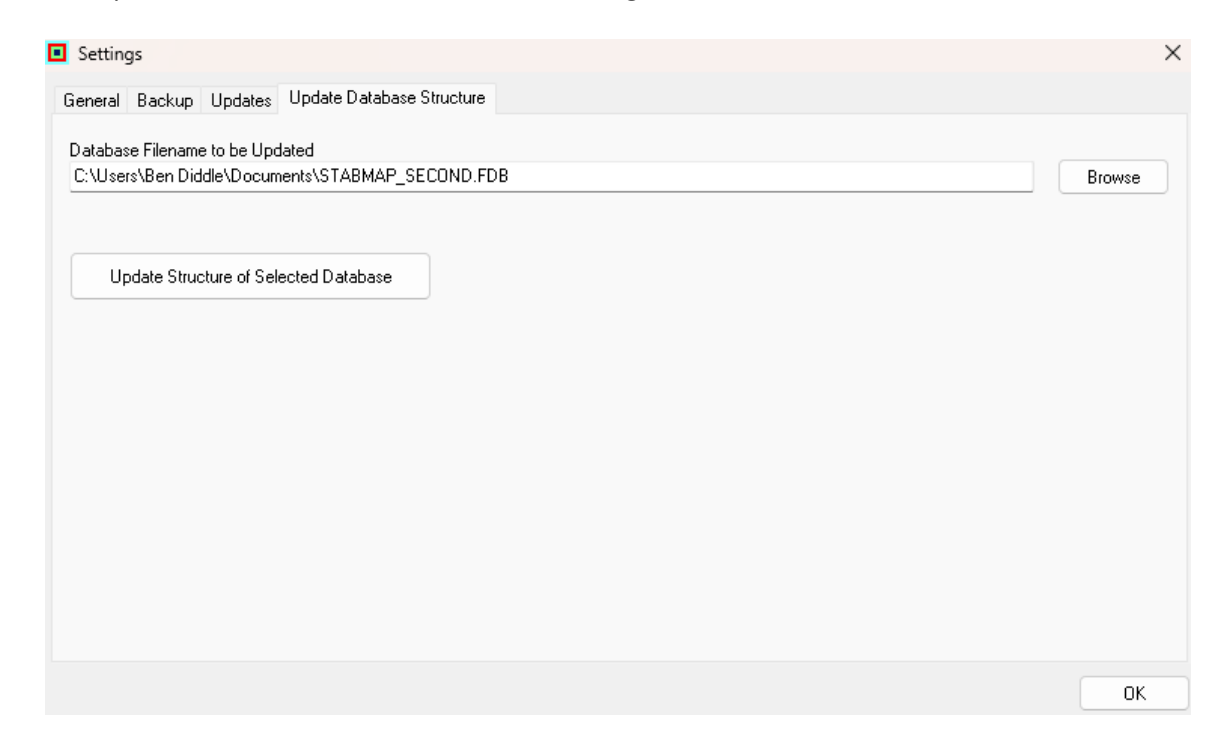


The utility of each of the fields in the updates tab is explained below:

- 1. The Application Updates region allows the user to determine how the program checks for updates.
- 2. Selecting "Automatically Check for Updates Every Time this Application is Executed" will prompt the program to search the server for updates whenever it is initiated.
- 3. Selecting "Manually Check for Updates" will prompt the program to immediately search the server for updates.
- 4. Selecting "Never Check for Updates" will prompt the program to stop searching the server for updates upon initiation.
- 5. The Select Folder for Program Updates allows the user to change where the program looks for program updates.
- 6. Selecting "Default" will save downloaded installers in the default folder, which is C: \Users\Username\AppData\Local\StabMap
- 7. Selecting "Alternate" will save downloaded installers to the folder specified in the Alternate Folder Specification for Downloading Program Updates field at the bottom of the tab, which displays the precise file location for that folder.

3.3.1.5 Update Database Structure

The update database structure tab under settings is shown below.



The installer only updates the active database.

When working with multiple databases, other databases will need to be updated manually before being utilized in the program. This feature allows the user to select other databases to be updated to the structure of the latest version.

3.3.1.6 Setup a New Database

This tab allows the user to create a new database.

The program will disconnect from the current database, copy that to a new database named "archive_yyyymmddhhnn" and will create a new (blank) database with the same name as the current database. The user can access the previous database by connecting to the "archive_yyyymmddhhnn" database.

Once created, the database may be linked to the program by providing the file location and name under the <u>General tab</u>.

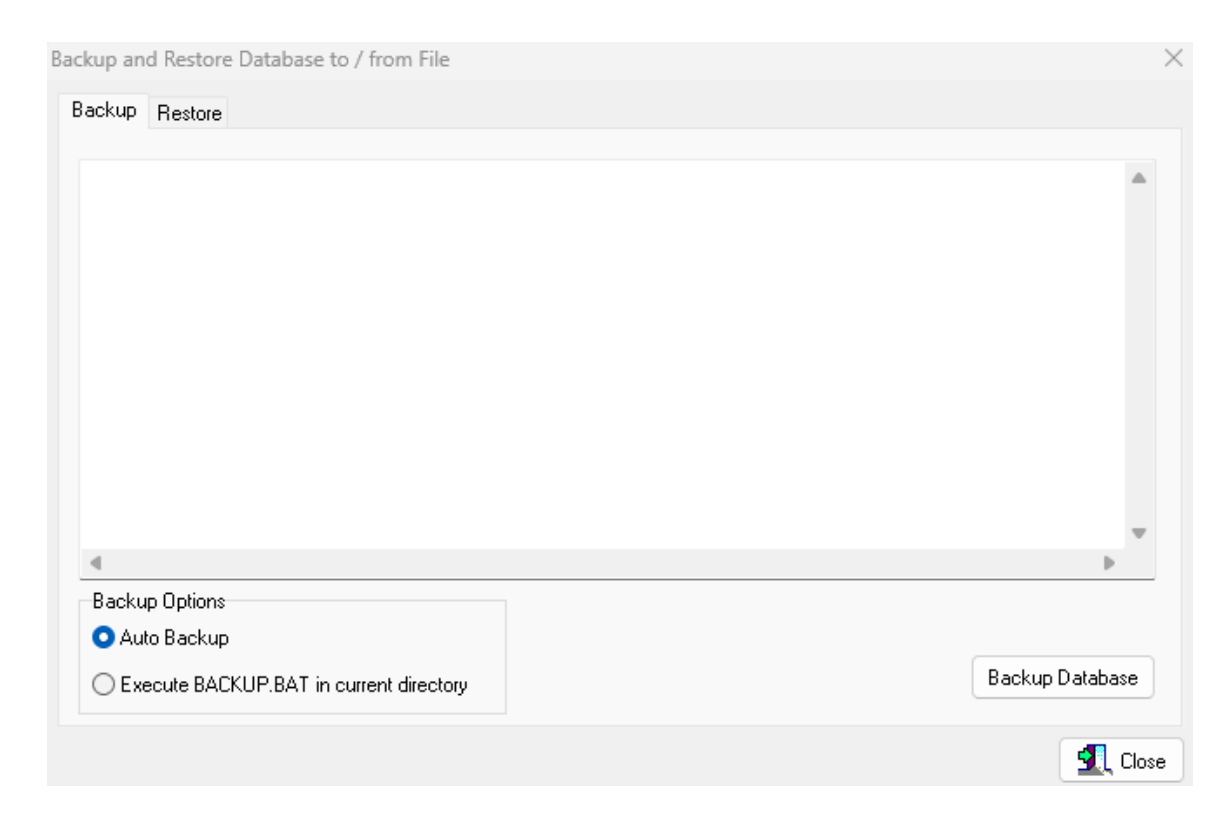
Button Functions

Setup a New Database

Creates of a new database.

3.3.2 Backup / Restore Database

The Backup tab allows the user to create a backup of the database. Backing up the database in this manner cleans up any incomplete records or transactions and reduced the file size of the database.



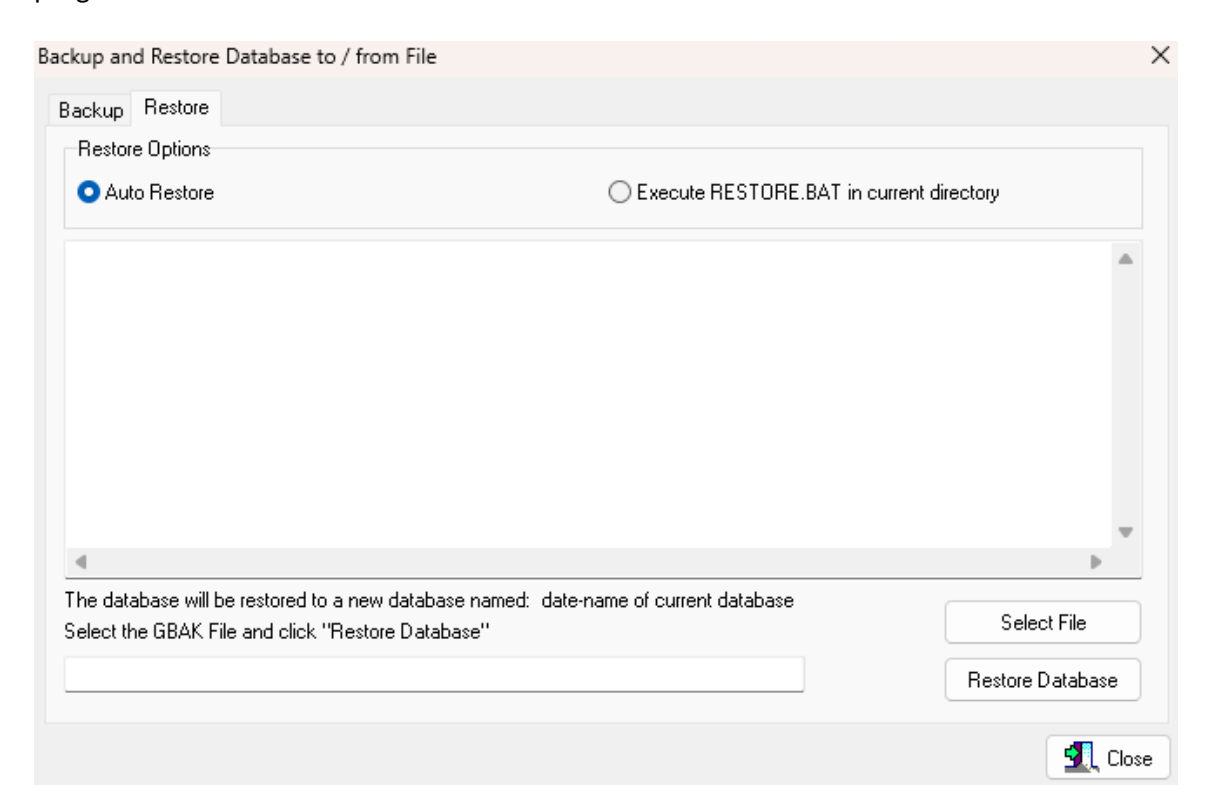
Selecting the Auto-Backup option will execute a simple one line script to backup the database into the folder specified in the <u>Settings tab</u>.

Selecting the Execute Backup.BAT in Current Directory option allows the user to build their own DOS script to backup the database.

Button Functions

Backup Database Executes the database backup.

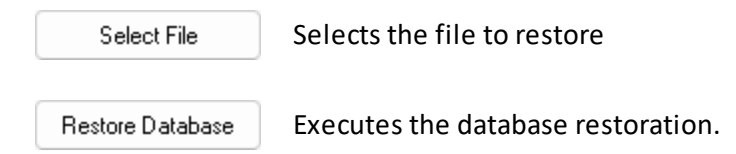
The Restore tab allows the user to restore a backed-up database to a format usable by the program.



Selecting the Auto-Restore option will execute a simple one line script to restore the database.

Selecting the Execute Restore.BAT in Current Directory option allows the user to build their own DOS script to restore the database.

Button Functions



3.4 Help

The Help window contains six options; <u>Context Sensitive Help File</u>, <u>StabMap Users Manual</u>, <u>Resource Files</u>, <u>Updates</u>, <u>Disclaimer</u>, and <u>About</u>.

3.4.1 Context Sensitive Help File

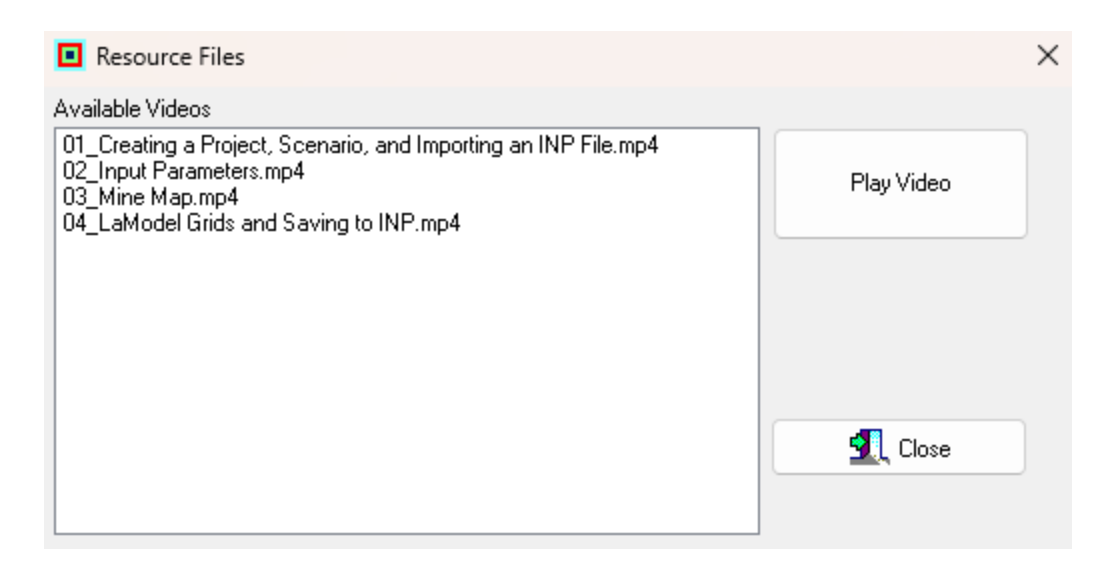
The Context Sensitive Help function allows the user to access help files for each aspect of the program. Press F1 on any open form and the respective help window will be displayed.

3.4.2 StabMap Users Manual (PDF)

Selecting this option will open the PDF version of the StabMap Users Manual.

3.4.3 Resource Files

This window houses a library of tutorial videos walking through the workflow of the program for both coal and stone scenarios.



3.4.4 Program Updates

The Program Updates option accesses a help file form that contains information regarding each specific program update.

3.4.5 Disclaimer

Selecting Disclaimer will open the Disclaimer window, the same that appears upon program startup.

End User License Agreement

This End User License Agreement ('Agreement') is between You and Owners (defined below) and governs your use of the StabMap software and its documentation.

By using StabMap, You are agreeing to be bound by the terms and conditions of this Agreement. If You are not willing to be bound by this Agreement, do not download, install, or use StabMap.

Grant of License

Owners grant You a personal, revocable, nonexclusive, nontransferable, limited license to download, install, and use StabMap subject to terms and conditions set forth in this Agreement.

Except as otherwise restricted by this Agreement, StabMap and any information derived from its use may be used by You for any lawful purpose, including educational, research, regulatory, and commercial uses.

Restrictions

You may not sell, charge for, sub-license, rent, or lease StabMap.

You are not permitted to decompile, disassemble, reverse engineer, or otherwise attempt to discover the source code of StabMap (except as expressly permitted by applicable law).

You may not repackage, translate, adapt, vary, modify, alter, create derivative works based on, or integrate any other computer programs with StabMap, in whole or in part, without the express written consent of Owners (except as expressly permitted by applicable law).

Warranty Disclaimer

OWNERS MAKE NO REPRESENTATION OR WARRANTY OF ANY KIND, WHETHER EXPRESS OR IMPLIED (EITHER IN FACT OR BY OPERATION OF LAW) WITH RESPECT TO StabMap, INCLUDING, WITHOUT LIMITATION, WITH RESPECT TO THE SUFFICIENCY, ACCURACY, OR UTILIZATION OF, OR ANY INFORMATION OR OPINION CONTAINED OR REFLECTED IN, StabMap, OR INFORMATION GENERATED BY OR THROUGH THE USE OF StabMap. OWNERS EXPRESSLY DISCLAIM ALL WARRANTIES OR CONDITIONS OF MERCHANTABILITY, FITNESS FOR A PARTICULAR PURPOSE, OR NON-INFRINGEMENT. StabMap and accompanying documentation, if any, is provided "as is".

Limitation of Liability

You are responsible for the consequences of any use of StabMap whether or not such use was consistent with this Agreement.

In no event shall the Owners, or any authors, contributors, employers (including universities), or other persons associated with the development and publishing of StabMap, be liable to any party (including You or any of your directors, officers, employees, agents, representatives, contractors, clients, or any third party) for direct, indirect, special, exemplary, incidental, or consequential

damages (including but not limited to lost profits, procurement of substitute goods or services; loss of use, data, or profits; or business interruption) however caused and on any theory of liability, whether in contract, strict liability, or tort (including negligence or otherwise), arising out of the use of StabMap and its documentation.

Governing Law

This Agreement shall be governed by the laws of the Commonwealth of Kentucky without reference to its conflict of laws provisions. You consent to exclusive jurisdiction and venue of the state and federal courts sitting in Kentucky.

Ownership of StabMap

StabMap was developed as a collaborative effort by Zach Agioutantis, and Deniz Tuncay with support from Alpha Foundation for the Improvement of Mine Safety and Health.

Direct any inquiries concerning this Agreement to:

Zach Agioutantis
Department of Mining Engineering
University of Kentucky
Lexington, KY 40506

Miscellaneous

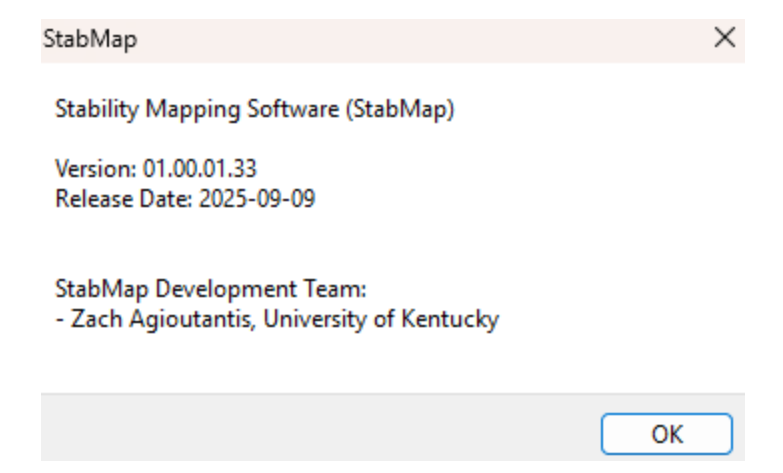
Failure to enforce any right under this Agreement will not waive that right. This Agreement may be terminated by Owners at any time and for any reason.

This Agreement does not grant You the right to distribute StabMap. Parties may obtain a licensed copy of StabMap by contacting the Owners or by downloading it from https://minegroundcontrol.com/.

Although this license to use StabMap is provided to You without charge, Owners reserve the right to charge maintenance fees, subscription fees, or other fees for future updates, expansions, services, or related products.

3.4.6 About

The About window displays the version information, release date, and authorship information.



This page is intentionally left blank. Remove this text from the manual template if you want it completely blank.

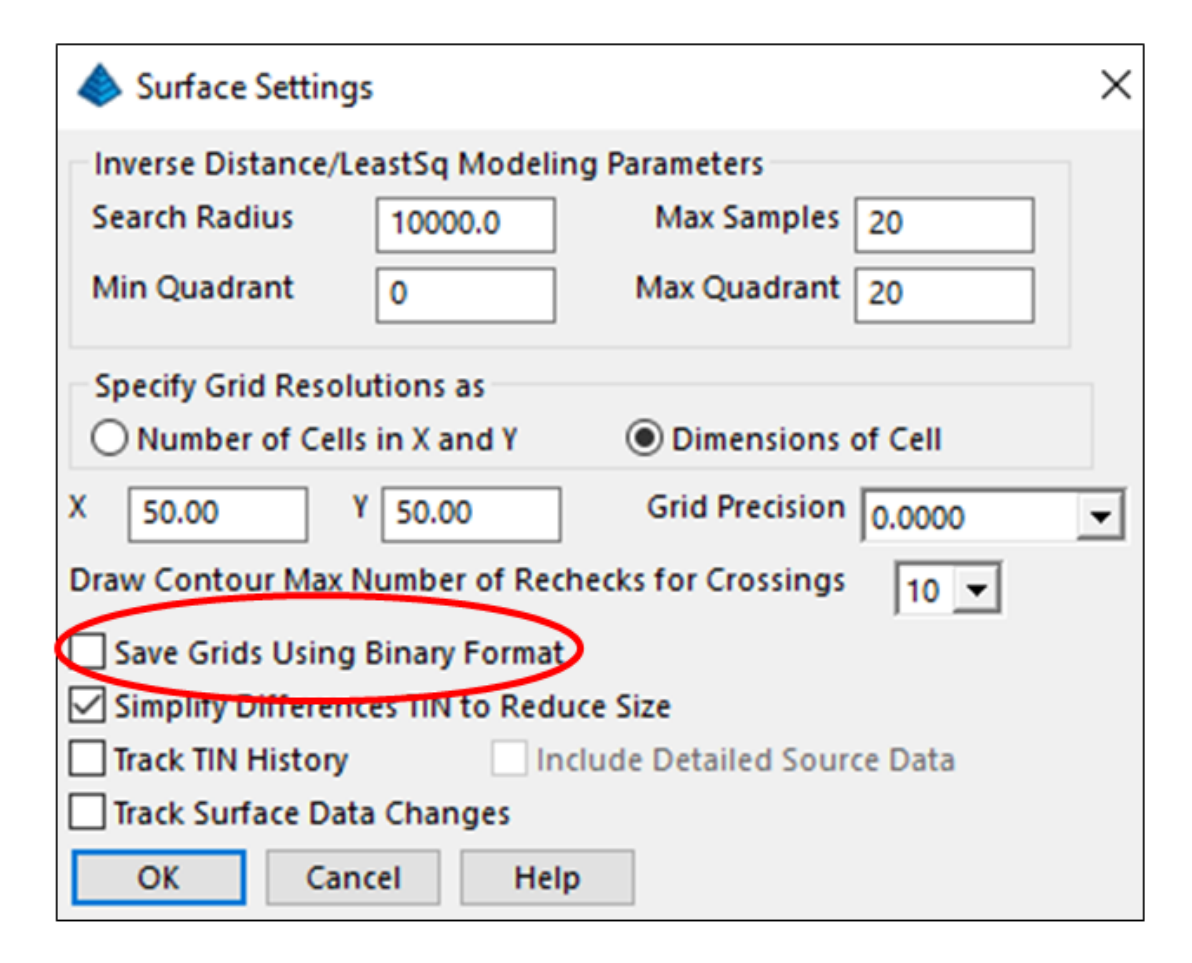


Using Carlson Grids in StabMap

4 Using Carlson Grids in StabMap

StabMap reads grid files in ASCII format, not binary. Carlson's default grid file (.grd) output is in a binary format.

To switch the output file type, go to Settings > Carlson Configure > Surface Settings. Then uncheck "Save Grids Using Binary Format" as shown below.



Lamination Thickness Calculation

5 Lamination Thickness Calculation

Rock mass stiffness is largely determined by two parameters: rock mass modulus and lamination thickness. To calibrate the model, it has been found most effective to keep the modulus the same while varying the lamination thickness. The metric for calibration is realistic loading at the extent of abutment zone. Because field measurements of abutment zones are difficult to obtain, it is best to use generalized equations based on historical measurements. This process is detailed below:

First, the known or estimated properties required for calculating the laminated load are input. These include:

- The Rock Mass Elastic Modulus (E, psi), Rock Mass Density $(\gamma, lbs/in^3)$, and Rock Mass Poisson's Ratio (v), which are generally weighted averages based on the geologic column.
- Seam Depth (*H*, inches)
- Seam Thickness (*M*, *inches*)
- Seam Elastic Modulus (E_s , psi)
- Half Width of Panel (L, inches)
- Location of Point (x, inches)

An initial estimate for Rock Mass Lamination Thickness (t, inches) is made. The following calculations are conducted to determine the Laminated Load at Point X (W):

Lambda (λ , *inches*) is calculated using Equation 1.

$$\lambda = \frac{t}{\sqrt{12(1-v^2)}}\tag{1}$$

Overburden Load (q, psi) is calculated using Equation 2.

$$q = \gamma * H \tag{2}$$

Parameter A (A, 1/inch) is calculated using Equation 3.

$$A = \sqrt{\frac{2E_s}{E\lambda M}} \tag{3}$$

Laminated Stress at Point X ($\sigma_i(x)$, psi) is calculated using Equation 4.

$$\sigma_i(x) = qL * A * e^{-(Ax)} \tag{4}$$

Laminated Load at Point X (W, lbs/inch) is calculated using Equation 5.

$$W = \int_{0}^{x} \sigma_i(x)dx = -mqL * e^{-(Ax)} + mqL$$
 (5)

Next, calculations begin to determine the Mark-Bieniawksi Load at Point X (W_{MB}). First, the Insitu Coal Strength (S_i , psi) is input.

Extent of Abutment Zone (D, inches) is calculated using Equation 6.

$$D = 9.3 \sqrt{\frac{H}{12}} * 12 \tag{6}$$

Percent of Gob Load on Abutment (m, percentage) is calculated using the process outlined below (Equations 7-12):

An Abutment Angle (α , degrees) is assumed , 21 degrees is the default. Then the panel is deemed supercritical or subcritical, based on Equations 7 & 8.

$$H * Tan(\alpha) < L : Supercritical$$
 (7)

$$H * Tan(\alpha) > L : Subcritical$$
 (8)

The Total Panel Load (TPL, lbs/inch) is calculated using Equation 9.

$$TPL = 2L * H * \gamma \tag{9}$$

The Ratio (R) is then determined using Equation 10 for a supercritical panel (R_{SS}) or Equation 11 for a subcritical panel (R_S) .

$$R_{ss} = \frac{H^2 * Tan(\alpha)}{H * 2L} * \frac{TPL}{2}$$
 (10)

$$R_{s} = \frac{\frac{H*2L}{2} - \frac{(2L)^{2}}{8Tan(\alpha)}}{\frac{H*2L}{2}} * \frac{TPL}{2}$$
 (11)

Finally, the Percent of Gob Load on Abutment (m) is calculated using Equation 12.

$$m = 1 - \frac{2R}{TPL} \tag{12}$$

Side Abutment Load (L_s , inch) is calculated using Equation 13.

$$L_{s} = mqL \tag{13}$$

Mark Abutment Stress ($\sigma_f(x)$, psi) is calculated using Equation 14.

$$\sigma_f(x) = \frac{36L_s}{(D/12)^3} * \frac{\left(\frac{D}{12} - \frac{x}{12}\right)^2}{144}$$
 (14)

Mark-Bieniawski Coal Stress ($S_e(x)$) is calculated using Equation 15.

$$S_e(x) = S_i(0.64 + 2.16(\frac{x}{M})) \tag{15}$$

Marl-Bieniawski Load at Point X (W_{MB} , lbs/inch) is calculated using Equation 16.

$$W_{MB} = \int_{0}^{x} S_{e}(x) = S_{i}(0.64x + 1.08(\frac{x^{2}}{M}))$$
 (16)

To calibrate, W and W_{MB} are made to be equal by varying the Location of Point, or, the value of x. Once equal, this value of x is used in Equation 18 to determine the Rock Mass Lamination Thickness (t, inches). You'll remember that this t-value was assumed earlier in order to begin these calculations.

$$D_{0.9} = (5\sqrt{\frac{H}{12}}) * 12 \tag{17}$$

$$t = \frac{2E_s\sqrt{12(1-v^2)}}{E*M}*\left(\frac{D_{0.9}-x}{ln(1-0.9)}\right)^2$$
 (18)

The new *t*-value is then plugged back into Equation 1, and the process is repeated iteratively until the changes between previous and new *t*-values are effectively null.

Material Model Generation

6 Material Model Generation

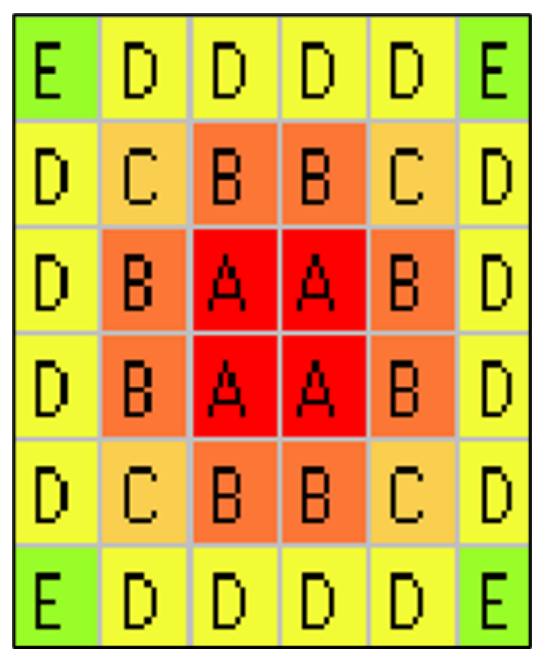
There are three different material model types in StabMap: Coal, Gob, and Stone.

6.1 Coal Properties Generation

Analytical equations based on empirical observations are used to generate seam material properties in StabMap. These calculations are detailed below, utilizing English units.

The process begins with user input of several parameters:

- Elastic Modulus (*E*, *psi*)
- Poisson's Ratio (v)
- Plastic Modulus (E_p , psi)
- Coal Strength (S_i, psi)
- Seam Height (h, inches)
- Element Size (*W*, *inches*)
- Number of Seams (N_s)
- Residual Stress Factor (RF_{Stress}), defaults to 0.2254.
- Residual Strain Factor (RF_{Strain}), defaults to 4.
- Number of Zones (N_Z) , each zone is composed of one side material and one corner material. This concept is displayed in the image below, where material pairs B & C and D & E compose one zone each.



Two zones surrounding the pillar core, which is represented by element A.

The Total Number of Models (M_T) to be created is determined using Equation 1.

$$M_T = 2N_Z + 1 \tag{1}$$

The Zone Number (Z_n) for each model is determined according to proximity to the pillar core. One pillar zone is composed of a side and corner model. The Z_n for both the corner and side models at the exterior of the pillar are designated "1", while the highest Z_n is reserved for the pillar core. In the example displayed in Figure 1, materials D & E would be Zone 1, B & C Zone 2, etc.

The Sequence Parameter (^{S}v) is then calculated using Equations 2 & 3.

$$S_{ps} = Z_n - \frac{1}{2} \tag{2}$$

$$S_{pc} = Z_n - \frac{2}{3} \tag{3}$$

Peak Stress is determined for each model using Equations 4 & 5 for side (${}^{\sigma}ps.psi$) and corner elements (${}^{\sigma}pc.psi$), respectively.

$$\sigma_{ps} = S_i(0.64 + (2.16(\frac{S_{ps} * W}{h})) \tag{4}$$

$$\sigma_{pc} = S_i(0.64 + (2.16(\frac{S_{pc} * W}{h}))$$
 (5)

Peak Strain is determined for each model using Equations 6 & 7 for side (ε_{es}) and corner elements (ε_{ec}), respectively.

$$\varepsilon_{es} = \frac{\sigma_{ps}}{E} \} \tag{6}$$

$$\varepsilon_{ec} = \frac{\sigma_{pc}}{E} \tag{7}$$

Residual Stress (${}^{\sigma}r,psi$) is then determined based upon the material model type. For an Elastic-Plastic model, the Plastic Modulus (${}^{E}p,psi$) takes over as the controlling parameter.

For a Strain-Softening model, Equation 8 is used to determine the Residual Stress for both side and corner elements.

$$\sigma_r = \sigma_p(0.2254 * ln(x)) \tag{8}$$

Where σ_p refers to both σ_{ps} & σ_{pc} and x represents the element midpoint (ft), which can be found using Equation 9.

$$x = \frac{W(Z_n - 0.5)}{12} \tag{9}$$

Residual Strain () for strain-softening models is determined using Equation 10.

$$\varepsilon_r = 4\varepsilon_e \tag{10}$$

Where ε_e refers to both ε_{es} & ε_{ec} .

6.2 Gob Properties Generation

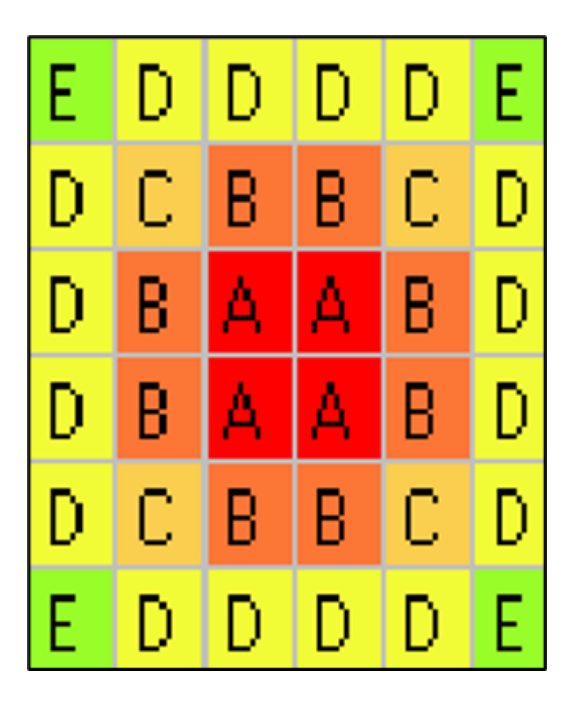
This section still under development.

6.3 Stone Properties Generation

Analytical equations based on empirical observations are used to generate seam material properties in StabMap. These calculations are detailed below, utilizing English units.

The process begins with user input of several parameters:

- Elastic Modulus (*E*, *psi*)
- Poisson's Ratio (v)
- Pillar Height (*h*, *inches*)
- Pillar Width (w, inches)
- Element Size (W, inches)
- Number of Seams (N_s)
- Rock Strength (σ_0 , psi), UCS x 0.92 for English units.
- Number of Zones (N_Z) , each zone is composed of one side material and one corner material. This concept is displayed in the image below, where material pairs B & C and D & E compose one zone each.



Two zones surrounding the pillar core, which is represented by element A. The character representing the benched pillar core will vary depending on the number of zones.

The Total Number of Models (M_T) to be created is determined using Equation 1.

$$M_T = 2N_Z + 1 \tag{1}$$

The Zone Number (Z_n) for each model is determined according to proximity to the pillar core. One pillar zone is composed of a side and corner model. The Z_n for both the corner and side models at the exterior of the pillar are designated "1", while the highest Z_n is reserved for the pillar core. In the example displayed in Figure 1, materials D & E would be Zone 1, B & C Zone 2, etc.

The Sequence Parameter (^{S}p) is then calculated using Equations 2 & 3.

$$S_{ps} = Z_n - \frac{1}{2} \tag{2}$$

$$S_{pc} = Z_n - \frac{2}{3} \tag{3}$$

Peak Stress is determined for each model using Equations 4 & 5 for side ($^{\sigma}_{ps,psi}$) and corner elements ($^{\sigma}_{pc,psi}$), respectively.

$$\sigma_{ps} = \left(\frac{1.23 * \sigma_0}{h^{0.59} * W^2}\right) \left[\left(x + \frac{W}{2}\right)^{2.3} - 2.3\left(x + \frac{W}{2}\right)\left(x - \frac{W}{2}\right)^{1.3} + 1.3\left(x - \frac{W}{2}\right)^{2.3}\right] \tag{4}$$

$$\sigma_{pc} = 1.84\sigma_0 \frac{x^{0.3}}{h^{0.59}} \tag{5}$$

Where x represents the element midpoint (ft), which can be found using Equation 6.

$$x = \frac{W(Z_n - 0.5)}{12} \tag{6}$$

Peak Strain is determined for each model using Equations 7 & 8 for side (ε_{es}) and corner elements (ε_{ec}), respectively.

$$\varepsilon_{es} = \frac{\sigma_{ps}}{E} \} \tag{7}$$

$$\varepsilon_{ec} = \frac{\sigma_{pc}}{E} \tag{8}$$

This page is intentionally left blank. Remove this text from the manual template if you want it completely blank.

- A -

Abutment Load Extent 21
Alternate Database 48
Apply Yield Zones 35
ASCII 43
Author Information 56
Automatic Updates 50

- B -

Backup Database 52
Backups Location 49
Benched Core 33
Benched Material 25
Binary Grids 60
Boundary Conditions 17

- C -

Clone Project 11, 12
Clone Scenario 15
Close 43
Coal Properties Calculation 66
Common Functions 12
Contact Developers 54
Contouring 40
Copy Grids 35
Cross Sections 40

- D -

Database Location 48
Define Project 10
Define Scenarios 10

- E -

Elastic Plastic 23
Exit 43
Exit Program 10
Export Grids 35

- F -

Firebird Location 49

- G -

Gob Core 33
Gob Material 23
Gob Properties Calculation 68
Grid Elements 30
Grid Generation 30, 32

- H -

Help 10 Help Manual 54

- | -

Import Benched Pillars 29
Import Gobs 27
Import Grids 35
Import Pillars 27, 29

- L -

Lamination Thickness Wizard 21
Latitude 12
Leave 43
Linear Elastic 23
Load Drawing 27, 29
Load F1 37
Load INP 16
Load Map 27, 29
Location 12
Log Files 48
Longitude 12

- M -

Main Menu 10
Manage Projects 11
Material Codes 23
Menu 10
Mine Name 11

Multiple Seam 27, 54

- N -

New Project 11 New Scenario 15

- O -

Options 10
Outline 8
Output Indices 38
Overburden Information 17

- P -

Parameters 10
Pillar Core 33
Program Controls 17
Project Summary 14
Projects 10

- R -

Release Date 56
Replace Grid Characters 35
Restore Database 52
Results Grid 39
Rock Mass Stiffness 62

- S -

Save INP 16
Scenarios in Project 14
Seam Grid Information 17
Seam Information 20
Seam Material 23, 25
Seam Parameters 21
Select Project 10, 42
Settings 47
Start 10
Stone Properties Calculation 68
Strain Hardening 23
Strain Softening 23

- T -

Tutorial 54

- U -

Units 11 updates 50,54 User Agreement 54

- V -

Version Number 56

- W -

Workflow 8